THE BIOLOGICAL EFFECTS OF PET SCANS WITH ^{18}F-FDG IN MICE

THE BIOLOGICAL EFFECTS OF PET SCANS WITH ^{18}F-FDG IN MICE

By

KRISTINA TAYLOR, B.Sc.

A Thesis

Submitted to the School of Graduate Studies

in Partial Fulfilment of the Requirements for the Degree

Doctor of Philosophy

McMaster University

DOCTOR OF PHILOSOPHY McMaster University

(Medical Physics) Hamilton, Ontario

TITLE: The Biological Effects of PET Scans with ^{18}F-FDG in Mice

AUTHOR: Kristina Taylor, B.Sc. (McMaster University)

SUPERVISOR: Professor D. Boreham

NUMBER OF PAGES: ix, 142

Abstract

This research addresses low dose ionizing radiation exposure and risk. While it is well understood that high doses of radiation lead to deleterious health effects, there is controversy surrounding the definitive level of risk associated with exposure to low doses of radiation. These types of low level exposures are relevant to patients undergoing medical imaging procedures. This thesis considers the health effects associated with nuclear medicine, specifically positron emission tomography (PET), with the radiopharmaceutical 2-deoxy-2-(^{18}F)fluoro-D-glucose (^{18}F-FDG). These effects were studied in mice to eliminate the high degree of variability among human patients.

The early response to various injection activities of ^{18}F-FDG was first considered in terms of the DNA damage response in the haematopoietic cells of wild-type *Trp53*+/+ mice. The late effects of PET scans with clinically relevant doses of ^{18}F-FDG, such as carcinogenesis, were evaluated in cancer prone *Trp53*+/- mice. The role of p53 in the response to low dose radiation was also investigated to explore how short term responses correlate with p53-mediated cancer risk. This work has helped to advance the understanding of low dose radiation biology and the health risks associated with medical imaging procedures.

Acknowledgements

This research was supported by the US Department of Energy Low Dose Radiation Program (DE-FG02-07ER64343). I would like to thank Mary Ellen Cybulski, Lisa Laframboise and Nicole McFarlane for their important technical contributions (laboratory, veterinary) to the experiments presented in this thesis. I'd also like to thank Caitlin Mills and Jeroen Thompson for proof reading parts of this thesis. I'd like to acknowledge Chantal Saab and Rod Rhem from the McMaster Center for Preclinical and Translational Imaging for their technical assistance with the ^{18}F-FDG injections, as well as Dr. Raman Chirakal for providing information on the ^{18}F-FDG chemistry. I'd like to thank Jackie Ferreira for her exemplary veterinary care of the mice. Thank you to Dr. Dean Percy for histopathological analysis of samples and consultation regarding diseases in *Trp53+/-* mice. The research presented in this thesis represents part of a large shared project on the biological effects of low dose ionizing radiation from diagnostic imaging shared with fellow graduate student Nghi Phan. Nghi contributed to various aspects of data acquisition and experimental design in the experiments presented here.

I would like to thank my wonderful family for encouraging me throughout my studies and for their unwavering positivity which kept me afloat during stressful times. I would like to thank Brendon for being supportive and encouraging me

throughout the endeavour of a PhD. It's not always easy living with a grad student, especially while they're writing their thesis.

I'd like to thank Doug for introducing me to the field of medical physics, for being a good mentor and for providing many opportunities for success. I'd like to thank all the members of the Boreham lab, past and present. You helped me do the research but more importantly, you made being a graduate student a great experience which I will not soon forget.

Table of Contents

List of Figures

Chapter 1

Chapter 2

Chapter 3

Chapter 4

Appendix B

List of Tables

Chapter 1

Chapter 3

Chapter 4

Chapter 1

Introduction

1.1 Diagnostic Imaging

The use of diagnostic imaging in health care has increased dramatically over the last two decades [1]. This may be attributed to advances in technology, increased availability and the fact that the population is aging and requires increased medical care. Computed tomography (CT) scans and nuclear medicine in particular saw the greatest increase in use between 1982 and 2006 within the United-States [1]. Many diagnostic imaging procedures expose the patient to low levels of ionizing radiation in order to generate the image. A list of doses to the patient from diagnostic imaging procedures involving ionizing radiation is provided below (Table 1). The values listed in Table 1.1 represent the estimated maximum absorbed organ dose.

Table 1.1 Doses from Diagnostic Imaging Procedures [2]

Examination Type	**Maximum Organ Dose (mGy)**
Chest x-ray (PA+LA)	0.14
Dental x-ray (panoramic)	0.7
Mammography	2 – 4
Head CT	30 – 50
Abdominal CT	22 – 60
Tc-99m Stress Test	6 – 12
^{18}F-FDG PET Scan	50 – 80

Abbreviations: PA = post-anterior, LA = lateral, CT = computed tomography, Tc-99m = Technetium-99m ^{18}F-FDG = 2-deoxy-2-(^{18}F)fluoro-D-glucose, PET = Positron Emission Tomography

While the increase in diagnostic imaging has led to an improvement in the quality of care, it has raised questions regarding the risk posed by radiation exposure during these procedures. The health risk of concern from low doses of radiation is carcinogenesis. A common approach to risk estimation at low doses employs the linear no threshold (LNT) model. The LNT model extrapolates biological effects observed in the atomic bomb survivors resulting from doses above 100 mGy into the low dose range. This assumption implies that the risk per unit dose is constant (no threshold), that risk is additive and that the absorbed dose is the most important determinant of the biological response. Originally introduced as a practical approach to radiation protection, the LNT model has been used by researchers to derive excess risk estimates for the procedures listed in Table 1 [3-5]. For example, it was recently concluded that 2% of cancers in the US population may be caused by current rates of CT scan usage [3]. This approach has been criticized because it favours the use of inappropriate epidemiological data and ignores a wealth of relevant biological data evaluated at low doses [6-9].

1.2 Biological Effects of Low Doses of Ionizing Radiation

Deoxyribonucleic acid (DNA) is considered the principle target for cell killing, mutation and carcinogenesis. Radiation particles interact with DNA within cells either directly, through the ionization or excitation of atoms, or indirectly, by generating free radicals which will subsequently interact with DNA. There are different types of DNA lesions

(base damage, single strand breaks (SSB), double strand breaks (DSB)) but the most biologically important are DNA DSBs. Once DNA damage occurs, there are generally three possible biological outcomes in a normal cell [9]. The cell can attempt to repair this damage and return to its original state (error free). If the damage is too extensive, the cell will undergo programmed cell death (apoptosis). It is also possible that the cell attempts repair and misrepairs the damage causing a mutation (error-prone). At this point, the mutation may be recognized and the cell can undergo apoptosis although it is also possible that division will progress as usual, leading to genomic instability. Genomic instability is a driving force in the process of carcinogenesis [10].

Cell culture work has provided mechanistic evidence that this process occurs differently following exposure to low doses of radiation than it does following high doses of radiation. It is important to first consider that ≈ 6000 DNA DSBs are generated per cell each hour by endogenous processes[11]. The DNA damage resulting from low rates of radiation are more likely to be repaired accurately as the efficiency of repair increases with decreasing amounts of damage simultaneously present in a cell (approaching the endogenous rate)[12]. The same principle applies to the function of antioxidants and free radical scavengers in response to reactive oxygen species. It has also been shown that low doses up-regulate repair mechanisms [13]. At low doses, apoptosis effectively eliminates small numbers of damaged cells but following high levels of apoptosis in response to high doses of radiation, tissue dysfunction becomes an issue [8, 14]. At the

tissue level, immune competence is up-regulated following exposure to low doses of radiation [15] but ablated following high doses. Microarray data supports these findings; the genes activated or repressed at low doses versus high dose (and dose-rates) are different [16, 17]. This pattern of low dose stimulation and high dose inhibition is called hormesis and has been identified for a number of substances in addition to ionizing radiation [18]. These mechanisms are thought to be responsible for the observation that low dose and low dose-rate radiation exposure reduces the level of transformation in cultured cells below background levels [19]. Moreover, these types of effects at low doses have also been shown to protect against subsequent exposure to genotoxins. This phenomenon is called the adaptive response. *In vivo* rodent work has shown that these low dose protective mechanisms are not only relevant on a tissue level but also applicable on a whole organism scale [20-25]. For example, it has been shown that a single 10 mGy dose (^{60}Co, 0.5 mGy/minute) increased the latency period of lymphoma and osteosarcoma in cancer prone p53 heterozygous mice (*Trp53*+/-) [21]. *Trp53*+/- mice are cancer prone due to a defective tumour suppressor gene (p53). This particular example highlights the importance of genetic background on the influence of the radiation exposure.

There is a wealth of low dose data chronicling the response of cells and tissues to x-rays or gamma-rays and while it has already been shown that gamma radiation can either increase or decrease the latency period of cancer depending upon genotype, the type of

cancer, and the magnitude of the radiation exposure, very little direct evidence concerning risk from diagnostic imaging is known.

1.3 Thesis Objective

The objective of this thesis it to investigate how radiation risk is modified in *Trp53* mice by exposure to ionizing radiation from 2-deoxy-2-(^{18}F)fluoro-D-glucose (^{18}F-FDG) used in positron emission tomography (PET). In order to satisfy this objective, there were 3 areas of investigation:

1. The role of biological endpoints such as apoptosis, micronucleated reticulocyte formation (MN-RET) and γH2A.X fluorescence in p53-mediated cancer risk in the haematopoietic cells of mice.
2. How DNA damage and repair is influenced by radiation quality from PET scans in wild-type mice (*Trp53*+/+).
3. How cancer risk in heterozygous mice (*Trp53*+/-) is influenced by radiation quality from PET scans.

Apoptosis and DNA damage assays are often used as surrogates for risk [26] and so an important first step would be establishing how important these processes were in littermates that had distinctly different cancer risks as a result of a p53 defect. The dose

response and kinetics were evaluated following radiation exposure to gain an improved understanding of the pathways responsible. The p53 gene is a tumour suppressor gene and its role in the response to radiation is described in detail in Chapter 2. The results acquired from the investigation described in Chapter 2 may shed light on the mechanisms responsible for any potential increase or decrease in the risk of cancer observed in Chapter 4.

In Chapter 3, the short term DNA damage response to ^{18}F-FDG used in PET scans was studied in the bone marrow of wild-type mice using 2 different assays; micronucleated reticulocyte formation and γH2A.X foci formation. DNA damage was evaluated because it is an important initiating event in the process of carcinogenesis. Wild-type mice were used because the primary goal was to isolate the effects of the radiation quality associated with ^{18}F-FDG. The induction of DNA damage was compared to that generated by external radiation exposure with Cesium-137 in order to determine the relative biological effectiveness (RBE) for ^{18}F-FDG. The possibility of an adaptive response was also investigated. A period of 24 hours was chosen between the ^{18}F-FDG injection and the high dose "challenge" to allow for decay of the isotope.

Chapter 3 only investigates the radiation risk of PET scans in bone marrow. While bone marrow is of importance due to its radiosensitivity [27] relative to other tissues, the biodistribution of ^{18}F-FDG results in certain organs (heart, brain, kidneys, bladder)

receiving much higher radiation doses than others based on their metabolic requirements. The introduction and methods of Chapter 3 and 4 discuss this in greater detail. Chapter 4 addresses the whole body radiation risk associated with a single 10 mGy ^{18}F-FDG by evaluating the latency and frequency of cancers in multiple tissues of *Trp53+/-* mice. A 10 mGy γ-ray dose was also administered to *Trp53+/-* mice to allow for a direct comparison of radiation quality, dose-rate and biodistribution on the modification of cancer risk. In addition, the short term adaptive response experiment was reproduced in the context of the lifetime cancer study as a period of 24 hours was chosen between the ^{18}F-FDG injection and the high dose "challenge".

1.4 Positron Emission Tomography with ^{18}F-FDG

PET is an imaging modality that allows visualization of metabolic activity within an organism (human patient, mouse). It achieves this through use of a biological molecule labelled with a short lived positron emitting isotope. The diagnostic image is created by the coincidence detection of photons (511 keV) created when the positrons emitted by the radioisotope annihilate with electrons in tissue.

^{18}F-FDG is the most commonly used radiopharmaceutical in clinical PET studies. There are a number of factors which shaped the choice of ^{18}F-FDG as a representative isotope to investigate the effects of nuclear medicine on cancer latency and frequency in *Trp53+/-*

mice. One, the McMaster University Medical Center houses a Siemens RDS112 11 MeV Proton-Cyclotron and routinely produces large volumes ^{18}F-FDG for clinical and research use which made the injection of hundreds of mice feasible and cost effective. Two, the timeline for this research fell during the worldwide reactor based isotope shortage. It was estimated that clinical use of Tc-99 during this time was restricted by 80% [28]. Three, when compared to other nuclear medicine compounds used for diagnostic purposes, ^{18}F-FDG is reported as resulting in one of the highest effective doses to patients [29]. Effective dose is a whole body dose parameter that allows comparison between medical imaging techniques by correcting absorbed dose values for radiation quality and tissue susceptibility to radiation detriment. Originally introduced by the ICRP as an operational radiation protection quantity, the value of using effective dose in evaluating diagnostic imaging procedures has been debated [30, 31]. It is expected that the use of PET with ^{18}F-FDG will only increase due to its versatility in detecting disease states and its improved sensitivity over single-photon emission computed tomography (SPECT) based methods.

The positron emitting isotope ^{18}F is produced by bombarding ^{18}O with high energy protons in a cyclotron. The radiopharmaceutical 2-^{18}FDG is synthesized using a nucleophilic substitution technique from the mannose triflate precursor (1, 3, 4, 6-tetraO-acetyl-2-O-trifluoro-methanesulfonyl-β-D-mannopyranose, TATM) as described in [32]. Once it has been taken up into the cell by facilitated transport, FDG mimics the behaviour of glucose until the phosphorylation of FDG to form flurodeoxyglucose-6-phophate

(FDG-6-P). Because of the substitution of the hydroxyl group with fluorine in 2-^{18}FDG, the compound can no longer progress through the glycolic pathway. FDG-6-P effectively becomes trapped in the cell since it has low membrane permeability and a slow rate of dephosphorylation [33].

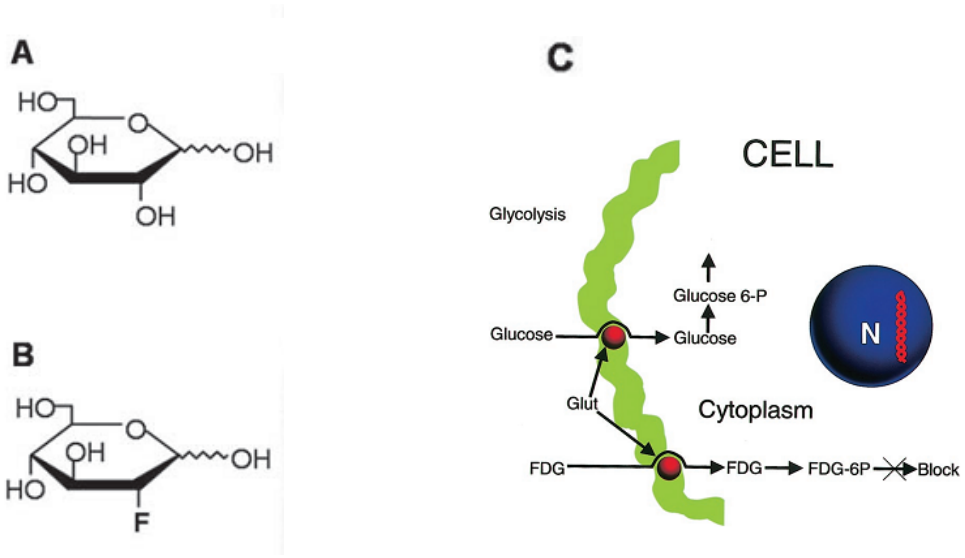

Figure 1.1 (A) D-Glucose (B) ^{18}F-FDG [33] (C) Metabolism of ^{18}F-FDG in the cell [34]

The ^{18}F isotope will decay to ^{18}O with a half life of 109 minutes and emit a positron (β^+) and a neutrino (ν):

$$^{18}F \rightarrow {}^{18}O + \beta^+ + \nu \qquad (1)$$

$$\beta^+ + \beta^- \rightarrow 2\,\gamma\,(0.511\ keV) \qquad (2)$$

This process is enhanced in areas of the body with high metabolic activity.

1.5 Model System & Biological Endpoints

Mice were used for this research as they represent the highest level of biological organisation. A breeding colony was established to generate the mice used. Male mice with a single defective copy of *Trp53* (B6.129S2-Trp53$^{tm1Tyj/1}$) were bred with wild-type female mice (129X1/SvJ) (Jackson Laboratory, Bar Harbour, Maine). A p53 gene targeting technique is used to inactivate 40% of the p53 coding sequence through insertion of a neocasette (exon 2→intron 6) as described in detail in [35]. The F1 female progeny produced from this cross were genotyped at 4-5 weeks of age and used in experiments at 7-9 weeks of age. Both wild-type (*Trp53*+/+) and heterozygous (*Trp53*+/-) F1 female mice were used for short term biology whereas *Trp53*+/- F1 female mice were used to investigate cancer risk. Most animal models and human populations are generally not well suited for carcinogenesis studies because of the long latency period and low frequency of cancers. *Trp53*+/- mice develop spontaneous tumours at a high frequency with an average lifespan of 375 ± 103 days [21] making them well-suited for this type of investigation. Lymphomas and sarcomas are the two major tumour types observed in *Trp53*+/- mice [35].

Three different flow cytometry based assays were used to detect short term changes in apoptosis and the induction and repair of DNA damage following radiation exposure.

Flow cytometry enables the analysis of large numbers of cells relative to traditional microscopy methods.

Apoptosis is a programmed mode of cell death that is characterized by distinct morphological changes. It is a mechanism by which damaged or unwanted cells are eliminated and is triggered by a number of stimuli including ionizing radiation. We have identified apoptotic lymphocytes in the peripheral blood of mice through detection of phophatidylserine (PS) on the outer leaflet of the cell using Annexin V. PS externalization is a downstream event of caspase activation and an early phenomenon associated with the execution phase of apoptosis [36]. We have used 7-Amino actinomycin D (7-AAD) as a counter stain to identify late apoptotic cells when there is permeabilization of the cell membrane.

Micronuclei represent residual extra-nuclear chromatin and occur when chromosome fragments or whole chromosomes fail to be incorporated into daughter nuclei [37]. In these experiments, micronuclei were evaluated in the circulating reticulocytes which are normally devoid of DNA. This flow cytometry technique was developed by Dertinger *et al.* [38]. In this assay, the frequency of micronucleated reticulocytes (MN-RET) 43 hours following radiation exposure is indicative of previous genotoxic damage to reticulocyte precursors (erythroblasts) in bone marrow. MN-RETs represent chromosome damage and offer insight into how DNA damage to bone marrow is processed.

It has been shown that γH2A.X foci form in response to DNA DSBs following radiation exposure [39]. Consequently, mean γH2A.X fluorescence has been established as a biomarker for the formation of DNA DSBs [37, 38]. The phosphorylation of H2A.X by ataxia telangiectasia mutated (ATM) to produce γH2A.X constitutes one of the initial activities in the DNA damage response (DDR) pathway [42]. This signals the recruitment of repair proteins to the site of the DSB to enable repair processes such homologous recombination (HR) or non homologous end joining (NHEJ). These measurements yield information about the initial recognition and subsequent repair, of DSBs.

These assays will also be briefly reviewed in each chapter.

1.6 ^{18}F-FDG Dosimetry in Mice

Previously published absorbed dose estimates for ^{18}F-FDG in mice [43, 44] were used to convert the injected activities used into whole body doses and doses to applicable organs. Small samples of mice were imaged at 7-8 weeks of age to verify the distribution of ^{18}F-FDG in our mouse model to ensure that the uptake was consistent with the dose distribution predicted by these models.

Individual isotope doses were calibrated using a CRC-12 radioisotope calibrator (Capintec). Bi-weekly quality control (voltage, zero, background, stability) was performed on this system using Cs-137 and Co-60 check sources. The pre-and post-

injection activity of the syringe in addition to the time of each measurement was recorded. This information was used to accurately calculate the activity administered to each individual mouse by correcting for decay:

$$A_1 e^{-\lambda(t_0 - t_1)} - \frac{A_2}{e^{-\lambda(t_2 - t_0)}} = A_0 \qquad (3)$$

where A_1 is the initial activity of the syringe measured at time t_1; A_2 is the residual activity of the syringe measured at time t_2; λ is the decay constant for ^{18}F (0.00632 minutes^{-1}); A_0 is the activity injected into the mouse at time t_0. The difference between the times is expressed in minutes.

The weight of each mouse was also recorded prior to the injection to justify the use of the model provided in [43].

The ^{18}F-FDG was diluted into a total volume of 200 µl with saline and administered by tail vein injection (30g needle, 1 cc syringe). Control mice were injected with 200 µl saline only. Mice were immobilized using a restraint device designed for mouse tail vein injections (Tailveiner® TV-150, Braintree Scientific Inc., MA). Anaesthesia was not used since image acquisition was not the objective of this work. Food was returned to the mice 2 hours after the injection to maximize uptake of the ^{18}F-FDG and to simulate the conditions of a typical PET procedure.

In a study by Taschereau and Chaztiioannou [44], voxel-based mouse phantoms (whole body, high resolution bladder only, high resolution femur head only, high resolution

vertebrae) were used to calculate the internal absorbed dose distribution from F-18 labelled compounds. Time activity curves obtained from dynamic *in vivo* studies were used to set the initial activity concentrations in the Monte Carlo simulation (GATE). For example, the absorbed dose per unit administered activity was found to be 14 mGy/MBq for the body mass of the mouse and 10 mGy/MBq for the bone marrow. See TABLE II in reference [44].

An earlier approach by Funk et al. [43] employed a different Monte Carlo code (MCNP 4c) and the Medical Internal Radiation Dose (MIRD) formulation to calculate the absorbed dose per cumulated activity and unit mass (S-value). The mouse was approximated by a 20 g soft tissue ellipsoid (2.2cm x 2.2cm x 8.4 cm) containing a homogeneously distributed source. According to the MIRD schema, the absorbed dose is the product of the cumulated activity $\tilde{A}$ (Bq) and the S value (Gy/Bq s), a term which reflects the geometry, absorption, radiation types, size and mass of the mouse.

$$\overline{D} = \tilde{A} \cdot \mathrm{S} \qquad (4)$$

The cumulated activity is the activity A_j (Bq) with residence time τ_j (s). This is summed for different fractions of the initial activity distributed throughout the mouse's body.

$$\tilde{A} = \sum_j A_j \cdot \tau_j \qquad (5)$$

The residence time τ_j depends on the physical half life (T=109.7 minutes) and biological half life (T_j) of the pharmaceutical in the tissue of interest.

$$\tau_j = \frac{1}{\ln(2)} \cdot \left(\frac{1}{T} + \frac{1}{T_j}\right)^{-1} \quad (6)$$

The whole body was treated as a single compartment. It was assumed that the cumulated activity within the whole body would be equal to the initial injected A_0 activity minus the activity that was immediately voided through the bladder. It was assumed that 25% of the initial activity was immediately lost through the bladder based on previous imaging experience and [45]. After this point, the physical decay of the isotope (T) was assumed to be the primary mode of decay. By applying these simplifications and combining equations (4), (5) and (6):

$$\overline{D} = 0.75 A_0 \frac{T}{ln2} \cdot S \quad (7)$$

The whole body dose estimates using both approaches were found to be in good agreement. Chapter 3 and Chapter 4 briefly review this approach and provide specific dose values for the experiments.

1.7 References

[1] F. A. Mettler et al., "Medical radiation exposure in the U.S. in 2006: preliminary results.," *Health physics*, vol. 95, no. 5, pp. 502-7, Nov. 2008.

[2] N. Metting, "US DOE Dose Ranges Chart," 2010. [Online]. Available: http://lowdose.energy.gov/imagegallery.aspx.

[3] D. J. Brenner and E. J. Hall, "Computed tomography--an increasing source of radiation exposure.," *The New England journal of medicine*, vol. 357, no. 22, pp. 2277-84, Nov. 2007.

[4] B. Huang, M. W. M. Law, and P. L. Khong, "Whole-Body PET/CT Scanning: Estimation of Radiation Dose and Cancer Risk," *Radiology*, vol. 251, no. 1, p. 166, 2009.

[5] A. Berrington de González and S. Darby, "Risk of cancer from diagnostic X-rays: estimates for the UK and 14 other countries.," *Lancet*, vol. 363, no. 9406, pp. 345-51, Jan. 2004.

[6] B. R. Scott, C. L. Sanders, R. E. J. Mitchel, and D. R. Boreham, "CT scans may reduce rather than increase the risk of cancer," *Journal of American Physicians and Surgeons*, vol. 13, no. 1, 2008.

[7] M. Tubiana, A. Aurengo, D. Averbeck, and R. Masse, "Recent reports on the effect of low doses of ionizing radiation and its dose-effect relationship," *Radiation and environmental biophysics*, vol. 44, no. 4, pp. 245-51, Mar. 2006.

[8] M. Tubiana, L. E. Feinendegen, C. Yang, and J. M. Kaminski, "The Linear No-Threshold Relationship Is Inconsistent with Radiation Biologic and Experimental Data1," *Radiology*, vol. 251, no. 1, p. 13, 2009.

[9] R. E. J. Mitchel, "Low doses of radiation reduce risk in vivo.," *Dose-response : a publication of International Hormesis Society*, vol. 5, no. 1, pp. 1-10, Jan. 2007.

[10] W. F. Morgan, "Non-targeted and delayed effects of exposure to ionizing radiation: II. Radiation-induced genomic instability and bystander effects in vivo, clastogenic factors and transgenerational effects.," *Radiation research*, vol. 159, no. 5, pp. 581-96, May. 2003.

[11] D. Billen, “Spontaneous DNA Damage and Its Significance for the ‘Negligible Dose ’ Controversy in Radiation Protection,” *Radiation Research*, vol. 124, no. 2, pp. 242-245, 1990.

[12] E. Dikomey and I. Brammer, “Relationship between cellular radiosensitivity and non-repaired double-strand breaks studied for different growth states, dose-rates and plating conditions in a normal human fibroblast line.,” *International journal of radiation biology*, vol. 76, no. 6, pp. 773-81, Jun. 2000.

[13] D. Boucher, H. Joelle, and A. Dietrich, “Increased repair of gamma -induced DNA double-strand breaks at lower dose-rate in CHO cells,” *Canadian Journal of Physiology and Pharmacology*, vol. 82, no. 2, 2004.

[14] D. I. Portess, G. Bauer, M. A. Hill, and P. O’Neill, “Low-dose irradiation of nontransformed cells stimulates the selective removal of precancerous cells via intercellular induction of apoptosis.,” *Cancer research*, vol. 67, no. 3, pp. 1246-53, Feb. 2007.

[15] S.-Z. Liu, “Cancer control related to stimulation of immunity by low-dose radiation.,” *Dose-response*, vol. 5, no. 1, pp. 39-47, Jan. 2007.

[16] S. A. Amundson, K. T. Do, and A. J. Fornace Jr, “Induction of stress genes by low doses of gamma rays,” *Radiation research*, vol. 152, no. 3, pp. 225–231, 1999.

[17] N. Franco et al., “Low-Dose Exposure to γ Rays Induces Specific Gene Regulations in Normal Human Keratinocytes,” *Radiation Research*, vol. 163, no. 6, pp. 623-635, Jun. 2005.

[18] E. J. Calabrese, *Hormesis*. Totowa, NJ: Humana Press, 2010.

[19] E. I. Azzam, S. M. de Toledo, G. P. Raaphorst, and R. E. J. Mitchel, “Low-Dose Ionizing Radiation Decreases the Frequency of Neoplastic Transformation to a Level below the Spontaneous Rate in C3H 10T1/2 Cells,” *Radiation Research*, vol. 146, no. 4, p. 369, Oct. 1996.

[20] R. E. Mitchel, J. S. Jackson, R. a McCann, and D. R. Boreham, “The adaptive response modifies latency for radiation-induced myeloid leukemia in CBA/H mice.,” *Radiation research*, vol. 152, no. 3, pp. 273-9, Sep. 1999.

[21] R. E. J. Mitchel, J. S. Jackson, D. P. Morrison, and S. M. Carlisle, “Low doses of radiation increase the latency of spontaneous lymphomas and spinal osteosarcomas

in cancer-prone, radiation-sensitive Trp53 heterozygous mice.," *Radiation research*, vol. 159, no. 3, pp. 320-7, Mar. 2003.

[22] R. E. J. Mitchel, J. S. Jackson, and S. M. Carlisle, "Upper dose thresholds for radiation-induced adaptive response against cancer in high-dose-exposed, cancer-prone, radiation-sensitive Trp53 heterozygous mice.," *Radiation research*, vol. 162, no. 1, pp. 20-30, Jul. 2004.

[23] Y. Ina and K. Sakai, "Prolongation of life span associated with immunological modification by chronic low-dose-rate irradiation in MRL-lpr/lpr mice.," *Radiation research*, vol. 161, no. 2, pp. 168-73, Feb. 2004.

[24] K. Sakai, Y. Hoshi, T. Nomura, and T. Oda, "Suppression of carcinogenic processes in mice by chronic low dose-rate gamma-irradiation," *International Journal of Low Radiation*, vol. 1, no. 1, pp. 142-146, 2003.

[25] Y. Ina, H. Tanooka, T. Yamada, and K. Sakai, "Suppression of thymic lymphoma induction by life-long low-dose-rate irradiation accompanied by immune activation in C57BL/6 mice.," *Radiation research*, vol. 163, no. 2, pp. 153-8, Feb. 2005.

[26] J. D. Tucker and R. J. Preston, "Chromosome aberrations, micronuclei, aneuploidy, sister chromatid exchanges, and cancer risk assessment.," *Mutation research*, vol. 365, no. 1-3, pp. 147-59, Sep. 1996.

[27] E. Hall and A. Giaccia, *Radiobiology for the Radiologist*. 2006.

[28] R. Collier, "Canadian hospitals rise to the occasion during isotope shortage.," *Canadian Medical Association journal*, vol. 178, no. 7, p. 815, Mar. 2008.

[29] F. A. Mettler, W. Huda, T. T. Yoshizumi, and M. Mahesh, "Effective doses in radiology and diagnostic nuclear medicine: a catalog.," *Radiology*, vol. 248, no. 1, pp. 254-63, Jul. 2008.

[30] G. Drexler, W. Panzer, N. Petoussi, and M. Zankl, "Effective dose--how effective for patients?," *Radiation and environmental biophysics*, vol. 32, no. 3, pp. 209-19, Jan. 1993.

[31] C. H. McCollough, J. a Christner, and J. M. Kofler, "How effective is effective dose as a predictor of radiation risk?," *American journal of roentgenology*, vol. 194, no. 4, pp. 890-6, Apr. 2010.

[32] R. Chirakal, "Base mediated Decomposition of a Mannose Triflate During the Synthesis of 2-Deoxy-2-18F-fluoro-D-glucose," *Applied Radiation and Isotopes*, vol. 46, no. 3, pp. 149-155, Mar. 1995.

[33] R. Alford, M. Ogawa, P. L. Choyke, and H. Kobayashi, "Molecular probes for the in vivo imaging of cancer.," *Molecular BioSystems*, vol. 5, no. 11, pp. 1279-91, Nov. 2009.

[34] V. Kapoor, B. M. McCook, and F. S. Torok, "An introduction to PET-CT imaging.," *Radiographics*, vol. 24, no. 2, pp. 523-43, 2004.

[35] T. Jacks et al., "Tumor spectrum analysis in p53-mutant mice.," *Current biology*, vol. 4, no. 1, pp. 1-7, Jan. 1994.

[36] M. Van Engeland, L. J. Nieland, F. C. Ramaekers, B. Schutte, and C. P. Reutelingsperger, "Annexin V-affinity assay: a review on an apoptosis detection system based on phosphatidylserine exposure.," *Cytometry*, vol. 31, no. 1, pp. 1-9, Jan. 1998.

[37] S. D. Dertinger et al., "Reticulocyte and micronucleated reticulocyte responses to gamma irradiation: dose-response and time-course profiles measured by flow cytometry.," *Mutation research*, vol. 634, no. 1-2, pp. 119-25, Dec. 2007.

[38] S. D. Dertinger, D. K. Torous, and K. R. Tometsko, "Simple and reliable enumeration of micronucleated reticulocytes with a single-laser flow cytometer.," *Mutation research*, vol. 371, no. 3-4, pp. 283-92, Dec. 1996.

[39] E. P. Rogakou, D. R. Pilch, A. H. Orr, V. S. Ivanova, and W. M. Bonner, "DNA double-stranded breaks induce histone H2AX phosphorylation on serine 139.," *The Journal of biological chemistry*, vol. 273, no. 10, pp. 5858-68, Mar. 1998.

[40] K. Rothkamm, M. Lo, and M. Löbrich, "Evidence for a lack of DNA double-strand break repair in human cells exposed to very low x-ray doses," *Proceedings of the National Academy of Sciences of the United States of America*, vol. 100, no. 9, pp. 5057-62, Apr. 2003.

[41] O. A. Sedelnikova, E. P. Rogakou, and I. G. Panyutin, "Quantitative detection of 125IdU-induced DNA double-strand breaks with y-H2AX antibody," *Radiation research*, vol. 158, no. 4, pp. 486–492, 2002.

[42] L.-J. Mah, A. El-Osta, and T. C. Karagiannis, “gammaH2AX: a sensitive molecular marker of DNA damage and repair.,” *Leukemia*, vol. 24, no. 4, pp. 679-86, Apr. 2010.

[43] T. Funk, M. Sun, and B. H. Hasegawa, “Radiation dose estimate in small animal SPECT and PET,” *Medical Physics*, vol. 31, no. 9, p. 2680, 2004.

[44] R. Taschereau and A. F. Chatziioannou, “Monte Carlo simulations of absorbed dose in a mouse phantom from 18-fluorine compounds,” *Medical Physics*, vol. 34, no. 3, p. 1026, 2007.

[45] FDA, “Fludeoxyglucose F 18 (Systemic).” [Online]. Available: http://www.drugs.com/mmx/fludeoxyglucose-f-18.html.

Chapter 2

Trp53 gene status influences low dose radiation-induced apoptosis and DNA damage in the haematopoietic cells of mice

2.1 Abstract

This study investigated the apoptotic and DNA damage response of haematopoietic cells from mice of differing *Trp53* gene status to low doses of radiation (0.1-2 Gy). No difference was observed in the formation of DNA double-strand breaks, as measured by γH2A.X fluorescence between 0 and 120 minutes post-irradiation, between wild-type (*Trp53*+/+) and heterozygous *(Trp53*+/-) bone marrow lymphocytes. To our knowledge, there are no reports that investigate the kinetics of radiation-induced apoptosis in the peripheral blood lymphocytes of p53-deficient mice. Here, peripheral blood lymphocytes from *Trp53*+/+ mice showed higher apoptosis levels relative to *Trp53*+/- in response to *in vitro* γ-ray doses between 0 and 1 Gy. This trend was observed up to 12 hours post-irradiation although both genotypes ultimately reached the same level of apoptosis at 14 hours, indicating that the influence of p53 is transient. *Trp53*+/+ and *Trp53*+/- mice showed similar MN-RET levels at 43 hours post-irradiation although *Trp53*+/- mice did show a slightly slower rate of MN-RET clearance between 43 and 137 hours post-irradiation. Again, the p53-mediated effect was transient as MN-RET levels returned to the same baseline level in both genotypes by 68 hours post-irradiation. Although p53 has an important role in cancer risk, its influence on biological pathways and cellular endpoints is variable, as shown in this research. When using these haematopoietic endpoints as surrogates for radiation-induced cancer risk estimation, the timing of the assays and understanding the steps in the various pathways is essential.

2.2 Introduction

The p53 knockout mouse strain developed by Tyler Jacks in 1994 carries a mutation deleting 40% of the p53 coding region which completely eliminates the production of p53 protein by that allele . This results in a reduced level of full length functional p53 protein in heterozygous (*Trp53+/-)* cells. The reduced level of p53 protein results in decreased survival and a shorter tumour latency period in *Trp53*+/- mice relative to *Trp53*+/+ mice. More specifically, a recent study showed that the median survival of female *Trp53*+/- mice that developed malignant tumours was 407 days (95% CI: 387–427) compared to 617 days (95% CI: 573–661) in female *Trp53*+/+ mice; a difference of 210 days [2]. Null mice (*Trp53*-/-) develop tumours at an even faster rate with a correspondingly shorter lifespan. In one study, all null mice succumbed to cancer by 10 months of age (≈300 days) [3]. Lymphomas and sarcomas predominate in the tumour spectrum observed in this p53-deficient strain indicating that certain tissues are more influenced by p53 deficiency than others [1]. High dose ionizing radiation exposure (1-4 Gy) has been shown to further reduce the lifespan and tumour latency in null, heterozygous and wild-type mice relative to unirradiated isogenic mice [4]. In *Trp53*+/- mice, the median lifespan of mice with malignant tumours was reduced by 45.4±2.6 days per Gy [2].

The quantity and activity of p53 in the cell is regulated through post-translational modifications [5]. Under normal, unstressed conditions, the p53 protein is maintained at a low concentration through a continual degradation process initiated by the

ubiquitinylation of p53 by MDM2 [6]. In response to ionizing radiation, a series of coordinated cellular responses forms what is known as the DNA damage response (DDR) pathway. Within minutes of a DNA double strand break (DSB) created by ionizing radiation exposure, the histone H2A.X is phosphorylated by PIK-kinases (ATM, DNA-PK) at the site of nascent DNA DSBs to form γH2A.X [7-9] . This acts as a scaffold for repair proteins to access the DSB. Activated ATM also acts as a transducer of the damage signal and phosphorylates p53 (directly or indirectly) to enable stabilization and accumulation of p53 in the nucleus where it forms a tetrameric complex [10]. This complex binds to specific downstream gene targets (p53 responsive elements), activating the transcription of proteins that will allow the cell to process the radiation damage via cell cycle arrest, apoptosis, senescence or repair. Cell cycle arrest occurs to enable repair of damage before the cell progresses to division. In mammalian cells, DSBs are repaired using non-homologous end-joining (NHEJ) or homologous recombination (HR). Once the break is repaired, de-phosphorylation of γH2A.X generally occurs [11, 12]. In the event that the damage sustained by the cell is too substantial, the cell undergoes apoptosis. Morphological changes, such as the appearance of phosphatidylserine on the outer membrane of the cell, signals the execution phase of apoptosis and may be identified with Annexin V [13]. The outcome of the cell in response to external signals ultimately depends on the genetic background, microenvironment, tissue type, and the strength/nature of the p53 activating stimuli [14]. In cells lacking p53 functionality, it is thought that the cell is not able to respond adequately to radiation response signals,

enabling the inappropriate survival of damaged cells [15]. Unrepaired or misrepaired DSBs in haematopoietic progenitors (erythroblasts) will lead to micronuclei in newly formed reticulocytes following mitosis [16]. As such, micronucleated reticulocytes (MN-RETs) are indicative of chromosome damage in the progenitor cells of bone marrow which may be related to genomic instability. Genomic instability is thought to be an important contributor to tumorigenesis in p53-deficient mice [17, 18].

The aim of this work was to compare the radiation sensitivity of haematopoietic cells in normal *Trp53+/+* mice to that of isogenic heterozygous *Trp53+/-* littermates. The spontaneous and radiation-induced responses for various doses and time points post-irradiation were evaluated in order to gain a comprehensive understanding of the role of p53 gene status in γH2A.X foci formation, apoptosis and micronucleus formation in this specific mouse strain because it was used in extensive life-time radiation-induced cancer risk studies in our laboratory.

2.3 Materials and Methods

2.3.1 Mice

Male mice with a single defective copy of *Trp53* (B6.129S2-Trp53$^{tm1Tyj/1}$) were bred with wild-type female mice (129X1/SvJ) (Jackson Laboratory, Bar Harbour, Maine). The F1

female progeny produced from this cross were genotyped at 4-5 weeks of age and used in experiments at 7-9 weeks of age. All F1 mice were housed five to a cage, in specific pathogen free conditions (SPF), in a housing room maintained on a 12 hour light/dark cycle at a temperature of 24 ± 1°C. Food and water were available *ad libitum*. Protocols were approved by the Animal Research Ethics Board (AREB) at McMaster University and carried out as per the Canadian Council on Animal Care (CCAC).

2.3.2 Genotyping

Tail snips were collected as a source of DNA to use for polymerase chain reaction (PCR) to identify whether mice were wild-type (*Trp53*+/+) or heterozygous (*Trp53*+/-). Mice were anaesthetized (1-2% Isoflurane™ via inhalation) and a tail snip was collected in 200 µl of 95% ethanol. Mice were ear punched at this time for subsequent identification and sorting. The PCR procedure has been described previously [1].

2.3.3 Irradiations

All irradiations were performed using a Cs-137 source (662 keV γ-rays) at the McMaster Taylor Radiobiology Source Facility. For *in vivo* irradiations, mice were placed in a customized sectioned polycarbonate restraint tube and irradiated at a dose-rate of 0.35 Gy/minute. *In vitro* samples were irradiated in an ice slurry (0 ^{o}C) at a dose-rate of 0.19 Gy/minute to temporarily arrest biological processes such as DNA repair.

2.3.4 Flow Cytometry

All 3 assays used (γH2A.X, apoptosis, MN-RET) were flow cytometry-based. Samples were analyzed using a Beckman Coulter EPICS XL flow cytometer which is equipped with a 488 nm argon laser and four detectors for fluorescence measurements. All samples were kept in an ice slurry (0 ^{o}C) during preparation unless otherwise specified.

2.3.5 γH2A.X Assay

Mean γH2A.X fluorescence was measured in the lymphocyte-rich bone marrow population. Briefly, fixed bone marrow cells were permeabilized and incubated with a primary antibody for γH2A.X which was then followed by incubation with a fluorescent secondary antibody. This bone marrow lymphocyte rich population was initially identified based on the forward-scatter/side-scatter (FSC/SSC) properties of the sample population. Within this population, only G0/G1 cells were analyzed for mean γH2A.X fluorescence. Cells in G2/M interfere with this assay and were consequently excluded by measuring relative DNA content using propidium iodide (PI).

Spontaneous and radiation-induced mean γH2A.X levels were measured in lymphocyte-rich bone marrow cultures from *Trp53+/+* and *Trp53+/-* mice in a single experiment. Mice were euthanized via cervical dislocation and a bone marrow sample was harvested by flushing both femurs with a 3 ml syringe with 23 gauge needle containing 1 mL of heparinised RPMI 1640 media (0^{o}C) (Lonza Inc., Allendale, New Jersey). This bone

marrow suspension was adjusted to a concentration of 1 x 10^6 cells/mL with complete media (RPMI 1640 supplemented with 10% Fetal Bovine Serum (FBS), 1% L-Glutamine (2mM), 1% Penicillin(100U/ml)-Streptomycin(100ug/ml)); all components from Invitrogen, Mississauga, ON) and irradiated according to the instructions above to produce the required doses (0, 0.5, 1, 2 or 4 Gy) in 5 ml propylene tubes. Following irradiation, samples were placed in a water bath (37^{o}C) for the incubation period. At 0, 15, 30, 60 or 180 minutes post-irradiation, 2 x 500µl sample aliquots were removed and placed in duplicate flow tubes. These samples were fixed by adding 3 mL of 70% ethanol (0^{o}C) and incubated on ice for 1 hour. Samples were then stored at -20^{o}C until staining and flow analysis. The first step in the staining procedure was to remove the ethanol by centrifugation (300 x *g*, 7 minutes) and decanting. A wash step followed where 3 mL of Tris-buffered saline (1x TBS; Trizma base + NaCl, Sigma Aldrich, Mississauga, Ontario) was added and the samples centrifuged and decanted once more (300 x *g*, 7 minutes). The second step, permeabilization, began with the addition of 1 ml of Tris–saline–triton [TST; TBS + 4% FBS (VWR International, Mississauga, Ontario) + 0.1% Triton X-100 (Sigma Aldrich, Mississauga, Ontario)] followed by a 10 minute incubation (0^{o}C). The samples were then centrifuged (300 x *g*, 7 minutes), the supernatant removed and 200 µL of a 1:400 dilution of anti-phospho-H2A.X (ser139) antibody in TST was added (γH2A.X; Upstate Cell Signaling, Charlottesville, VA). After an incubation period of 2 hours (RT), the samples were washed with 3 mL TST(0^{o}C) and re-suspended in 200 µL of AlexaFluor™ 488-conjugated goat anti-rabbit IgG F(ab')2 antibody (Invitrogen Canada,

Burlington, Ontario) at a 1:500 dilution in TST followed by a 1 hour incubation in the dark. Prior to flow cytometry, the samples were washed in 3 mL TBS, centrifuged (300 x *g*, 7 minutes), decanted and re-suspended in 300 µL TBS + PI solution (5 µl PI x 1 mg/mL + 295 µl TBS; Sigma Aldrich). Per sample, $5x10^3$cells within the lymphocyte-rich bone marrow gate were acquired.

2.3.6 Apoptosis Assay

Annexin V and 7-Amino Actinomycin D (7-AAD), in combination with platelet specific antibody CD61 and leukocyte specific antibody CD45, were used to indentify lymphocytes in various stages of apoptosis. The Annexin V-FITC/ 7-AAD stains are available as a commercial kit (Annexin V-FITC/7-AAD; IM3614, Beckman Coulter, Mississauga, Ontario). The lymphocyte population was isolated by gating on CD45 PE-TR (MCD4517, Caltag Laboratories) bright positive cells with low side scatter. Events identified as CD61PE (Beckman Coulter, Mississauga, Ontario) positive were eliminated to minimize platelet contamination within this lymphocyte population.

Four independent experiments were performed to determine if differences existed in the spontaneous and radiation-induced responses of peripheral blood lymphocytes from *Trp53+/-* and *Trp53+/+* mice. In these experiments, mice were anaesthetized with Isoflurane™ and 0.5 ml of blood was collected by cardiac puncture into a 1 ml syringe with 23 gauge needle containing 0.1 ml heparinized RPMI 1640. The blood was further

diluted into 0.5 ml of complete medium ((RPMI 1640 supplemented with 10% Fetal Bovine Serum (FBS), 1% L-Glutamine (2mM), 1% Penicillin(100U/ml)-Streptomycin(100ug/ml) all components from Invitrogen, Mississauga, ON) (≈ 1:1 ratio). The diluted blood samples ($1x10^6$ cells/ml lymphocytes) were aliquoted into 100 µl samples, which were irradiated to yield the required doses (0, 0.25, 0.5, 0.75 or 1 Gy). These samples were then incubated at 37˚C (5% CO_2, 98% humidity) for the required time period (0, 4, 6, 8, 10, 12 or 14 hours). Following incubation, red blood cells were lysed using an ammonium chloride (NH_4Cl) solution (0.154M ammonium chloride, 1.5 mM potassium bicarbonate, 0.1mM EDTA). Two ml of 37˚C NH_4Cl solution was added to the samples followed by an incubation (5 minutes) at room temperature (RT). The lysed samples were centrifuged at 300 x *g* for 5 minutes at RT and subsequently decanted. The pellet in each sample was resuspended by vortexing and stained using 100 µl of an antibody cocktail containing CD45 PE-TR(1.25 µl), CD61 PE(0.17 µl), 5 µl Annexin V(5 µl) and 7-AAD(10 µl), in binding buffer. Samples were incubated for 15 minutes (4°). Immediately prior to running samples on the flow cytometer, 300 µl binding buffer was added. A total of $2x10^4$ lymphocytes (CD45+CD61-) were analyzed for each sample.

2.3.7 MN-RET Assay

The MN-RET assay used has been described previously [19] and is based on the idea that an elevation in the frequency of micronucleated reticulocytes (MN-RETs) is indicative of recent genotoxic damage. Newly formed erythrocytes, also known as reticulocytes

(RETs), are identified within a peripheral blood sample using an antibody to the transferrin receptor (CD71) and a platelet specific antibody (CD61). This allows differentiation of RETS from mature erythrocytes and platelets. DNA content is then analyzed within the RET population using PI; the MN-RETs are differentially identified through calibration with a malaria infected erythrocyte biostandard. A comprehensive kit provided all antibodies, stains and reagents necessary for the fixation and analysis of peripheral blood samples for the purpose of MN-RET analysis (Mouse MicroFlowPLUS®, Litron Laboratories, Rochester NY).

A total of three independent experiments were performed to assess potential differences in MN-RET formation between *Trp53+/+* and *Trp53+/-* mice. In these experiments, mice were irradiated *in vivo* to yield absorbed whole body doses of 0, 0.1, 0.25, 0.5, 0.75, 1 or 2 Gy. For dose response experiments, blood was collected by cardiac puncture from mice anaesthetized with Isoflurane™ at 43 hours post-irradiation into a 1 ml syringe with 23 gauge needle containing 0.01 ml heparinized RPMI 1640. The needle was removed and two drops (60-120µl) of blood were transferred into 350 µl anticoagulant (RT). For time course experiments, blood was collected using a repeat facial vein bleeding technique with a lancet (goldenrod 3 mm lancet, MEDIpoint inc., NY USA) at 41, 43, 44, 51, 68 and 137 hours following irradiation with 0 or 1 Gy. A reduced amount of blood (1 drop or 30-50 µl) was collected in a reduced amount of anticoagulant (180 µl) to maintain the same cell density while minimizing side effects on the mice for the duration of the

experiment. Blood samples were fixed within 4 hours of collection. Using a specialized fixing technique described in the Mouse MicroFlowPLUS® instruction manual, 180 µl of the blood/anticoagulant mix was forcefully added to 2 ml ultra cold (-80^{0}C) 100% methanol (MeOH) (CAS no. 67-56-1, Sigma Aldrich, Mississauga, Ontario). Fixed blood specimens were stored at -80^{0}C until staining and flow analysis. For the staining procedure, the MeOH-fixed blood samples were first washed by adding 12 ml of kit supplied buffer, centrifuged at 300 x *g* (0^{0}C) for 5 minutes and the pellet was resuspended after thoroughly decanting. Eighty µl of a labelling solution containing binding buffer (69.4 µl), RNAase (9.5 µl), antiCD71-FITC (0.8 µl) and antiCD61PE (0.4 µl) was added to each tube followed by two incubation periods: 30 minutes at 0°C followed by 30 minutes at RT. The sequential gating logic used in the assay has been published. Prior to acquisition, 1 mL of cold (4^{o}C) PI solution (1.25 µg/mL in buffer) was added to each tube. For each sample, 2x10^4 CD71+CD61- events (RETs) were collected at a rate of less than 4x10^3 cells per second. The percentage of MN-RETs was then identified within this RET population based on PI content.

2.3.8 Statistical Analysis

Statistics were performed using Sigma Plot version 11.0 (Systat Software, Germany). Experimental results are presented as the mean ± the standard error of the mean (SEM). Two sided P values ≤ 0.05 were considered statistically significant. Analysis of Variance (ANOVA) was used to assess the relationship between gene status, dose, time and the

resulting biological response for the 3 endpoints used. Statistically significant differences were probed using the Bonferroni post hoc test. Additional t-tests were performed, where appropriate, to determine if significant differences existed between any groups. Dose responses between *Trp53+/+* and *Trp53+/-* mice were compared using multiple linear regression analysis.

2.4 Results

2.4.1 γH2A.X

The spontaneous levels of γH2A.X were measured at 0, 15, 30, 60 and 120 minutes post-irradiation (Figure 2.1 A). Genotype did not affect spontaneous γH2A.X levels at any time point (P=0.294). Time, however, was found to affect spontaneous γH2A.X levels (P=0.006); the 0 minute samples showed a slight increase (P=0.01-0.05) over all other time points. Radiation-induced γH2A.X was measured following 1 Gy at the aforementioned time points. The spontaneous level was subtracted at each time point for each genotype to yield radiation-induced values (Figure 2.1 B). Both genotypes showed similar time dependent (P<0.001) kinetic patterns as fluorescence increased rapidly between 0 and 15 minutes post-irradiation, reached a maximum at 30 minutes post-irradiation, and decreased at a comparatively slower rate between 30 and 120 minutes post-irradiation. Genotype did not influence the kinetics of γH2A.X foci formation or

removal (P=0.198). The dose responses of *Trp53*+/+ and *Trp53*+/- bone marrow lymphocytes were investigated at 30 minutes post-irradiation (Figure 2.1 C). Again, spontaneous values were subtracted from each genotype curve. There was a significant dose response for both *Trp53*+/+ and *Trp53*+/- ($P<0.001$) but genotype did not affect this dose response (P=0.590).

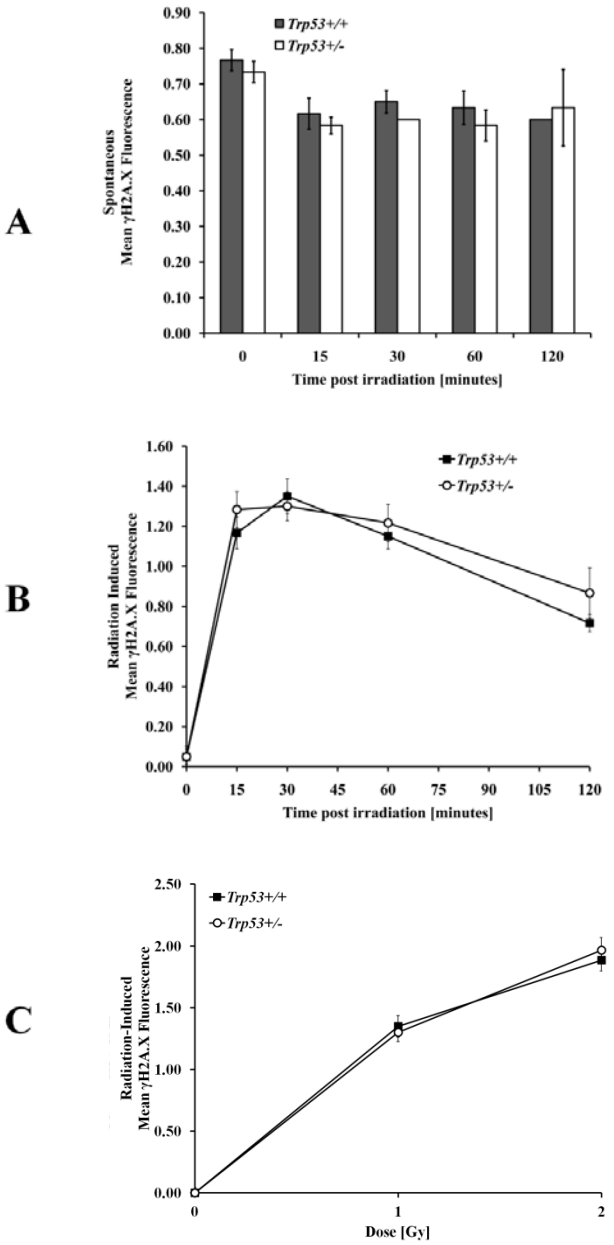

Figure 2.1 γH2A.X fluorescence in the bone marrow of wild-type *Trp53+/+* (closed squares) and heterozygous *Trp53+/-* (open circles) mice **(A)** Spontaneous and (**B**) radiation-induced kinetics were evaluated at 0, 15, 30, 60, 120 minutes post-irradiation (n=3 in duplicate). The radiation-induced values were obtained by subtracting spontaneous γH2A.X (0 Gy) from total γH2A.X (1 Gy). **(C)** The γH2A.X dose response was evaluated at 30 minutes following 0, 1 or 2 Gy (n=3 in duplicate). Only radiation-

induced γH2A.X is displayed; spontaneous γH2A.X has been subtracted from total γH2A.X. All data points shown represent mean ± standard error.

2.4.2 Apoptosis

Time dependent changes were measured in irradiated (1 Gy) and sham-irradiated (0 Gy) lymphocyte cultures from both genotypes up to 14 hours following irradiation (Figure 2.2 A). The spontaneous level of apoptosis was found to increase with time ($P<0.001$) and depended on genotype ($P=0.043$). *Trp53+/-* lymphocytes generally demonstrated higher spontaneous apoptosis levels.

Radiation-induced kinetics were determined by subtracting this background level of apoptosis from that induced by a 1 Gy acute radiation exposure for all time points (Figure 2.2 B). Both genotypes displayed similar kinetic patterns throughout the 14 hour incubation period. Radiation-induced apoptosis increased between 4 and 10 hours. Both genotypes decreased at 12 hours and then increased to reach the same level of radiation-induced apoptosis at 14 hours ($P=0.825$). The wild-type lymphocytes generally experienced higher levels of radiation-induced apoptosis at all time points with the exception of 14 hours, although these differences were only significant at 6 ($P=0.018$) and 8 hours ($P<0.001$) post-irradiation. The difference between the apoptotic responses of the two genotypes was greatest at 8 hours post-irradiation; the lymphocytes from wild-type mice were found to be 27% more radiation sensitive than the lymphocytes from heterozygous mice. The 8 hour time point was subsequently used in dose response

experiments. Spontaneous apoptosis levels (0 Gy) were subtracted from the apoptosis induced by doses of 0, 0.25, 0.5, 0.75 and 1 Gy to assess radiation-induced effects at 8 hours post-irradiation (Figure 2.2 C). Both wild-type and heterozygous lymphocytes showed a dose dependent increase in radiation-induced apoptosis ($P<0.001$). The relationship between genotype and radiation-induced apoptosis levels ($P<0.001$) was also significant with wild-type lymphocytes displaying consistently higher apoptosis levels for all doses other than 0 Gy ($P=0.624$).

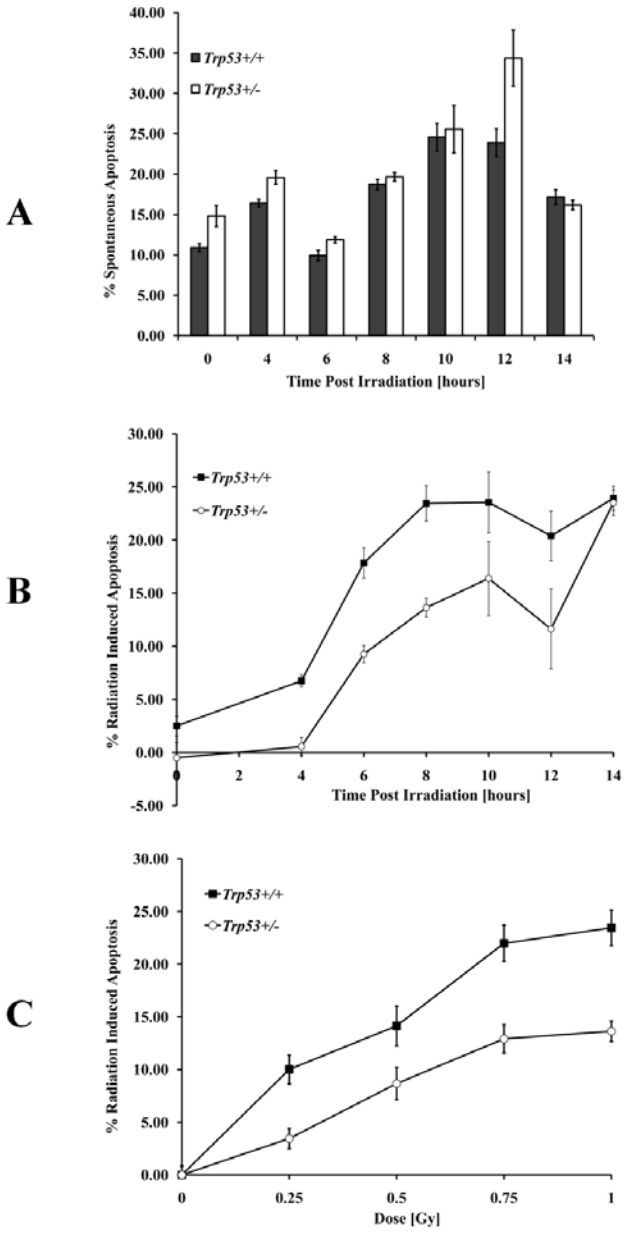

Figure 2.2 Apoptosis in the peripheral blood lymphocytes of wild-type *Trp53+/+* (closed squares) and heterozygous *Trp53+/- (open circles)* mice**. (A)** Spontaneous and (**B**) radiation-induced kinetics were evaluated at 0, 4, 6, 8, 10, 12 and 14 hours following 0 or 1 Gy (n=6-16). The radiation-induced values were obtained by subtracting spontaneous apoptosis (0 Gy) from total apoptosis (1 Gy) **(C)** The apoptotic dose response was evaluated at 8 hours following 0, 0.25, 0.5, 0.75 or 1 Gy (n=10-20). Only radiation-

induced apoptosis is displayed; spontaneous apoptosis (0 Gy) has been subtracted from total apoptosis. All data points shown represent mean ± standard error.

2.4.3. MN-RET

Experiments to assess differences in blood collection techniques on levels of spontaneous MN-RET formation showed no difference (Figure 2.3).

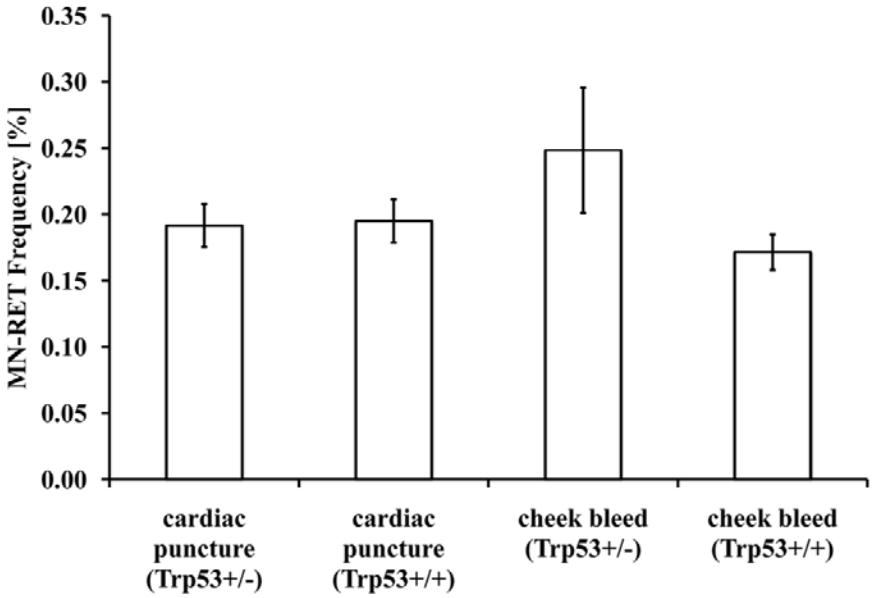

Figure 2.3 Spontaneous micronucleated reticulocyte frequency (MN-RET) in wild-type (*Trp53+/+*) and heterozygous (*Trp53+/-*) mice using 2 different blood collection techniques (n=3 in duplicate)). All data points shown represent mean ± standard error.

The spontaneous frequency of MN-RET in sham-irradiated mice did not vary with time (P=0.197) or genotype (P=0.823) throughout the sampling period (Figure 2.4 A).

Radiation-induced kinetics were determined by subtracting this spontaneous MN-RET frequency from that induced by a 1 Gy acute radiation exposure, for all time points

(Figure 2.4 B). Radiation-induced MN-RET levels varied with time (P<0.001). Both genotypes reached a peak level of MN-RETs at 43 hours post-irradiation, subsequently decreasing and returning to spontaneous levels by 137 hours post-irradiation. Genotype appeared to affect the kinetics of processing MN-RETs with *Trp53*+/- mice showing a slightly slower rate of MN-RET clearance which are typically at a maximum after 43 hours. This was particularly evident at 51 hours when there was a significant difference between the different mouse strains (P=0.052). *Trp53*+/+ and *Trp53*+/- responses however returned to the same level of MN-RET at 68 and 137 hours post-irradiation (P=0.375). The 43 hour time point was used in subsequent dose response experiments. *Trp53*+/+ and *Trp53*+/- mice were irradiated with 0, 0.1, 0.25, 0.75, 1 and 2 Gy *in vivo* and the spontaneous MN-RET frequency was subtracted to examine radiation-induced effects for each genotype (Figure 2.4 C). There was a dose dependent increase in the frequency of MN-RETs for both genotypes up to 0.75 Gy (P<0.001) above which dose there was no further increase in micronuclei indicating a saturation level for this endpoint. The lowest dose tested (0.1 Gy) showed a significant increase over spontaneous frequencies (P=0.012) for both groups of mice. Genotype did not affect the nature of the dose response curve as there was no difference in the frequency of MN-RETs between genotypes at any dose, including 0 Gy (P=0.520).

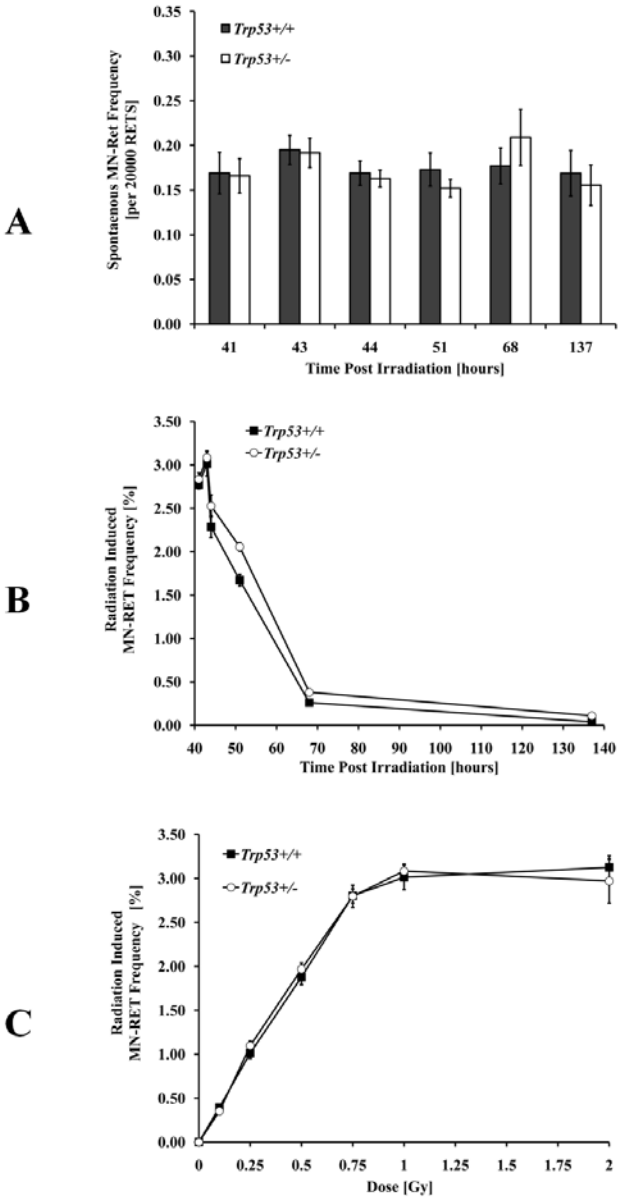

Figure 2.4 Micronucleated reticulocyte (MN-RET) frequency in wild-type *Trp53+/+* (closed squares) and heterozygous *Trp53+/-* (open circles) mice. **(A)** Spontaneous and (**B**) radiation-induced kinetics were evaluated at 41, 43, 44, 51, 68 and 137 hours post-irradiation (n=5 in duplicate)). The radiation-induced values were obtained by subtracting spontaneous MN-RETs (0 Gy) from total MN-RETs (1 Gy) **(C)** The MN-RET dose response was evaluated at 43 hours following 0, 0.1, 0.25, 0.5, 0.75, 1 or 2 Gy (n=3-6 in duplicate)). Only radiation-induced MN-RET levels are displayed; spontaneous MN-

RETs have been subtracted from total MN-RETs. All data points shown represent mean ± standard error.

2.5 Discussion

Discovered in 1979 [20], the *TP53* gene acts as a tumour suppressor by regulating many facets of the cellular stress response. Located on chromosome 17 in humans, it codes for a 53 kDa protein which acts as a transcriptional activator of genes responsible for maintaining the integrity of the organism. Early evidence for the critical role of p53 in tumour growth suppression came from analysis of human colon carcinoma, the majority of which contained mutant p53 alleles [21]. It was later discovered that the p53 gene is mutated in over 50% of human cancers [22]. Moreover, individuals with p53 germ line mutations are affected by Li-Fraumeni syndrome which is characterized by a high frequency and early onset of tumours, particularly sarcomas [23].

A p53 gene defect in mice of a C57BL6 x 129SVJ background has been shown to augment cancer risk by increasing the rate of tumorigenesis and consequently decreasing lifespan [1]. Moreover, exposure to high doses of radiation (1 - 4 Gy) has been shown to cause a further reduction in the latency period of cancer [1, 4], which is associated with an inability to effectively eliminate radiation-induced initiating events via p53 mediated pathways. In contrast, low doses of radiation (0.01-0.1 Gy) have been shown to increase the latency period for lymphoma in Trp53+/- mice [24].

In order to better define DNA repair processes and apoptosis in this p53 knockout mouse model, the acute response to low doses of radiation (0.1-2 Gy) were compared between heterozygous *Trp53+/-* and wild-type *Trp53+/+* mice.

Cells from the haematopoietic system were evaluated because of their radiosensitivity and because one of the primary cancer types observed in the *Trp53+/-* mouse model is haematopoietic in origin (lymphoma) [3, 4]. Lymphocytes are often chosen for cytogenetic studies because they are long-lived, radiosensitive, contain DNA and are easy to harvest from circulating blood. While lymphocytes were used to evaluate γH2A.X and apoptosis, erythrocytes were used for cytogenetic analyses. It has been shown that there is a close correlation between the induction of chromosomal aberrations in bone marrow and the production of micronuclei in erythrocytes [25, 26].

2.5.1 Spontaneous Differences between Trp53+/+ and Trp53+/- mice

Despite distinctly different rates of spontaneous tumour formation in *Trp53+/-* versus *Trp53+/+* mice, the spontaneous levels of γH2A.X, apoptosis, MN-RET were not significantly different in the hematopoietic cells of these mice at any of the time points examined. We conclude that any decrease in p53 function associated with *Trp53+/-* status may not have adversely impacted the cellular processes under normal conditions (sham-irradiated) in the tissues and endpoints studied here. Wild-type p53 has a very short half-life (5-20 minutes) and is maintained at very low intracellular levels [27, 28]. In contrast,

upon exposure to ionizing radiation, the half-life of p53, and therefore concentration, increases seven-fold [28]. Our findings are congruent with those of Merritt *et al*. [29] and Di Masi *et al.* [30] who found no difference in spontaneous apoptosis levels the tissues of mice of differing p53 gene status. Radiation exposure was required to potentiate the difference in the apoptotic response of mice with differing *Trp53* status. Moreover, Di Masi *et al.* studied protein levels in various tissues from *Trp53+/+* and *Trp53+/-* mice (spleen, colon, kidneys, lungs, liver). No significant differences existed in basal levels between the 2 strains but after whole body irradiation (7.5 Gy); the induction of p53 was much lower in heterozygous mice [30].

The baseline levels of apoptosis and γH2A.X were found to vary with time whereas the MN-RET values did not. The variation in baseline apoptotic levels could be attributed to *ex vivo* culture stress. These same conditions would not be expected to increase the baseline frequency of DNA DSBs (as measured by MN-RET and γH2A.X). This was the case for MN-RET but, unexpectedly, an elevation in γH2A.X foci was seen at 0 hrs post-irradiation relative to the other time points measured. It is possible that one of technical aspects of the assay (bone marrow collection) generated γH2A.X foci which were repaired at later time points. It has been shown that not all γH2A.X foci correspond to DSBs [11].

2.5.2 Radiation-induced differences in γH2A.X between Trp53+/+ and Trp53+/- mice

The initial recognition of DNA damage, as measured by mean γH2A.X fluorescence levels in bone marrow lymphocytes, responded to ionizing radiation in a dose dependent manner. No significant difference was detected between *Trp53+/+* and *Trp53+/-* cells as measured by the kinetics of over 120 minutes post-irradiation following 1 Gy. Similarly, there was no significant difference detected between *Trp53+/+* and *Trp53+/-* cells in the magnitude of the radiation response to 1 and 2 Gy at 30 minutes. Consistent with earlier reports, we found that cells exhibited maximum γH2A.X levels at 30 minutes post-irradiation for both strains of mice [31, 32]. The results between 0 and 30 minutes are reflective of damage recognition through foci formation. It has been demonstrated that there is a strong correlation between mean γH2A.X fluorescence detected via flow cytometry and foci formation as detected with microscopy. The fact that no difference was found between *Trp53+/+* and *Trp53+/-* lymphocytes supports the concept that p53 is activated downstream of γH2A.X foci formation in response to ionizing radiation [8, 9]. γH2A.X levels at the 60 and 120 minute time points will show the repair of lesions. Our expectation was that p53-deficient cells would show a slower elimination of γH2A.X foci due to impaired DSB repair. For example, Mirzayans *et al*. [33] showed that Li-Fraumeni fibroblast cell lines (heterozygous p53 function) exhibited a reduced rate of DSB joining (comet assay) and removal of γH2A.X foci relative to fibroblast cell lines expressing WT p53 following 8 Gy γ-rays. We found no significant difference in the rate of repair

between *Trp53+/+* and *Trp53+/-* bone marrow lymphocytes between 30 and 120 minute following 1 Gy of γ-rays. It is possible that differences in the repair of DSBs would manifest themselves beyond 120 minutes as γH2A.X levels remained significantly elevated beyond background at this time point in both genotypes. Alternatively, it is possible that the magnitude of the stress response induced by 1 Gy was inadequate to demonstrate the difference between the two genotypes.

2.5.3 Radiation-induced differences in apoptosis between Trp53+/+ and Trp53+/- mice

Apoptosis has been shown to be one of the key mechanisms by which radiation-induced DNA damage is processed and utilizes both p53-dependent and independent pathways [34]. It is the primary mode of death for peripheral blood lymphocytes. In this work, a dose response was observed for various doses between 0 and 1 Gy at 8 hours post-irradiation in the peripheral blood lymphocytes of *Trp53+/+* and *Trp53+/-* mice. In response to a 1 Gy challenge, wild-type lymphocytes generally experienced higher levels of apoptosis between 0 and 10 hours post-irradiation. These results confirm that peripheral blood lymphocytes undergo p53-mediated apoptosis in a dose dependent manner since p53-deficient cells showed a resistance to apoptosis. Similar findings have been demonstrated in the thymocytes, myeloid progenitor cells, splenic cells and intestinal cells [29, 34-36]. Moreover, if heterozygous peripheral blood lymphocytes are not undergoing p53-mediated apoptosis in response to ionizing radiation, it is possible that they are evading surveillance. This was shown in the thymocytes of p53-deficient

mice which were resistant to apoptosis but maintained higher levels of viability following irradiation relative to wild-type thymocytes [35]. In our work, radiation induced apoptosis in lymphocytes from both genotypes increased to reach the same level at 14 hours despite showing clear differences before that time point. As suggested by Brown and Wouters [37] examining later time points is crucial in not under- or over-estimating the impact of p53 function. The 14 hour time point suggests that the effect of reduced p53 levels in the lymphocytes is transient. To our knowledge, there are no reports that investigate the kinetics of radiation-induced apoptosis in the peripheral blood lymphocytes of p53-deficient mice.

2.5.4 Radiation-induced differences in MN-RET levels between Trp53+/+ and Trp53+/- mice

The frequency of micronuclei in the peripheral blood of mice provides a means by which to evaluate genomic instability in hematopoietic stem cells *in vivo*. The kinetics of MN-RET formation were evaluated following a 1 Gy acute dose between 41 and 137 hours post-irradiation in the same cohort of mice (n=5 per genotype) using a serial bleed technique. The radiation-induced MN-RET frequency reached a maximum at 43 hours post-irradiation and declined at 44, 51 and 68 hours, returning to spontaneous levels at 68 and 137 hours. This kinetics pattern is in agreement with previous findings [16]. Furthermore, no difference was observed in the MN-RET values between *Trp53+/+* and *Trp53+/-* mice at 41 or 43 hours, but *Trp53+/-* values remained elevated relative to

Trp53+/+ values at 44 and 51 hours. This indicates that p53 gene status affects the removal of radiation-induced chromosomal aberrations *in vivo*. Chang *et al.* [38] identified a similar trend in mice of differing p53 status following exposure to energetic iron particle radiation. Following 1 Gy (1 GeV/amu) irradiation *in vivo* (or sham irradiation), MN-RET% were measured at 3, 9, 38, 56 and 91 days in *Trp53*+/+, *Trp53*+/- *and Trp53*-/- mice. At 91 days post-irradiation, MN-RET% in irradiated *Trp53*-/- mice remained elevated whereas by 9 days, MN-RET% in irradiated *Trp53*+/+ and *Trp53*+/- mice had returned to control levels. It was hypothesized that the p53 deficiency altered the ability of DNA damage recognition or repair in the haematopoietic stem cell population which lead to increased MN-RET levels.

At 43 hours post-irradiation, both *Trp53*+/+ and *Trp53*+/- mice had an identical, dose dependent increase in MN-RET between 0 and 0.75 Gy (Figure 4C) but there was no difference between the levels of MN-RET at 0.75, 1 and 2 Gy. The presence of a saturation point for this assay is consistent with earlier reports [16, 39]. It has been suggested that a proportion of erythroblasts cannot withstand the damage induced by doses approaching 1 Gy of radiation and therefore undergo apoptosis before dividing and completing the maturation process [16]. Recently, it was shown that various categories of reticulocyte precursors in C57BL6 mice are eliminated in response to 1 Gy by undergoing apoptosis as measured by Annexin V without changes in steady state cell proliferation [40]. Based on this hypothesis, we would expect less erythroblasts to undergo apoptosis

in *Trp53+/-* mice following radiation exposure to 1 and 2 Gy, leading to a higher frequency of MN-RETs at 43 hours. However, we found no difference in the MN-RET frequency at 43 hours between *Trp53+/+* and *Trp53+/-* mice at any of the doses tested. This indicates that while apoptosis may be responsible for the removal of precursors, it proceeds by means of a p53 independent pathway. It has been shown previously that defective erythroblasts (folate-deficient) also undergo p53 independent apoptosis [41] however the relationship between those studies and ours in unclear. Nonetheless, damage to marrow precursor cells and subsequent manifestation of the damage as MN-RETs in circulating blood could be p53 independent.

However, it might also be possible that heterozygous mouse cells have sufficient p53 protein to regulate a response similar to wild-type mice. This result could indicate that the signalling mechanisms which trigger changes in MN-RET frequency are very sensitive and may be induced by very low levels of p53 activity. Prior studies have identified that the radiosensitivity of heterozygous cells represents an intermediate response between those of null and wild-type cells, although generally more similar to wild-type [42].

2.5.5 Linking short term radiation responses to increased tumorigenesis in Trp53+/- mice

There is considerable interest in linking short term biological indicators, such as chromosome damage, gene mutation, apoptosis, and DNA damage and repair, to

radiation-induced cancer risk in p53-deficient mice. The consensus is that p53 prevents the progression of initiating events [5, 43-45]. These events could be the result of unrepaired DNA damage induced by ionizing radiation, although many other exogenous and endogenous processes are also thought to influence genomic instability in *Trp53+/-* mice [46]. The inappropriate recombination of DSBs during V(D) J recombination, for example, is thought to increase the number of potential oncogenic lesions in maturing T-Cells in p53-deficient mice which is why they develop lymphoma earlier than wild-type mice [45] .

Many studies have used variations on the p53 knockout model to elucidate the connection between p53 deficiency and the process of carcinogenesis [43]. Schmitt *et al.* [44] showed that apoptosis is selected against during the development of lymphoma in Myc-transgenic p53+/- and p53+/+ mice. Another study [47] used wild-type and transgenic mice expressing *p53*193Pro or *p53*Vall35, which are mutant forms of normal p53 protein, to show that irradiated *p*53 transgenic mice and *p*53 null mice had twice the level of chromosome damage than did irradiated wild-type mice and suggested that this was a means by which tumorigenesis was enhanced.

Loss of heterozygosity (LOH) is another important factor governing the development of cancer in *Trp53+/-* mice. Since many human tumours exhibit loss of heterozygosity, it was assumed that this was a critical step in the cancer phenotype of *Trp53+/-* mice. The two hit theory proposes that individuals who possess only a single functional copy of a

tumour suppressor gene are more likely to progress to carcinogenesis because they already have one inactivated allele [48]. This theory assumes that inactivation of both alleles is required for carcinogenesis. Contrary to the two hit theory, Venkatachalam [49] showed that a reduction in p53 functional gene product was sufficient for the development of tumours in *Trp53*+/- mice. This conclusion was derived from analysis of tumours in which wild-type characteristics had been maintained by the one allele.

2.6 Conclusion

This research offers new insight into the relationship between p53 status and radiation-induced γH2A.X foci formation, apoptosis and MN-RET formation in various haematopoietic cell subtypes. The lack of difference in γH2A.X fluorescence between mouse strains indicates this process is independent of p53. *Trp53*+/- mice had less apoptosis per unit dose and therefore apoptosis is p53-dependent in the haematopoietic cells of these mice. Both strains had virtually identical responses for MN-RET formation. Therefore, DNA damage in reticulocyte precursors (erythroblasts in bone marrow) and the subsequent repair or removal of those cells was largely p53 independent, although small differences in kinetics were observed. This information contributes further to our understanding of the role of p53 in carcinogenesis since the role of p53 in radiation responses is highly variable between cell and tissue types [43, 50, 51]. The usefulness of

using short term biological endpoints, like those used in these experiments, to predict cancer risk remains unclear although lower levels of radiation-induced apoptosis discovered here correlates with higher cancer risk in *Trp53+/-* mice [4, 24] .

2.7 References

[1] T. Jacks et al., "Tumor spectrum analysis in p53-mutant mice.," *Current biology*, vol. 4, no. 1, pp. 1-7, Jan. 1994.

[2] S. M. Carlisle, P. A. Burchart, and R. E. J. Mitchel, "Cancer and non-cancer risks in normal and cancer-prone Trp53 heterozygous mice exposed to high-dose radiation.," *Radiation research*, vol. 173, no. 1, pp. 40-8, Jan. 2010.

[3] L. A. Donehower and G. Lozano, "20 Years Studying P53 Functions in Genetically Engineered Mice.," *Nature reviews. Cancer*, vol. 9, no. 11, pp. 831-41, Nov. 2009.

[4] C. Kemp, "p53-deficient mice are extremely susceptible to radiation induced tumorigenesis," *Nature Genetics*, vol. 8, pp. 66-69, 1994.

[5] P. Fei and W. S. El-Deiry, "P53 and radiation responses.," *Oncogene*, vol. 22, no. 37, pp. 5774-83, Sep. 2003.

[6] J. Momand, G. P. Zambetti, D. C. Olson, D. George, and a J. Levine, "The mdm-2 oncogene product forms a complex with the p53 protein and inhibits p53-mediated transactivation.," *Cell*, vol. 69, no. 7, pp. 1237-45, Jun. 1992.

[7] K. Rothkamm and S. Horn, "γ-H2AX as protein biomarker for radiation exposure," *Ann Ist Super Sanita*, vol. 45, no. 3, pp. 265-271, 2009.

[8] O. Fernandez-Capetillo, A. Lee, M. Nussenzweig, and A. Nussenzweig, "H2AX: the histone guardian of the genome.," *DNA repair*, vol. 3, no. 8-9, pp. 959-67, 2004.

[9] T. Stiff, "ATM and DNA-PK Function Redundantly to Phosphorylate H2AX after Exposure to Ionizing Radiation," *Cancer Research*, vol. 64, no. 7, pp. 2390-2396, Apr. 2004.

[10] K.-X. Shu, B. Li, and L.-X. Wu, "The p53 network: p53 and its downstream genes.," *Colloids and surfaces. B, Biointerfaces*, vol. 55, no. 1, pp. 10-8, Mar. 2007.

[11] W. M. Bonner et al., "γH2AX and cancer," vol. 8, no. DEcEMBER, 2008.

[12] C. E. Redon, J. S. Dickey, A. J. Nakamura, O. A. Martin, and W. M. Bonner, "Molecular Determinants of Radiation Response," *Response*, pp. 3-33, 2011.

[13] M. Van Engeland, L. J. Nieland, F. C. Ramaekers, B. Schutte, and C. P. Reutelingsperger, "Annexin V-affinity assay: a review on an apoptosis detection system based on phosphatidylserine exposure.," *Cytometry*, vol. 31, no. 1, pp. 1-9, Jan. 1998.

[14] J. S. Fridman and S. W. Lowe, "Control of apoptosis by p53.," *Oncogene*, vol. 22, no. 56, pp. 9030-40, Dec. 2003.

[15] N. Kunugita, H. Kakihara, T. Kawamoto, and T. Norimura, "Micronuclei induced by low dose-rate irradiation in early spermatids of p53 null and wild mice.," *Journal of radiation research*, vol. 43, pp. S205-7, Dec. 2002.

[16] S. D. Dertinger et al., "Reticulocyte and micronucleated reticulocyte responses to gamma irradiation: dose-response and time-course profiles measured by flow cytometry.," *Mutation research*, vol. 634, no. 1-2, pp. 119-25, Dec. 2007.

[17] G. Liu et al., "Chromosome stability, in the absence of apoptosis, is critical for suppression of tumorigenesis in Trp53 mutant mice.," *Nature genetics*, vol. 36, no. 1, pp. 63-8, Jan. 2004.

[18] H. Symonds et al., "p53-Dependent Apoptosis and Progression In Vivo Suppresses Tumor Growth," *Cell*, vol. 76, pp. 703-711, 1994.

[19] S. D. Dertinger, D. K. Torous, and K. R. Tometsko, "Simple and reliable enumeration of micronucleated reticulocytes with a single-laser flow cytometer.," *Mutation research*, vol. 371, no. 3-4, pp. 283-92, Dec. 1996.

[20] D. Lane and L. Crawford, "T antigen is bound to a host protein in SY40-transformed cells," *Nature*, vol. 278, p. 261, 1979.

[21] S. J. Baker, S. Markowitz, E. R. Fearon, J. K. Willson, and B. Vogelstein, "Suppression of human colorectal carcinoma cell growth by wild-type p53.," *Science*, vol. 249, no. 4971, pp. 912-5, Aug. 1990.

[22] M. Hollstein, D. Sidransky, B. Vogelstein, and C. C. Harris, "p53 mutations in human cancers," *Science*, vol. 253, no. 5015, p. 49, 1991.

[23] D. Malkin, “Li-Fraumeni Syndrome,” in *Adrenocortical Carcinoma*, G. D. Hammer and T. Else, Eds. New York, NY: Springer New York, 2011, pp. 173-191.

[24] R. E. J. Mitchel, J. S. Jackson, D. P. Morrison, and S. M. Carlisle, “Low doses of radiation increase the latency of spontaneous lymphomas and spinal osteosarcomas in cancer-prone, radiation-sensitive Trp53 heterozygous mice.,” *Radiation research*, vol. 159, no. 3, pp. 320-7, Mar. 2003.

[25] M. Shelby and K. Witt, “Comparison of results from mouse bone marrow chromosome aberration and micronucleus tests,” *Environmental and molecular mutagenesis*, vol. 25, no. 4, pp. 302–313, 1995.

[26] M. Hayashi, T. Sofuni, and M. Ishidate, “Kinetics of micronucleus formation in relation to chromosomal aberrations in mouse bone marrow.,” *Mutation research*, vol. 127, no. 2, pp. 129-37, Jul. 1984.

[27] M. V. Blagosklonny, “Loss of function and p53 protein stabilization.,” *Oncogene*, vol. 15, no. 16, pp. 1889-93, Oct. 1997.

[28] A. J. Giaccia and M. B. Kastan, “The complexity of p53 modulation: emerging patterns from divergent signals,” *Genes & Development*, vol. 12, no. 19, pp. 2973-2983, Oct. 1998.

[29] A. J. Merritt et al., “The role of p53 in spontaneous and radiation-induced apoptosis in the gastrointestinal tract of normal and p53-deficient mice.,” *Cancer research*, vol. 54, no. 3, pp. 614-7, Feb. 1994.

[30] A. Di Masi et al., “Gene expression and apoptosis induction in p53-heterozygous irradiated mice.,” *Mutation research*, vol. 594, no. 1-2, pp. 49-62, Feb. 2006.

[31] S. H. Macphail, J. P. BanÁth, T. Y. Yu, E. H. M. Chu, H. Lambur, and P. L. Olive, “Expression of phosphorylated histone H2AX in cultured cell lines following exposure to X-rays,” *International Journal of Radiation Biology*, vol. 79, no. 5, pp. 351-359, Jan. 2003.

[32] E. P. Rogakou, D. R. Pilch, A. H. Orr, V. S. Ivanova, and W. M. Bonner, “DNA double-stranded breaks induce histone H2AX phosphorylation on serine 139.,” *The Journal of biological chemistry*, vol. 273, no. 10, pp. 5858-68, Mar. 1998.

[33] R. Mirzayans, D. Severin, and D. Murray, “Relationship between DNA double-strand break rejoining and cell survival after exposure to ionizing radiation in

human fibroblast strains with differing ATM/p53 status: Implications for evaluation of clinical radiosensitivity," *International Journal of Radiation Oncology• Biology• Physics*, vol. 66, no. 5, pp. 1498–1505, 2006.

[34] A. Clarke et al., "Thymocyte apoptosis induced by p53-dependent and independent pathways," *Nature*, vol. 362, no. 6423, pp. 849–852, 1993.

[35] S. W. Lowe, E. M. Schmitt, S. W. Smith, B. A. Osborne, and T. Jacks, "p53 is required for radiation-induced apoptosis in mouse thymocytes," *Nature*, vol. 362, no. 6423, pp. 847–849, 1993.

[36] K. Fujikawa, Y. Hasegawa, S. Matsuzawa, A. Fukunaga, T. Itoh, and S. Kondo, "Dose and dose-rate effects of X rays and fission neutrons on lymphocyte apoptosis in p53(+/+) and p53(-/-) mice.," *Journal of radiation research*, vol. 41, no. 2, pp. 113-27, Jun. 2000.

[37] J. M. Brown and B. G. Wouters, "Apoptosis, p53, and tumor cell sensitivity to anticancer agents.," *Cancer research*, vol. 59, no. 7, pp. 1391-9, Apr. 1999.

[38] P. Y. Chang, D. Torous, L. Lutze-Mann, and R. Winegar, "Impact of p53 status on heavy-ion radiation-induced micronuclei in circulating erythrocytes.," *Mutation research*, vol. 466, no. 1, pp. 87-96, Mar. 2000.

[39] S. D. Dertinger et al., "Reticulocyte and micronucleated reticulocyte responses to gamma irradiation: effect of age.," *Mutation research*, vol. 675, no. 1-2, pp. 77-80, Apr. 2009.

[40] S. A. Peslak et al., "Sublethal radiation injury uncovers a functional transition during erythroid maturation," *Experimental Hematology*, vol. 39, pp. 434-445, 2011.

[41] M. J. Koury, J. O. Price, and G. G. Hicks, "Apoptosis in megaloblastic anemia occurs during DNA synthesis by a p53-independent, nucleoside-reversible mechanism.," *Blood*, vol. 96, no. 9, pp. 3249-55, Nov. 2000.

[42] X. Wang et al., "p53 accumulation in the organs of low-dose X-ray-irradiated mice," *Cancer letters*, vol. 104, no. 1, pp. 79–84, 1996.

[43] D. Kenzelmann Broz and L. D. Attardi, "In vivo analysis of p53 tumor suppressor function using genetically engineered mouse models.," *Carcinogenesis*, vol. 31, no. 8, pp. 1311-8, Aug. 2010.

[44] C. A. Schmitt, J. S. Fridman, M. Yang, E. Baranov, R. M. Hoffman, and S. W. Lowe, "Dissecting p53 tumor suppressor functions in vivo.," *Cancer cell*, vol. 1, no. 3, pp. 289-98, Apr. 2002.

[45] L. D. Attardi, "The role of p53-mediated apoptosis as a crucial anti-tumor response to genomic instability: lessons from mouse models.," *Mutation research*, vol. 569, no. 1-2, pp. 145-57, Jan. 2005.

[46] L. D. Attardi and T. Jacks, "The role of p53 in tumour suppression: lessons from mouse models.," *Cellular and molecular life sciences : CMLS*, vol. 55, no. 1, pp. 48-63, Jan. 1999.

[47] J. Lee, J. Abrahamson, R. Kandel, L. Donehower, and A. Bernstein, "Susceptibility to radiation-carcinogenesis and accumulation of chromosomal breakage in p53-deficient mice," *Oncogene*, vol. 9, pp. 3731-3736, 1994.

[48] A. G. Knudson, H. W. Hethcote, and B. W. Brown, "Mutation and childhood cancer: a probabilistic model for the incidence of retinoblastoma.," *Proceedings of the National Academy of Sciences of the United States of America*, vol. 72, no. 12, pp. 5116-20, Dec. 1975.

[49] S. Venkatachalam et al., "Retention of wild-type p53 in tumors from p53 heterozygous mice: reduction of p53 dosage can promote cancer formation.," *The EMBO journal*, vol. 17, no. 16, pp. 4657-67, Aug. 1998.

[50] E. A. Komarova, K. Christov, A. I. Faerman, and A. V. Gudkov, "Different impact of p53 and p21 on the radiation response of mouse tissues.," *Oncogene*, vol. 19, no. 33, pp. 3791-8, Aug. 2000.

[51] P. J. Coates, S. A. Lorimore, K. J. Lindsay, and E. G. Wright, "Tissue-specific p53 responses to ionizing radiation and their genetic modification: the key to tissue-specific tumour susceptibility?," *The Journal of pathology*, vol. 201, no. 3, pp. 377-88, Nov. 2003.

Chapter 3

PET scans with ^{18}F-FDG cause radiation induced biological changes in mice

3.1 Abstract

The specific aim of this study was to assess the effects of ^{18}F-FDG exposure in the bone marrow of mice. The induction and repair of DNA damage and the relative biological effectiveness (RBE) of radiation from ^{18}F-FDG relative to 662 keV γ-rays were investigated. The study also tested whether low dose radiation exposure from ^{18}F-FDG induced an adaptive response in bone marrow cells. 7-9 week old wild-type female mice (B6.129S2 x 129X1/SvJ) were used in these experiments. DNA damage to the bone marrow erythroblast population was measured using micronucleus formation (MN-RET). DNA damage to the bone marrow lymphocyte population was measured by assessing the levels of γH2A.X fluorescence. To test the RBE of ^{18}F-FDG (β+, E_{max}=634 keV and γ-rays, 511 keV), mice were injected with various activities of ^{18}F-FDG (0-14.80 MBq) or irradiated with Cs-137 γ-rays (0-100mGy, 662 keV). The adaptive response was investigated 24 hours after the ^{18}F-FDG injection by irradiating mice with 1 Gy challenges doses for MN-RET formation or 1, 2, 4 Gy *in vitro* challenges doses for γH2A.X formation. A significant increase in MN-RET formation above controls occurred following injection activities of 3.70, 7.40 or 14.80 MBq ($P<0.001$) which correspond to bone marrow doses of ≈ 35 mGy, 75 mGy, and 150 mGy, respectively. Per unit dose, the Cs-137 radiation exposure caused significantly more damage than the ^{18}F-FDG injections (RBE=0.79±0.04). A 20% reduction in γH2A.X fluorescence was observed in mice injected with 14.80 MBq relative to controls at 24 hours ($P=0.019$).^{18}F-FDG injection

activities (0.74 MBq) that caused doses in mice which would be similar to human exposure during clinical PET scans did not cause a significant increase in DNA damage nor did they generate an adaptive response. Typical ^{18}F-FDG injection activities used in small animal imaging (14.80 MBq) caused a decrease in DNA damage, as measured by γH2A.X formation, below spontaneous levels observed in control mice. The RBE of ^{18}F-FDG was less than 1.0 indicating that the mixed radiation quality and/or low dose-rate from PET scans is less damaging than equivalent doses of gamma radiation.

3.2 Introduction

The use of diagnostic imaging in health care has seen a dramatic increase over the last two decades. In the US, nuclear medicine procedures have grown from 7.5 million in 1982 to 19.6 million in 2005 [1]. Positron Emission Tomography (PET) is expected to continue to increase because it offers unprecedented sensitivity for the detection of biological processes [2]. Clinically, the most commonly used PET radiotracer is the glucose analog 2-[^{18}F] fluoro-2-deoxy-D-glucose (^{18}F-FDG). PET scans with ^{18}F-FDG are used to image disease states characterized by alterations in metabolism: epilepsy [3], Alzheimer's [4], infection [5], heart disease [6, 7] but most often, malignancy [8, 9]. ^{18}F-FDG is transported into the cytoplasm of metabolically active cells by glucose transport membrane proteins (GLUT) and undergoes phosphorylation to form ^{18}F-FDG-6-

phosphate by hexokinase [10]. At this point, ^{18}F-FDG becomes trapped in the cell because of the substitution at the hydroxyl group [11]. The absorbed radiation dose in a tissue depends on the glucose requirements of that tissue. The radiation exposure is a result of positrons (β+, E_{max}= 634 keV) emitted by ^{18}F-FDG and subsequent annihilation photons (γ-rays, 511 keV). During a typical clinical protocol involving the administration of 350-750 MBq ^{18}F-FDG [12], most tissues will be irradiated throughout the patient's body (*4-9 mGy*). However, in organs with high energy requirements doses can be much higher, such as the brain (*10-36 mGy*) and heart (*16-51 mGy*) or organs within the excretory system such as the kidneys (*7-23 mGy*) or bladder (*13-233mGy*) through which the radiopharmaceutical is voided [13-17]. Dose is delivered at a low decaying dose-rate reflective of the physical (109.7 minutes) and biological half-life of ^{18}F-FDG. The biological half-life depends on the residence times of the radiopharmaceutical in different parts of the body. The MIRD Dose Estimate Report for ^{18}F-FDG provides a whole body residence time of 2.38 ± 0.12 hours [15]. It is important to note that regardless of the site being imaged, an injection of the radiopharmaceutical ^{18}F-FDG will result in uptake, and therefore radiation exposure, throughout the entire body [18]. It has been reported that, when compared to all other nuclear medicine procedures, PET scans with ^{18}F-FDG deliver one of the highest effective doses to patients (14.1 mSv) [18]. The effective dose is a value which allows the summation of dose contributions from radionuclides non-uniformly distributed throughout the body to evaluate the associated stochastic effects (cancer & hereditary) relative to other radiation exposures. It requires a calculation using

radiation weighting factors (w_R) and tissue weighting factors (w_T) published by the International Commission on Radiological Protection (ICRP) [19].

The increase in nuclear medicine procedures has stimulated interest in whether a rise in radiation-induced cancers should be expected. Certain studies, utilizing the linear no threshold (LNT) model of risk estimation, assert that PET scans will result in a measurable increase in the lifetime risk of cancer among patients [20]. These types of studies use dose as a surrogate for risk. While accurate dosimetry in nuclear medicine is important, it should only be used as a starting point in evaluating the possible health effects associated with nuclear medicine procedures.

Nuclear medicine examinations involve protracted dose-rates which have been shown to significantly reduce the biological risk associated with a given dose of ionizing radiation [21-24]. In fact, many studies have shown that low dose-rate exposures may be protective to an organism by generating an adaptive response. For example, a number of experiments using cell lines have shown that low dose-rate radiation exposures reduced the level of transformation or damage below that of controls [25-27]. In addition, both low dose [28, 29] and lose dose-rate [26, 30, 31] exposures have been shown to reduce the full detriment of a subsequent high dose radiation exposure. In contrast, there are certain elements of nuclear medicine procedures that may augment the associated risk. Certain groups have identified that decaying dose-rates generate more damage than fixed

low dose-rates [32] or that damage delivered at a low dose-rate (9.4 cGy/hr) evades DNA damage surveillance mechanisms [33].

Current investigations into medical isotope health effects have been focused almost exclusively on radioiodine (I-131, I-125) [34-38]. There are few investigations that address the possible health effects of radiation exposure from newer imaging agents [39] and none that are focused on PET imaging. Moreover, many radiobiological investigations into the characteristics associated with nuclear medicine procedures (low dose-rates, changing dose-rates) have been investigated in cell lines.

In this study, the response to ^{18}F-FDG was investigated in mice to gain a better understanding of the *in vivo* radiation induced health effects associated with PET scans. Inbred mice were chosen as the model system to eliminate the high degree of inter-individual variability observed in patient studies [35, 40]. DNA double-strand breaks (DSBs) following ^{18}F-FDG injections were measured by γH2A.X fluorescence at 24 hours post-injection and micronucleated reticulocyte (MN-RET) formation at 43 hours post-injection. Additionally, the potential of this injection to induce an adaptive response was evaluated using these same endpoints by irradiating mice or cells at 24 hours post-injection with high doses of radiation (1, 2, 4 Gy). We hypothesize that the low dose-rate associated with PET scans employing ^{18}F-FDG reduces the detrimental effects of the radiation exposure and that this exposure may have the capacity to generate an adaptive response.

3.3 Materials and Methods

3.3.1 Mice

In these experiments, 7-9 week old wild type female mice (B6.129S2-Trp53$^{tm1Tyj/1}$x 129X1/SvJ, Jackson Laboratory; Bar Harbor, Maine) were used. Mice were housed five per cage in specific pathogen free (SPF) conditions. The housing room was maintained on a 12 hour light/dark cycle at a temperature of 24 ± 1°C. Protocols were approved by the Animal Research Ethics Board (AREB) at McMaster University and carried out as per the Canadian Council on Animal Care (CCAC).

3.3.2 ^{18}F-FDG

Mice were injected with ^{18}F-FDG prepared at Hamilton Health Sciences (Hamilton, Ontario).

The ^{18}F was produced by ^{18}O(*p*,n)^{18}F reaction using a Siemens RDS112 11MeV Proton-Cyclotron and the FDG was prepared as per the procedure listed in [41], meeting all USP and Health Canada regulatory requirements.

3.3.3 ^{18}F-FDG Injections

All mice were fasted overnight prior to the isotope injection (12-14 hours) and water was available *ad libitum.* Mice were housed individually for the duration of the experiment to minimize inter-mouse irradiation following the isotope injection.

Individual isotope doses were calibrated using a CRC-12 radioisotope calibrator (Capintec). Bi-weekly quality control (voltage, zero, background, stability) was performed on this system using Cs-137 and Co-60 check sources. The pre-and post-injection activity of the syringe in addition to the time of each measurement was recorded. This information was used to accurately calculate the activity administered to each individual mouse by correcting for decay. The weight of each mouse was also recorded prior to the injection. The average weight of mice used in these experiments was 20 ± 0.08 g. The ^{18}F-FDG was diluted into a total volume of 200 µl with saline and administered by tail vein injection (30g needle, 1 cc syringe). Control mice were injected with 200 µl saline only. Mice were immobilized using a restraint device designed for mouse tail vein injections (Tailveiner® TV-150, Braintree Scientific Inc., MA). Anaesthesia was not used since image acquisition was not the objective of this work and may interfere with the radiation biology under investigation. Food was returned to the mice 2 hours after the injection to maximize uptake of the ^{18}F-FDG and to simulate the conditions of a typical PET procedure.

3.3.4 Calculation of absorbed doses from ^{18}F-FDG

Previously published absorbed dose estimates for ^{18}F-FDG in mice [42, 43] were used to convert the injected activities used into whole body doses and bone marrow doses (Table 3.1). The whole body dose estimates using both approaches are in good agreement. Small samples of mice were imaged at 7-8 weeks of age to verify the distribution of ^{18}F-FDG in the mouse model (Figure 3.1).

3.3.5 Biological Experiments

Two flow cytometry based assays were used to evaluate the biological effects of ^{18}F-FDG injections in mice: micronucleated reticulocyte (MN-RET) formation and γH2A.X mean fluorescence. These assays were performed exactly as described in detail previously [44]. All samples were kept in ice slurry (0 ^{o}C) during preparation and analyzed using a Beckman Coulter EPICS XL flow cytometer.

An experiment was first performed to evaluate the kinetics of MN-RET formation induced by a single injection of ^{18}F-FDG. Mice were injected with saline (n=1-3 in duplicate per time point) or ≈ 18.5 MBq ^{18}F-FDG (n=3 in duplicate per time point). Blood samples were collected at various times post injection (30, 43, 47, 51, 72 hours). In each sample, the percentage of MN-RETs within a population of 20,000 reticulocytes (RET) was determined.

For the activity response experiments, mice were injected with various activities of ^{18}F-FDG (0, 0.74, 1.48, 3.70, 7.40 or 14.80 MBq) and the MN-RET frequency was evaluated at 43 hours post-injection in a blood sample obtained from each mouse in duplicate. In each sample, the percentage of MN-RETs within a population of 20,000 reticulocytes (RET) was determined.

In order to compare the effectiveness of the radiation exposure from PET scans employing ^{18}F-FDG to that of a reference dose of radiation (662 keV γ-rays), the bone marrow dose was determined for the injection activities listed in Table 1 using conversion values determined by Taschereau *et al*. [43] . The gamma-irradiated mice received acute doses of 0 (n=3), 10 (n=5), 20 (n=5), 50(n=5), 100 mGy (n= 5) at a dose-rate of 0.018 Gy/minute. Gamma doses were delivered using a Cs-137 source (662 keV γ-rays) at the McMaster Taylor Radiobiology Source Facility and mice were placed in a customized sectioned polycarbonate restraint tube for the γ-ray irradiation. These doses were corrected for attenuation through the mouse to the site of bone marrow using previously determined experimental values from our laboratory [45].

For the *in vivo* adaptive response experiments, mice were injected with 0, 0.74, 1.48 or 3.70 MBq of ^{18}F-FDG (n=9-11, duplicate samples) and irradiated with 1 Gy whole body (662 keV γ-rays, 0.35 Gy/minute) 24 hours post-injection. The micronucleated reticulocyte (MN-RET) frequency was evaluated 43 hours after the 1 Gy dose.

For the *in vitro* adaptive response experiments, mice were injected with 0, 0.74, 1.48 or 3.70 MBq of ^{18}F-FDG (n=6-10, duplicate samples). The bone marrow was extracted at 24 hours post-injection and irradiated with 0, 1, 2 or 4 Gy in vitro (662 keV γ-rays, 0.19 Gy/minute, 0°C). Bone marrow cultures (1 x 10^6 cells/mL) were fixed with 70% EtOH 30 minutes after irradiation. Mean γH2A.X fluorescence was measured within 5000 bone marrow cells (lymphocyte rich) using flow cytometry. Only G0/G1 cells were analyzed for mean γH2A.X fluorescence.

3.3.6 Statistics

Statistical analysis of the biological data was performed using Sigma Plot version 11.0 (Systat Software, Germany). Data points represent the mean ± the standard error of the mean (SEM). Two sided P values ≤ 0.05 were considered statistically significant. One-way ANOVA was performed on ranks (Kruskal-Wallis). Two-way ANOVA with Bonferroni was also used. T-tests, when appropriate, were performed to examine differences between 2 groups in particular. Dose response curves were analyzed using linear regression analysis and multiple linear regression analysis was used for comparisons.

3.4 Results

3.4.1 Validation of Isotope Distribution

The pattern of uptake is consistent with the predicted distribution of absorbed doses from [42] listed in Table 3.1. A representative image is provided in Figure 3.1. The image shows that the isotope preferentially accumulated in certain organs and consequently increases the absorbed dose to that organ relative to the whole body average.

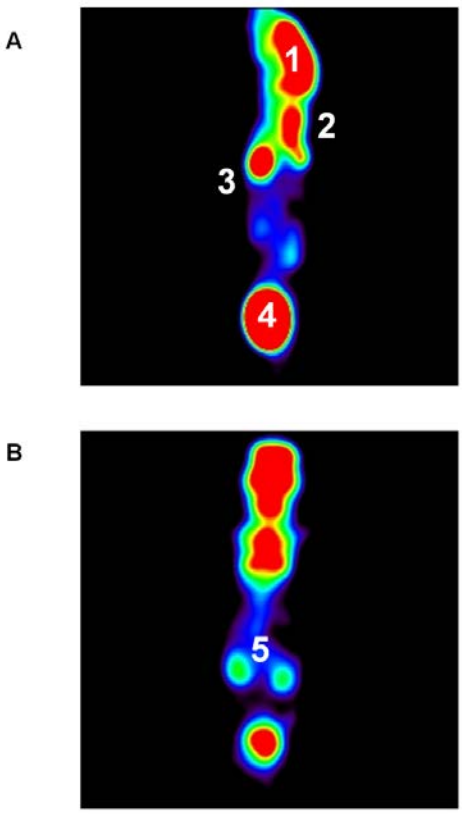

Figure 3.1 Representative PET scan of an 8 week old female healthy wild-type mouse from this study acquired with a Philips MOSIAC animal PET scanner at the McMaster Center for Pre-Clinical and Translational Imaging. Mouse (fasted) was injected with 18.5 MBq ^{18}F-FDG. Static scan (15 minutes in duration) was acquired 45 minutes post-injection. (A) Coronal view: increased ^{18}F-FDG uptake in the bladder(4), heart(3), brain(1) and active skeletal muscle/brown fat(2) is evident (B) Sagittal view: reveals ^{18}F-FDG uptake in kidneys(5). The pattern of uptake is generally consistent with the predicted distribution of absorbed doses.

Table 3.1 Injection activities & corresponding doses for 20 g mice injected with ^{18}F-FDG

n	Nominal Activity	Activity Injected	WB Dose*	WB Dose†	BM Dose‡
8	14.80 (400)	15.03 ± 0.41	210.44 ± 5.77	236.80 ± 6.49	150.32 ± 4.12
10	7.40 (200)	7.43 ± 0.15	104.02 ± 2.33	117.05 ± 2.40	74.30 ± 1.59
9	3.70 (100)	3.59 ± 0.06	50.25 ± 0.86	56.55 ± 0.97	35.89 ± 0.62
10	1.48 (40)	1.42 ± 0.04	19.88 ± 0.56	22.37 ± 0.64	14.20 ± 0.40
10	0.74 (20)	0.66 ± 0.03	9.21 ± 0.41	10.36 ± 0.47	6.58 ± 0.30
10	0.00 (0)	0.00 ± 0.00	0.00 ± 0.00	0.00 ± 0.00	0.00 ± 0.00

Data are expressed mean ± SEM.
Activities are expressed in MBq (μCi). Absorbed dose estimates are expressed in mGy.
n = number of mice per group, WB= whole body, BM = bone marrow
* Obtained using absorbed dose values (14 mGy/MBq) from Taschereau *et al*. [43]
† Obtained using an approximate dose calculation and S value (22.1×10^{-13} Gy/Bq s) from Funk *et al*. [42]
‡ Obtained using the absorbed dose in marrow (10 mGy/MBq) from Taschereau *et al*. [43]

3.4.2 Kinetics of MN-RET formation following an ^{18}F-FDG injection

Emphasis was placed on time points after 43 hours as it was suspected that the protracted exposure associated with the isotope may lead to a persistent elevation in MN-RET levels. The injection caused a significant increase in MN-RETS relative to controls ($P<0.001$) (Figure 2). The level of MN-RETS in the saline injected mice (controls) did not appear to vary with time. Following the injection, the maximum level of MN-RETs occurred at 43 hours and subsequently decreased to control levels by 72 hours post-injection. The level of MN-RETS at 43 hours was not significantly different from that at 47 hours ($P= 1.000$) but decreased significantly at 49 hours ($P<0.001$) (Figure 3.2). At 72

hours, the average level of MN-RETS in the ^{18}F-FDG injected mice (0.19 ± 0.01) decreased below control levels (0.22 ± 0.05) although this decrease was not found to be significant (P=0.600). The 43 hour time point was subsequently used to further characterize the *in vivo* response to ^{18}F-FDG in mice.

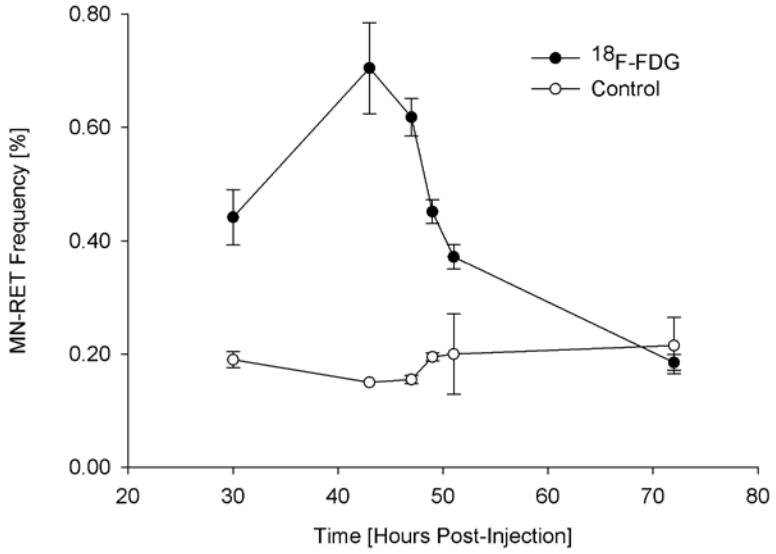

Figure 3.2 Kinetics *In vivo* formation of micronucleated reticulocytes (MN-RET) following injection with 18.5 MBq ^{18}F-FDG (n=3, duplicate samples) or saline (n=1-3, duplicate samples). Blood samples were collected at 30, 43, 47, 51, 72 hours post-injection. Results displayed are mean ± SEM.

3.4.3 ^{18}F-FDG Dose Response (MN-RET)

The induction of micronuclei in bone marrow by ^{18}F-FDG was found to vary linearly with the activity injected (R^2=0.9933) (see Figure 3.3). Specifically, all injection activities caused an increase in micronuclei relative to controls although this increase was only significant following injections of 3.70, 7.40 and 14.80 MBq (P<0.001). These injection activities corresponded to bone marrow doses of 35.89 ± 0.62, 74.30 ± 1.59 and 150.32 ± 4.12 mGy, respectively (Table 3.1).

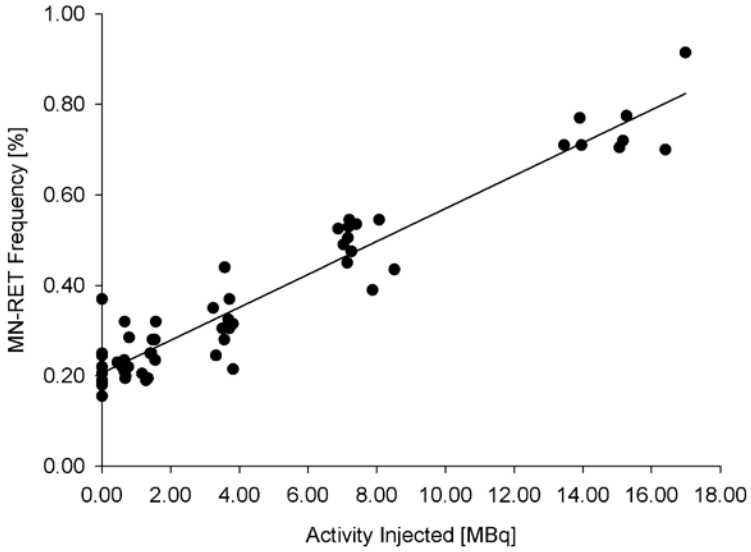

Figure 3.3 Activity- Response Curve *In vivo* formation of micronucleated reticulocytes (MN-RET) following injection with 0, 0.74, 1.48, 3.70, 7.40 or 14.80 MBq ^{18}F-FDG (n=8-10, duplicate samples). Each point (x,y) represents 1 mouse (duplicates averaged) with corresponding injected activity.

3.4.4 Relative Biological Effectiveness (RBE) of ^{18}F-FDG measured (MN-RET)

The dose curves are compared in Figure 3.4. The gamma dose response was also found to be linear (R^2=0.9933). Multiple linear regression analysis determined that the type of radiation exposure (^{18}F-FDG or 662 keV γ-rays) was a significant determinant of the MN-RET dose response (P=0.004) with 662 keV γ-rays generating significantly more damage per unit dose. The RBE for ^{18}F-FDG was calculated by taking the ratio of the linear regression coefficients from the 2 dose response curves (^{18}F-FDG: 662 keV γ-rays). Using this approach, the RBE for ^{18}F-FDG was determined to be 0.79 ± 0.04.

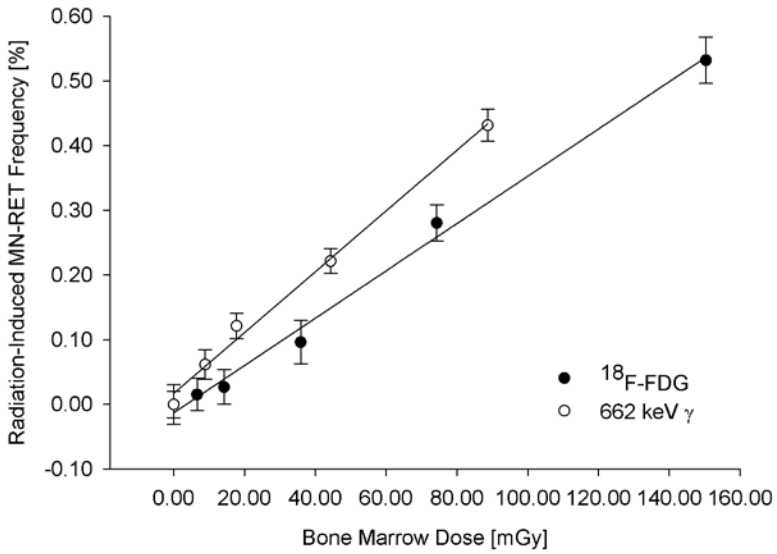

Figure 3.4 Relative Biological Effectiveness Comparison of the micronucleated reticulocyte (MN-RET) frequency per unit dose between ^{18}F-FDG (internal) and 662 keV γ-rays (external). For the ^{18}F-FDG curve, mice were injected with 0, 0.74, 1.48, 3.70, 7.40 or 14.80 MBq ^{18}F-FDG (n=8-10, duplicate samples) and converted to bone marrow doses. For the 662 keV γ-rays, mice were irradiated whole body with 0, 10, 20, 50 or 100 mGy (n=3-5, duplicate samples) at a dose rate of 18 mGy/minute which were also

converted to bone marrow doses using an attenuation factor. Radiation-induced values are displayed; the background level of MN-RET was subtracted from the MN-RET value for each dose point. Results displayed are mean ± SEM.

3.4.5 In vivo induction of an adaptive response by ^{18}F-FDG injections (MN-RET)

Four independent experiments were performed and pooled to examine whether injections of 0(0), 0.74(20), 3.70(100) or 14.80 (400) MBq (μCi) could modify the effect of subsequent 1 Gy (662 keV γ-rays) challenge dose *in vivo*. The time between the injection and the challenge was 24 hours. The PET injection did not significantly increase or decrease the effect of the 1 Gy challenge dose *in vivo* as measured by the MN-RET assay ($P = 0.959$) (Figure 3.5).

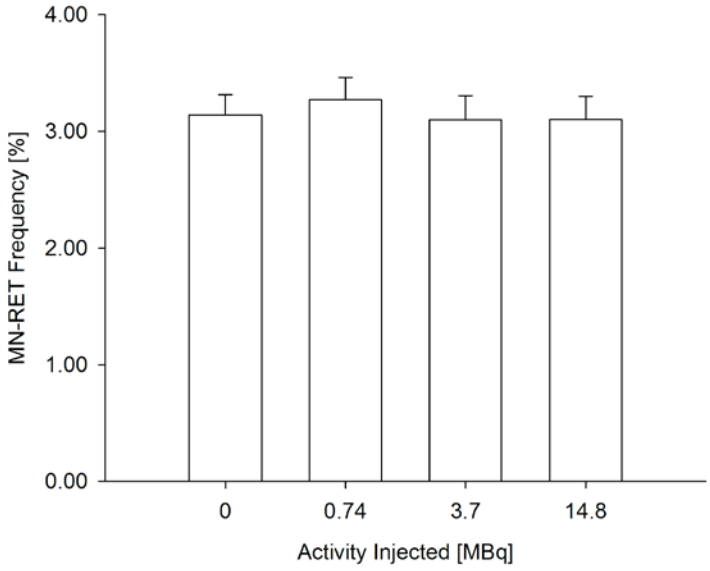

Figure 3.5 *In Vivo* Adaptive Response Mice were injected with 0, 0.74, 1.48 or 3.70 MBq of ^{18}F-FDG (n=9-11, duplicate samples) and irradiated 24 hours post-injection with 1 Gy whole body (662 keV γ-rays, 0.35 Gy/minute). The micronucleated reticulocyte (MN-RET) frequency was evaluated 43 hours after the 1 Gy dose. Results displayed are mean ± SEM.

3.4.6 In vitro induction of an adaptive response by ^{18}F-FDG injections (γH2A.X)

The lower limit of detection of the flow cytometry based γH2A.X assay is 100 mGy for acute radiation exposures [46], consequently, this assay would consequently not be useful in measuring the direct effects of low dose ^{18}F-FDG injections. It was used instead to measure the potential modification of an acute radiation exposure by ^{18}F-FDG (adaptive response). Mice were injected with 0(0), 0.74(20), 3.70(100) or 14.80 (400) MBq (μCi). At 24 hours post injection, bone marrow lymphocytes from these mice were extracted and

irradiated in culture with 0, 1, 2 or 4 Gy (662 keV γ-rays). The mean γH2A.X fluorescence in the lymphocyte rich population was measured 30 minutes after the challenge irradiation as this has been shown previously to be the optimal time for measurement [44].

The level of γH2A.X increased significantly with the magnitude of the challenge dose ($P<0.001$) (Figure 3.6 A). None of the injection activities (0.74, 3.70 or 14.80 MBq) significantly modified the effect of any of the challenge doses (1, 2, 4 Gy) relative to the saline injected controls ($P=0.322$) (Figure 3.6 A). It was observed in the non-challenged mice (0 Gy) that γH2A.X levels decreased with increasing injection activity ($P=0.019$) (Figure 3.6 B) at 24 hours. The 14.80 MBq injection of ^{18}F-FDG, in particular, caused a significant decrease in γH2A.X below controls ($P=0.014$).

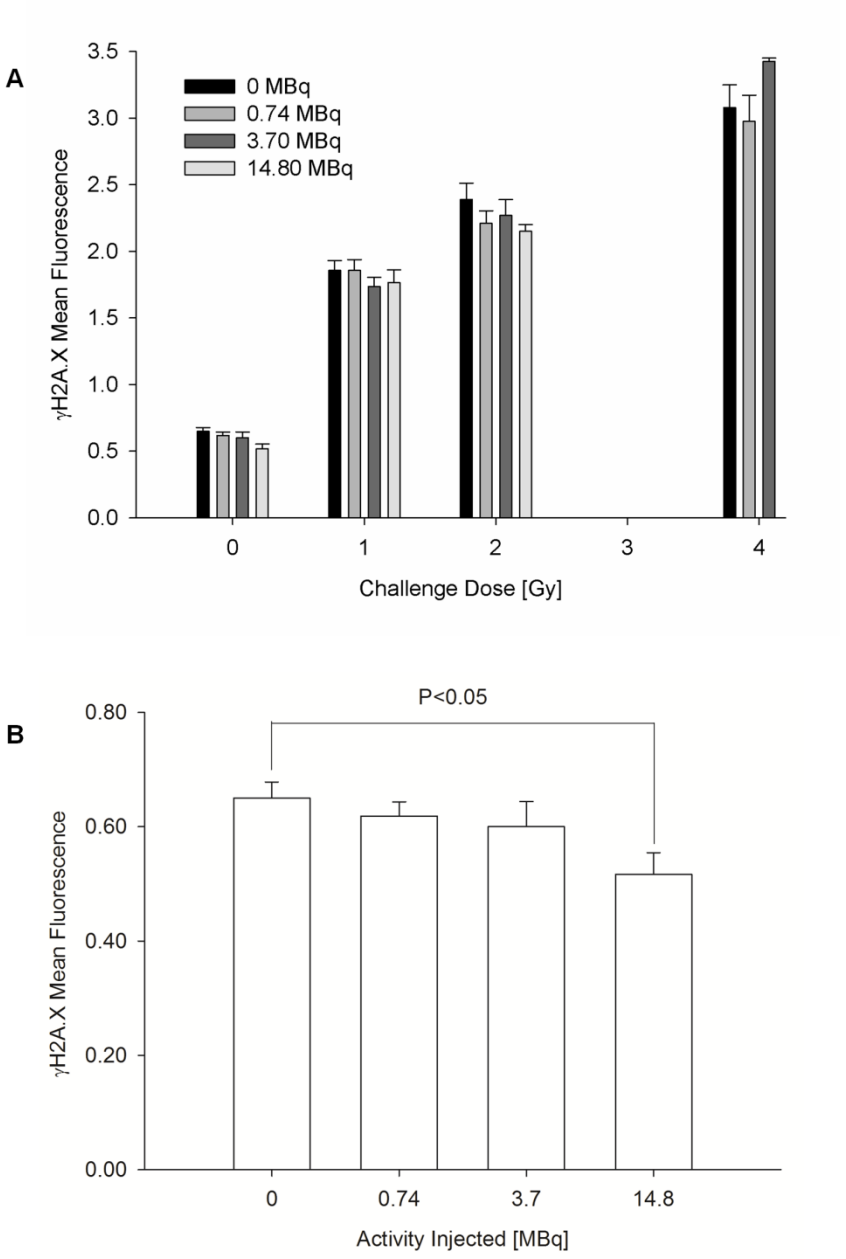

Figure 3.6 *In Vitro* Adaptive Response Mice were injected with 0, 0.74, 1.48 or 3.70 MBq of ^{18}F-FDG (n=6-10, duplicate samples) and irradiated at 24 hours post-injection with 0, 1, 2 or 4 Gy *in vitro*. Mean γH2A.X fluorescence was measured 30 minutes after the challenge dose (A). Sham-irradiated samples only (B) Results displayed are mean ± SEM.

3.5 Discussion

The short term DNA damage response to ^{18}F-FDG PET scans in mice was evaluated using two well established radiation biology assays: micronucleated reticulocyte formation and γH2A.X fluorescence.

Micronuclei occur in newly formed reticulocytes in the blood stream of mice following DNA damage to precursors in bone marrow. This process generally takes between 43-55 hours and varies with mouse strain [47]. Irradiation of the bone marrow will generate DNA DSBs in erythroblasts which, depending on the severity of the damage, undergo apoptosis, repair the DSBs, or proceed to division without repairing or misrepairing the DSBs. The latter will generate an acentric fragment outside the nucleus in daughter cells. These erythroblast daughter cells will expel their nucleus as they mature into polychromatic erythrocytes (PCE) but the acentric fragment can remain. These PCEs transition into the blood stream 12-24 hours later [48]. The lifespan of an erythrocyte is 4 weeks. This technique has been adopted by genetic toxicology and product safety research programs [49] because of its' exceptional sensitivity for measuring the mutagenic potential of low level exposures. It has been shown to be a reliable bio-dosimeter for acute radiation exposures and various clastogenic/aneugenic chemicals [47, 50, 51]. We have demonstrated previously that a 1 Gy acute radiation exposure (662 keV γ-rays) induces a maximum MN-RET frequency at 43 hours and returns to

spontaneous levels by 137 hours [44]. To our knowledge, this assay has never been used to measure the radiation exposure associated with radioisotopes.

The formation of γH2A.X foci occurs at the site of new DSBs within minutes. The phosphorylation of histone H2A.X to form γH2A.X is a key component in sensing damage and recruiting repair proteins. The maximum level of foci occurs at 30 minutes post-irradiation [41,44,47]. As DSBs are repaired, γH2A.X is de-phosphorylated and the foci disappear. It has been shown that the majority of radiation induced foci disappear by 8 hours post-irradiation following exposure to doses below 1 Gy [53]. Paris *et al.* [52] showed that γH2A.X foci disappeared in bone marrow cells specifically by 24 hours post-irradiation following 4 Gy. Measuring γH2A.X foci in bone marrow lymphocytes (via mean fluorescence measurements) at 24 hours post-irradiation would consequently provide information about residual damage.

We have investigated the response to various injection activities of ^{18}F-FDG between 0.74(20) and 14.80(400) MBq (μCi) in mice using these 2 endpoints. The lowest activity used (0.74MBq) produces absorbed doses in a mouse which is similar to the absorbed dose experienced by patients during clinical PET scans. The highest dose (14.80 MBq) represents a typical injection activity used in small animal imaging investigations. A proportionally larger amount of activity is needed to generate diagnostically useful images in mice; this is related to the higher spatial resolution requirements in small animal imaging [54].

A small preliminary experiment was performed to determine the appropriate sampling time for the measurement of MN-RET following injection with 18.5 MBq ^{18}F-FDG. This value was determined to be 43 hours in our strain of mouse. The pattern of decay following the 43 hour maximum was similar to that seen with acute exposures but with a reduced magnitude. A prolonged elevation in MN-RETS beyond the 43 hour maximum was not observed as might have been expected following the isotope injection. This illustrates that the ability to repair DSBs accurately is increased at low dose-rates. By 72 hours, the level of MN-RETS had returned to spontaneous levels. At 72 hours, the MN-RET level in the ^{18}F-FDG injected mice decreased slightly below control levels (by 14%) although this decrease was not found to be significant. It is important to note that food was returned to the mice within 2 hours of the injection for this part of the study. This would be predicted to cause a slight reduction in ^{18}F-FDG uptake among tissues for the amount injected but should not impact the MN-RET kinetics.

The dose response to various injections of ^{18}F-FDG was therefore determined at 43 hours post-injection and compared to that obtained with 662 keV γ-ray whole body exposures at a dose-rate of 0.018 Gy/minute. We have shown that a single 10mGy acute whole body radiation exposure will cause a significant increase in the MN-RET frequency above controls. In contrast, a 3.70 MBq injection of ^{18}F-FDG was required to significantly elevate the MN-RET frequency above control levels. This injection corresponds to a whole body dose of 50-57 mGy and a bone marrow dose of 36 mGy. Again, this

highlights the increased resistance to DNA damage *in vivo* when the radiation exposure is protracted. As the dose-rate decreases, the temporal abundance of damage in the cell is decreased and the ability to accurately repair DNA damage increases [55]. This stems from the fact that the cell has evolved mechanisms of repair to deal with endogenous damage generated during replication. It is estimated that endogenous DSBs are generated at a rate of 6000 per cell each hour [56]. When the exogenous rate of damage induced by ionizing radiation approaches this frequency, the cell is particularly efficient at repairing the damage.

The RBE for ^{18}F-FDG, a combined exposure from 634 keV positrons and 511 keV γ-rays, was calculated to be 0.79±0.04 in mice for the MN-RET endpoint. RBE is used to derive radiation weighting factors for use in radiation protection. The 2007 ICRP report advises to use a radiation weighting factor of 1 for all low LET radiations (x-rays, gamma rays, beta particles) [57]. We have shown that the dose-rate and radiation quality associated with PET scans reduces its effectiveness in generating micronuclei in bone marrow. The RBE has been shown to vary substantially based on the radiation quality, biological endpoint, organism and dose-rate.

It has been shown previously that single low dose or low dose-rate exposures have the capacity to modify a biological system's subsequent response to a large dose of radiation [26, 28-31, 58]. We investigated the potential for ^{18}F-FDG to generate an adaptive response at 24 hours post injection using the MN-RET and γH2A.X endpoints. The 24

hour gap was chosen to allow for complete decay of the isotope in order to capture the full extent of biological changes induced by the injection. A single injection of 0.74, 3.70 or 14.80 MBq ^{18}F-FDG did not modify the magnitude of the response to a 1 Gy acute dose of radiation *in vivo* as measured with the MN-RET endpoint. Injections of 0.74, 3.70 or 14.80 MBq correspond to approximate whole body doses of 10, 50, 200 mGy and approximate bone marrow doses of 7, 35 and 150 mGy (Table 3.1). Similarly, 0.74, 3.70 or 14.80 MBq ^{18}F-FDG injections did not modify the response of bone marrow lymphocytes to 1, 2 or 4 Gy *in vitro* as measured by γH2A.X foci formation. While protection from the high dose challenge has not been demonstrated, the biological effect has not been augmented by prior low dose radiation exposure. Certain models of risk would predict that the total damage from this combination of treatments would be equal to the damage due to the isotope injection plus that induced by the high dose radiation exposure. Consistent with the other observations in this research, the damage induced by the radiation exposure from the 0.74, 3.70 or 14.80 MBq ^{18}F-FDG injections was effectively repaired and did not add to the high dose challenge. The presence of an adaptive response has been shown to depend on the timing and the magnitude of the challenge dose [30]. It has been shown that the adaptive response will be maximal if the interval between the low dose priming signal and the high dose challenge is optimal for the cell or tissue type. Too short or too long a time period between the prime and challenge will result in diminished response [59].

There was a dose dependent decrease in γH2A.X following injections of ^{18}F-FDG at 24 hours in the sham challenged mice (0 Gy) and more specifically, a significant reduction (20%) in γH2A.X following the 14.80 MBq injections relative to saline injected mice. A reduction in transformation frequency below control levels following low dose-rate radiation exposure has been demonstrated previously in cell lines [25]. There are two plausible explanations behind our observation: that the isotope exposure has stimulated damaged cells to undergo apoptosis or has stimulated enhanced repair. Both mechanisms have been demonstrated previously in response to low dose/low dose-rate exposures [60], [61].

It is arguable that studying the biological effects associated with ^{18}F-FDG injections may not be representative of the full radiation detriment associated with a typical PET procedure. Stand-alone PET scanners use a germanium transmission source to correct for the attenuation of the annihilation photons through the patient. It has been shown however that the dosimetric contribution of the transmission scan to the procedure is negligible [62]. At present, PET images are often combined with computed tomography (CT) images for attenuation correction and anatomical information. The combined absorbed radiation dose from these procedures is not expected to exceed 100 mGy, a dose below which beneficial effects have been reported. It has been shown in mice that single and repeated CT scans may initially cause an increase in DNA damage (sensitization) which leads to an up-regulation of protective cellular mechanisms [58]. Moreover, there

is a growing interest in combining PET with MRI [63] in which case the PET component would be the only source of ionizing radiation exposure.

We have studied the DNA damage response to radiation exposure from PET scans and found a dose dependent increase in radiation induced damage. This initial damage response, as measured by MN-RET formation, offers insight into the biophysical properties of the energy deposition in bone marrow associated with ^{18}F-FDG. By studying later time points, we were able to understand the biological amplification of this initial response. For example, the highest injection activities used (14.80 - 18.5 MBq) did not lead to residual DNA damage but in fact decreased the level of damage below controls. This illustrates the importance of examining later time points in these types of investigations and that while the initial response may be linear, the subsequent biological response is not. The current understanding of radiation induced cancers is that it is a result of initiating events such as unrepaired or misrepaired DNA damage but also of systemic influences (immune response), tissue architecture and non-targeted effects [64]. We have studied the bone marrow erythrocytes and lymphocytes due to their radiosensitivity. Different effects would be expected in other tissues receiving higher doses such as the bladder. A concurrent lifetime cancer study currently being completed in our laboratory will provide insight into the whole body consequences of these types of injections.

This work has also shown that the injection activities used in small animal imaging have the capacity to generate an adaptive response in mice. Small animal imaging often involves longitudinal PET studies to investigate disease processes and potential therapies. The radiation exposure from the PET scan could potentially modify the physiological process under examination and emphasizes the importance of *imaging-only* controls in these types of studies. Conversely, this work has shown that from a radiation toxicity point of view, the large doses associated with small animal imaging are well tolerated due to dose protraction. This is confirmed by a study which showed that doses up to 185 MBq (5 mCi) of ^{18}F-FDG did not cause any evidence of radio toxicity in both transgenic and normal mice 1 month after exposure when assessed by complete histological analysis of tissues [65].

The linear no threshold model represents a practical approach to radiation protection and extrapolates epidemiological high dose effects into the low dose range using a linear relationship. In doing so, certain assumptions are made: that dose is a surrogate for risk, that there is no threshold for radiation effects and that risk is additive and can only increase. Our results indicate that in the context of ^{18}F-FDG exposure from PET scans, this does not hold true. We have shown that there is threshold for DNA damage to bone marrow following injections of ^{18}F-FDG. We have also shown that the added radiation exposure (low dose isotope + high dose challenge) does not result in added detriment.

3.6 Conclusions

We have examined the radiobiological changes induced by ^{18}F-FDG to improve the current understanding of the health effects associated with radiation exposure from PET scans. We have tested injection activities relevant to both human imaging and small animal studies. These experiments show that the low dose-rate associated with exposure to ^{18}F-FDG during a PET scan substantially reduces the DNA damage generated for a given dose. Later sampling times revealed that certain injection activities may actually reduce the level of DNA damage below that of controls. A single PET scan was not found to modify the effect of a subsequent high dose of radiation when administered 24 hours later. Together, these results provide evidence against the use of LNT to predict the risk to patients from nuclear medicine procedures such as PET.

3.7 References

[1] F. A. Mettler et al., "Nuclear medicine exposure in the United States, 2005-2007: preliminary results.," *Seminars in nuclear medicine*, vol. 38, no. 5, pp. 384-91, Sep. 2008.

[2] A. Rahmim and H. Zaidi, "PET versus SPECT: strengths, limitations and challenges.," *Nuclear medicine communications*, vol. 29, no. 3, pp. 193-207, Mar. 2008.

[3] S. Kim, N. Salamon, H. A. Jackson, S. Blüml, and A. Panigrahy, "PET imaging in pediatric neuroradiology: current and future applications.," *Pediatric radiology*, vol. 40, no. 1, pp. 82-96, Jan. 2010.

[4] S. Minoshima, K. A. Frey, R. A. Koeppe, N. L. Foster, and D. E. Kuhl, "A diagnostic approach in Alzheimer's disease using three-dimensional stereotactic surface projections of fluorine-18-FDG PET," *Journal of Nuclear Medicine*, vol. 36, no. 7, p. 1238, 1995.

[5] F. Gemmel, P. C. Rijk, J. M. P. Collins, T. Parlevliet, K. D. Stumpe, and C. J. Palestro, "Expanding role of 18F-fluoro-D-deoxyglucose PET and PET/CT in spinal infections.," *European Spine Journal*, vol. 19, no. 4, pp. 540-51, Apr. 2010.

[6] C. Grandin et al., "Delineation of myocardial viability with PET," *Journal of Nuclear Medicine*, vol. 36, no. 9, pp. 1543-52, Sep. 1995.

[7] R. W. Burt et al., "Direct comparison of fluorine-18-FDG SPECT, fluorine-18-FDG PET and rest thallium-201 SPECT for detection of myocardial viability.," *Journal of Nuclear Medicine*, vol. 36, no. 2, pp. 176-9, Feb. 1995.

[8] J. W. Fletcher et al., "Recommendations on the use of 18F-FDG PET in oncology.," *Journal of Nuclear Medicine*, vol. 49, no. 3, pp. 480-508, Mar. 2008.

[9] L. K. Shankar et al., "Consensus recommendations for the use of 18F-FDG PET as an indicator of therapeutic response in patients in National Cancer Institute Trials.," *Journal of Nuclear Medicine*, vol. 47, no. 6, pp. 1059-66, Jun. 2006.

[10] V. Kapoor, B. M. McCook, and F. S. Torok, "An introduction to PET-CT imaging.," *Radiographics*, vol. 24, no. 2, pp. 523-43, 2004.

[11] S. Yu, "Review of F-FDG Synthesis and Quality Control.," *Biomedical imaging and intervention journal*, vol. 2, no. 4, p. e57, Oct. 2006.

[12] H. R. Schelbert et al., "Society of Nuclear Medicine procedure guideline for tumor imaging using F-18 FDG," *Society of Nuclear Medicine Procedure Guidelines Manual*, 2002.

[13] H. M. Deloar, T. Fujiwara, M. Shidahara, T. Nakamura, A. Yamadera, and M. Itoh, "Internal absorbed dose estimation by a TLD method for -FDG and comparison with the dose estimates from whole body PET," *Physics in Medicine and Biology*, vol. 44, no. 2, pp. 595-606, Feb. 1999.

[14] H. M. Deloar et al., "Estimation of absorbed dose for 2-[F-18] fluoro-2-deoxy-D-glucose using whole-body positron emission tomography and magnetic resonance imaging," *European Journal of Nuclear Medicine and Molecular Imaging*, vol. 25, no. 6, pp. 565–574, 1998.

[15] M. T. Hays, E. E. Watson, S. R. Thomas, and M. Stabin, "MIRD dose estimate report no. 19: radiation absorbed dose estimates from (18)F-FDG.," *Journal of Nuclear Medicine*, vol. 43, no. 2, pp. 210-4, Feb. 2002.

[16] G. Brix et al., "Radiation exposure of patients undergoing whole-body dual-modality 18F-FDG PET/CT examinations," *Journal of Nuclear Medicine*, vol. 46, no. 4, p. 608, 2005.

[17] A. A. Mejia, T. Nakamura, I. Masatoshi, J. Hatazawa, M. Masaki, and S. Watanuki, "Estimation of absorbed doses in humans due to intravenous administration of fluorine-18-fluorodeoxyglucose in PET studies," *Journal of Nuclear Medicine*, vol. 32, no. 4, p. 699, 1991.

[18] F. A. Mettler, W. Huda, T. T. Yoshizumi, and M. Mahesh, "Effective doses in radiology and diagnostic nuclear medicine: a catalog.," *Radiology*, vol. 248, no. 1, pp. 254-63, Jul. 2008.

[19] International Commission on Radiological Protection, *ICRP Publication 92 Relative Biological Effectiveness (RBE), Quality Factor (Q), and Radiation Weighting Factor (wr)*, vol. 34, no. 3-4. 2004, pp. iii, 15-267, 269-80.

[20] B. Huang, M. W. M. Law, and P. L. Khong, "Whole-Body PET/CT Scanning: Estimation of Radiation Dose and Cancer Risk," *Radiology*, vol. 251, no. 1, p. 166, 2009.

[21] *NCRP Report No. 64 Influence of Dose and its Distribution in Time on Dose-Response Relationships for Low-LET Radiations*, no. 64. Washington, DC: , 1980.

[22] D. R. Boreham, J. A. Dolling, S. R. Maves, N. Siwarungsun, and R. E. Mitchel, "Dose-rate effects for apoptosis and micronucleus formation in gamma-irradiated human lymphocytes.," *Radiation research*, vol. 153, no. 5 Pt 1, pp. 579-86, May. 2000.

[23] Y. Ina, H. Tanooka, T. Yamada, and K. Sakai, "Suppression of thymic lymphoma induction by life-long low-dose-rate irradiation accompanied by immune activation in C57BL/6 mice.," *Radiation research*, vol. 163, no. 2, pp. 153-8, Feb. 2005.

[24] E. Elmore, X. Y. Lao, R. Kapadia, and J. L. Redpath, "The effect of dose-rate on radiation-induced neoplastic transformation in vitro by low doses of low-LET radiation.," *Radiation research*, vol. 166, no. 6, pp. 832-8, Dec. 2006.

[25] E. I. Azzam, S. M. de Toledo, G. P. Raaphorst, and R. E. J. Mitchel, "Low-Dose Ionizing Radiation Decreases the Frequency of Neoplastic Transformation to a Level below the Spontaneous Rate in C3H 10T1/2 Cells," *Radiation Research*, vol. 146, no. 4, p. 369, Oct. 1996.

[26] E. Elmore, X. Y. Lao, R. Kapadia, E. Giedzinski, C. Limoli, and J. Redpath, "Low doses of very low-dose-rate low-LET radiation suppress radiation-induced neoplastic transformation in vitro and induce an adaptive response," *Radiation research*, vol. 169, no. 3, pp. 311–318, 2008.

[27] S. M. de Toledo et al., "Adaptive responses to low-dose/low-dose-rate gamma rays in normal human fibroblasts: the role of growth architecture and oxidative metabolism.," *Radiation research*, vol. 166, no. 6, pp. 849-57, Dec. 2006.

[28] R. E. J. Mitchel, J. S. Jackson, and S. M. Carlisle, "Upper dose thresholds for radiation-induced adaptive response against cancer in high-dose-exposed, cancer-prone, radiation-sensitive Trp53 heterozygous mice.," *Radiation research*, vol. 162, no. 1, pp. 20-30, Jul. 2004.

[29] T. K. Day et al., "Adaptive response for chromosomal inversions in pKZ1 mouse prostate induced by low doses of X radiation delivered after a high dose.," *Radiation research*, vol. 167, no. 6, pp. 682-92, Jun. 2007.

[30] E. J. Broome, D. L. Brown, and R. E. J. Mitchel, “Dose Responses for Adaption to Low Doses of 60 Co Rays and H3 Particles in Normal Human Fibroblasts,” *Radiation research*, vol. 186, pp. 181-186, 2002.

[31] G. Olivieri, J. Bodycote, and S. Wolff, “Adaptive response of human lymphocytes to low concentrations of radioactive thymidine,” *Science*, vol. 223, no. 4636, p. 594, 1984.

[32] K. Brehwens, E. Staaf, S. Haghdoost, A. J. González, and A. Wojcik, “Cytogenetic damage in cells exposed to ionizing radiation under conditions of a changing dose-rate,” *Radiation research*, vol. 173, no. 3, pp. 283-9, Mar. 2010.

[33] S. J. Collis et al., “Evasion of early cellular response mechanisms following low level radiation-induced DNA damage.,” *The Journal of biological chemistry*, vol. 279, no. 48, pp. 49624-32, Nov. 2004.

[34] D. Boreham and J. Dolling, “Risks associated with therapeutic 131I radiation exposure.,” *Journal of Nuclear Medicine*, vol. 49, no. 5, pp. 691-3, May. 2008.

[35] M. A. Monsieurs, H. M. Thierens, A. M. Vral, C. Van De Wiele, L. I. De Ridder, and R. A. Dierckx, “Adaptive response in patients treated with 131I,” *Journal of Nuclear Medicine*, vol. 41, no. 1, p. 17, 2000.

[36] M. Lassmann et al., “In vivo formation of gamma-H2AX and 53BP1 DNA repair foci in blood cells after radioiodine therapy of differentiated thyroid cancer.,” *Journal of Nuclear Medicine*, vol. 51, no. 8, pp. 1318-25, Aug. 2010.

[37] *Health Risks From Exposure to Low Levels of Ionizing Radiation Beir VII Phase 2*. Washington, DC: , 2006.

[38] R. W. Howell, “Patient exposures and consequent risks from nuclear medicine procedures.,” *Health physics*, vol. 100, no. 3, pp. 313-7, Mar. 2011.

[39] O. Ulker, S. Genç, H. Ateş, H. Durak, and N. Atabey, “99mTc-HMPAO labelling inhibits cell motility and cell proliferation and induces apoptosis of NC-NC cells.,” *Mutation research*, vol. 631, no. 2, pp. 69-76, Jul. 2007.

[40] K. Schnarr, I. Dayes, J. Sathya, and D. Boreham, “Individual radiosensitivity and its relevance to health physics.,” *Dose-response*, vol. 5, no. 4, pp. 333-48, Jan. 2007.

[41] R. Chirakal, "Base mediated Decomposition of a Mannose Triflate During the Synthesis of 2-Deoxy-2-18F-fluoro-D-glucose," *Applied Radiation and Isotopes*, vol. 46, no. 3, pp. 149-155, Mar. 1995.

[42] T. Funk, M. Sun, and B. H. Hasegawa, "Radiation dose estimate in small animal SPECT and PET," *Medical Physics*, vol. 31, no. 9, p. 2680, 2004.

[43] R. Taschereau and A. F. Chatziioannou, "Monte Carlo simulations of absorbed dose in a mouse phantom from 18-fluorine compounds," *Medical Physics*, vol. 34, no. 3, p. 1026, 2007.

[44] K. Taylor, N. Phan, and D. Boreham, "Trp53 gene status influences low dose radiation-induced apoptosis and DNA damage in the haematopoietic cells of mice," *Mutagenesis (In Press)*, 2011.

[45] L. Churchley, "The Relative Biological Effectiveness of 30 kV mammography x-rays at low doses in vivo," McMaster University, 2008.

[46] K. Rothkamm and S. Horn, "γ-H2AX as protein biomarker for radiation exposure," *Ann Ist Super Sanita*, vol. 45, no. 3, pp. 265-271, 2009.

[47] S. D. Dertinger et al., "Reticulocyte and micronucleated reticulocyte responses to gamma irradiation: dose-response and time-course profiles measured by flow cytometry.," *Mutation research*, vol. 634, no. 1-2, pp. 119-25, Dec. 2007.

[48] K. H. Mavournin, D. H. Blakey, M. C. Cimino, M. F. Salamone, and J. a Heddle, "The in vivo micronucleus assay in mammalian bone marrow and peripheral blood. A report of the U.S. Environmental Protection Agency Gene-Tox Program.," *Mutation research*, vol. 239, no. 1, pp. 29-80, Jul. 1990.

[49] S. D. Dertinger, D. K. Torous, M. Hayashi, and J. T. MacGregor, "Flow cytometric scoring of micronucleated erythrocytes: an efficient platform for assessing in vivo cytogenetic damage.," *Mutagenesis*, vol. 26, no. 1, pp. 139-45, Jan. 2011.

[50] N. Asano, D. K. Torous, C. R. Tometsko, S. D. Dertinger, T. Morita, and M. Hayashi, "Practical threshold for micronucleated reticulocyte induction observed for low doses of mitomycin C, Ara-C and colchicine.," *Mutagenesis*, vol. 21, no. 1, pp. 15-20, Jan. 2006.

[51] N. Kunugita et al., “Increased frequencies of micronucleated reticulocytes and T-cell receptor mutation in Aldh2 knockout mice exposed to acetaldehyde.,” *The Journal of toxicological sciences*, vol. 33, no. 1, pp. 31-6, Feb. 2008.

[52] L. Paris et al., “Kinetics of gamma-H2AX induction and removal in bone marrow and testicular cells of mice after X-ray irradiation.,” *Mutagenesis*, vol. 26, no. 4, pp. 563-72, Jul. 2011.

[53] C. E. Redon, J. S. Dickey, A. J. Nakamura, O. A. Martin, and W. M. Bonner, “Molecular Determinants of Radiation Response,” *Response*, pp. 3-33, 2011.

[54] A. F. Chatziioannou, “Instrumentation for molecular imaging in preclinical research: Micro-PET and Micro-SPECT.,” *Proceedings of the American Thoracic Society*, vol. 2, no. 6, pp. 533-6, 510-11, Jan. 2005.

[55] M. Tubiana, A. Aurengo, D. Averbeck, and R. Masse, “Recent reports on the effect of low doses of ionizing radiation and its dose-effect relationship,” *Radiation and environmental biophysics*, vol. 44, no. 4, pp. 245-51, Mar. 2006.

[56] D. Billen, “Spontaneous DNA Damage and Its Significance for the ‘Negligible Dose’ Controversy in Radiation Protection,” *Radiation Research*, vol. 124, no. 2, pp. 242-245, 1990.

[57] *ICRP publication 103: The 2007 Recommendations of the International Commission on Radiological Protection*, vol. 37, no. 2-4. 2007, pp. 1-332.

[58] N. Phan, M. De Lisio, G. Parise, and D. R. Boreham, “Biological Effects and Adaptive Response from Single and Repeated Computed Tomography Scans in Reticulocytes and Bone Marrow of C57BL/6 Mice,” *Radiation Research (In Press)*.

[59] G. Esposito, A. Campa, M. Pinto, G. Simone, M. A. Tabocchini, and M. Belli, “Adaptive response: modelling and experimental studies.,” *Radiation protection dosimetry*, vol. 143, no. 2-4, pp. 320-4, Feb. 2011.

[60] D. I. Portess, G. Bauer, M. A. Hill, and P. O’Neill, “Low-dose irradiation of nontransformed cells stimulates the selective removal of precancerous cells via intercellular induction of apoptosis.,” *Cancer research*, vol. 67, no. 3, pp. 1246-53, Feb. 2007.

[61] M. C. Pant, X. Liao, Q. Lu, S. Molloi, E. Elmore, and J. L. Redpath, “Mechanisms of suppression of neoplastic transformation in vitro by low doses of low LET radiation.,” *Carcinogenesis*, vol. 24, no. 12, pp. 1961-5, Dec. 2003.

[62] T.-H. Wu et al., “Radiation exposure during transmission measurements: comparison between CT- and germanium-based techniques with a current PET scanner.,” *European journal of nuclear medicine and molecular imaging*, vol. 31, no. 1, pp. 38-43, Jan. 2004.

[63] B. J. Pichler, A. Kolb, T. Nägele, and H.-P. Schlemmer, “PET/MRI: paving the way for the next generation of clinical multimodality imaging applications.,” *Journal of Nuclear Medicine*, vol. 51, no. 3, pp. 333-6, Mar. 2010.

[64] M. H. Barcellos-Hoff and D. H. Nguyen, “Radiation carcinogenesis in context: how do irradiated tissues become tumors?,” *Health physics*, vol. 97, no. 5, pp. 446-57, Nov. 2009.

[65] R. M. Moadel et al., “Positron emission tomography agent 2-deoxy-2-[18F]fluoro-D-glucose has a therapeutic potential in breast cancer.,” *Breast cancer research : BCR*, vol. 5, no. 6, pp. R199-205, Jan. 2003.

Chapter 4

PET scans with ^{18}F-FDG do not modify cancer frequency or latency in *Trp53+/-* mice

4.1 Abstract

There is considerable interest in the health effects associated with low level radiation exposure from medical imaging procedures. There is a concern that imaging procedures will be responsible for increased cancer risk among patients. Conversely, low dose radiation exposure (γ-rays) has been shown to increase the latency period of lymphoma and spinal osteosarcoma in cancer prone *Trp53+/-* mice. The goal of this research was to investigate how modification of cancer associated with exposure to low dose ionizing radiation in *Trp53+/-* mice is influenced by radiation quality from Positron Emission Tomography (PET). PET scans are an increasingly used nuclear medicine procedure involving the radiopharmaceutical 2-[^{18}F] fluoro-2-deoxy-D-glucose (^{18}F-FDG) which exposes tissue to a mixed radiation quality: 634 keV β+, 511 keV γ-rays. At 7-8 weeks of age, *Trp53+/-* female mice were exposed to one of 5 treatments: 0 Gy, 10 mGy γ-rays, 10 mGy PET, 4 Gy γ-rays, 10 mGy PET + 4 Gy γ-rays (n>185). Mice were monitored on a daily basis for abnormal indications and euthanized when specific criteria associated with the cancer phenotype were observed. Formalin fixed tissues from these mice were subjected to complete histological analysis by a veterinary pathologist. The 4 Gy radiation dose significantly reduced the lifespan and latency period of cancer to unirradiated controls and caused a significant increase in the number of mice with malignancies. The 10 mGy γ-rays and 10 mGy PET doses did not significantly modify the frequency or the latency period of cancer relative to unirradiated mice. Similarly, the

PET scan administered prior to the 4 Gy dose did not significantly modify the latency or frequency of cancer relative to mice receiving only 4 Gy. When tissue specific lesions were considered, it was found that the 10 mGy PET group had significantly fewer mice with kidney lesions ($P = 0.021$). An injection of 0.75 ± 0.0050 MBq ^{18}F-FDG results in an approximate absorbed dose of 20 ± 0.13 mGy to the kidneys.

4.2 Introduction

It is well established that exposure to high doses of ionizing radiation increases the risk of cancer in humans [1-8]. The definitive carcinogenic risk associated with low level radiation exposures however is less clear. Using human epidemiological data (atom bomb survivor cohort), regulatory agencies linearly extrapolate high dose responses into the low dose range to offer a conservative approach to radiation protection. This model is referred to as the linear no threshold model of risk estimation and implies that every dose causes an increase in the risk of developing cancer above background levels. In contrast, there is a large body of *in vivo* evidence which shows that low doses of radiation may not cause any detrimental health effects [9-13] or, that these exposures may be beneficial to the irradiated organism by increasing lifespan and/or reducing carcinogenesis [14, 15] . The latter phenomenon is called radiation hormesis [16]. It has also been demonstrated *in vivo* that low doses of radiation can modify cellular processes and protect against the

effects of a subsequent high, carcinogenic dose of radiation [12,17]. This effect is referred to as an adaptive response [18].

The use of diagnostic imaging continues to expand [19] and newer technologies such as positron emission tomography (PET) are expected to play an important role in the future. The most commonly used PET radiotracer is the glucose analog 2-[^{18}F] fluoro-2-deoxy-D-glucose (^{18}F-FDG). A typical clinical scan involving the administration of 350-750 MBq ^{18}F-FDG [20] will expose most tissues within the patient to a maximum absorbed dose of approximately 10mGy as a result of positrons (β+, E_{max}=634 keV) and annihilation photons (γ-rays, 511 keV). However, tissues with increased uptake of the radiopharmaceutical will receive higher absorbed doses than the whole body average such as the brain (*10-36 mGy*), heart (*16-51 mGy*), kidneys (*7-23 mGy*) and bladder (*13-233mGy*) [21-25]. Recently, studies have emerged indicating that diagnostic imaging procedures may cause an increase in cancer among patients due to ionizing radiation exposure[26-28]. These studies infer an increased risk based using the linear no threshold model.

It has been shown previously that a single 10 mGy γ-ray dose (^{60}Co, 0.5 mGy/minute) can significantly extend the latency period of lymphoma and spinal osteosarcoma in cancer prone *Trp53+/-* mice relative to unirradiated controls [15]. When a 10 mGy γ-ray dose was administered 24 hours prior to an acute 4 Gy γ-ray dose (^{60}Co, 0.5 Gy/minute), the latency period of lymphoma was significantly extended relative to *Trp53+/-* mice

receiving 4 Gy only [17]. No changes in the frequency of cancers were observed in both experiments. These protective effects however seem to be dose and tissue dependent since in these same studies, a 100 mGy γ-ray dose extended the latency period of lymphoma but decreased the latency period of spinal osteosarcoma.

The goal of this research was to investigate how modification of cancer associated with exposure to low dose ionizing radiation is influenced by radiation quality from PET scans. There were two specific aims: to determine if a single PET scan could alter cancer risk and to determine if a single PET scan could alter cancer risk associated with a subsequent large dose exposure. Cancer risk was measured in terms of the frequency and latency of cancers in *Trp53+/-* mice. The 2007 ICRP report advises to use a radiation weighting factor of 1 for all low LET radiations (x-rays, γ-rays, β particles) [29], therefore we hypothesized that a 10mGy PET scan would replicate previous results in *Trp53+/-* mice[15, 17]. Based on these previous studies, a sample size of 180 would have sufficient statistical power (0.8) to detect differences of 30 days between the 10mGy exposed mice and unirradiated controls (α=0.05). It is postulated that a 10 mGy PET scan will significantly extend the mean latency of period of lymphoma and spinal osteosarcoma by 30 days and protect against a 4 Gy dose by extending the mean latency period of lymphoma by 30 days. The null hypothesis is that a PET scan will not significantly extend the mean latency period of lymphoma and spinal osteosarcoma relative to unirradiated mice or 4 Gy mice (in the context of 10 mGy PET + 4 Gy).

Despite an average whole body dose of 10 mGy, PET scans deliver doses ≥ 10 mGy in certain tissues. It has been shown previously that higher doses (100 mGy) cause detrimental effects, therefore, the expectation is that tissues receiving a higher absorbed dose from PET scans would demonstrate increased risk.

4.3 Materials & Methods

4.3.1 Mice

A breeding colony was established to generate the *Trp53+/-* female mice used in this study. Male mice with a single defective copy of the *Trp53* gene (B6.129S2-Trp53$^{tm1Tyj/1}$) were bred with wild-type female mice (129X1/SvJ) (Jackson Laboratory, Bar Harbour, Maine). The p53 knockout mouse strain carries a mutation deleting 40% of the p53 coding region which completely eliminates the production of p53 protein by that allele [30].

The F1 female progeny produced from this cross were genotyped at 4-5 weeks of age to determine whether mice were wild-type (*Trp53+/+*) or heterozygous (*Trp53+/-*) for *Trp53*. Mice were anaesthetized (1-2% Isoflurane™ via inhalation) and a tail snip was collected in 200 µl of 95% ethanol. Mice were ear punched at this time for subsequent

identification and sorting. This PCR procedure has been described previously [30]. *Trp53+/-* mice were subsequently assigned to treatment groups.

All mice were housed five to a cage, in specific pathogen free conditions (SPF), in a housing room maintained on a 12 hour light/dark cycle at a temperature of 24 ± 1°C. Food and water were available *ad libitum*. Protocols were approved by the Animal Research Ethics Board (AREB) at McMaster University and carried out as per the Canadian Council on Animal Care (CCAC).

4.3.2 Mouse Treatments

Trp53+/ - mice (7-8 weeks old) were randomly assigned to one of five treatment groups throughout the duration of the breeding program (see Table 1), each containing >180 mice: 0 Gy, 10 mGy γ-rays, 10 mGy PET, 4 Gy γ-rays, 10 mGy PET + 4 Gy γ-rays.

4.3.2.1 Unirradiated mice treatment (0 Gy)

Each week of treatments, untreated mice of the appropriate age were placed into the 0 Gy group.

4.3.2.2. Low dose radiation treatment (10 mGy γ-rays)

The 10 mGy γ-ray dose was delivered using a Cs-137 source (662 keV γ-rays) at the McMaster Taylor Radiobiology Source Facility. Mice were placed in a customized

sectioned polycarbonate restraint tube for immobilization during radiation exposure. The 10 mGy doses were delivered at a dose-rate 0.018 Gy/minute (whole body).

4.3.2.3 Low dose radiation treatment (10 mGy PET)

Mice were injected with 0.75 ± 0.00050 MBq (20.00 ± 0.13 μCi) ^{18}F-FDG prepared at Hamilton Health Sciences (Hamilton, Ontario) to simulate a radiation exposure similar to that associated with a clinical PET scan. This activity yields a whole body dose of ≈ 10 mGy in a 20 g mouse [31] but absorbed doses between 9-400 mGy depending on the organ (Table 2). The ^{18}F was produced by ^{18}O(*p*,n)^{18}F reaction using a Siemens RDS112 11MeV Proton-Cyclotron and the FDG was prepared as per the procedure listed in [32], meeting all USP and Health Canada regulatory requirements. All mice were fasted overnight prior to the isotope injection (12-14 hours) but water was available *ad libitum.* Mice were housed individually for a period of 24 hours following the injection to minimize inter-mouse irradiation.

Individual isotope doses were calibrated using a CRC-12 radioisotope calibrator (Capintec). Bi-weekly quality control (voltage, zero, background, stability) was performed on this system using Cs-137 and Co-60 check sources. The pre-and post-injection activity of the syringe in addition to the time of each measurement was recorded. This information was used to accurately calculate the activity administered to each individual mouse by correcting for decay. The weight of each mouse was also

recorded prior to the injection. The average weight of mice at the time of treatment was 20 ± 0.07 g. The ^{18}F-FDG was diluted into a total volume of 200 µl with saline and administered by tail vein injection (30g needle, 1 cc syringe). Mice were immobilized using a restraint device designed for mouse tail vein injections (Tailveiner® TV-150, Braintree Scientific Inc., MA). Anaesthesia was not used since image acquisition was not the objective of this work. Food was returned to the mice 2 hours after the injection to maximize uptake of the ^{18}F-FDG and to simulate the conditions of a typical PET procedure. Previously published absorbed dose estimates for ^{18}F-FDG in mice [34, 35] were used to convert the injected activity into whole body doses and structure specific absorbed doses (see Table 2).

4.3.2.4 High dose radiation treatment (4 Gy γ-rays)

The 4 Gy γ-ray dose was delivered using a Cs-137 source (662 keV γ-rays) at the McMaster Taylor Radiobiology Source Facility. Mice were placed in a customized sectioned polycarbonate restraint tube for immobilization during radiation exposure. The 4 Gy doses were delivered at a dose-rate 0.35 Gy/minute (whole body).

4.3.2.5 High dose adaptive response treatment (10 mGy PET + 4 Gy γ-rays)

Mice were injected with ^{18}F-FDG as described in the instructions for 10 mGy PET treatment. Mice were then irradiated whole body according to the instructions for 4 Gy γ-rays, 24 hours after this injection.

4.3.3 Cancer Endpoints

Following treatment, mice were returned to the housing room and examined daily for abnormal indications. The mouse treatment status was coded and undisclosed to veterinary staff. Objective criteria were set *a priori* to determine endpoint for euthanasia, which were consistent with previous studies performed with *Trp53+/-* mice [9,10]. Lymphoma and osteosarcoma are the cancer types most often observed in *Trp53+/-* mice [30].

Following euthanasia, mice were subjected to complete necropsy and histological assessment. Standard tissues (sternum, thymus, heart, lungs, liver, spleen, kidneys, thoracic spine, lumbar spine, brain) and any abnormalities (tumours, enlarged organs or lymph nodes etc) were collected. All tissues were fixed in 10% buffered formalin. Vertebrae and other mineralized tissues were further processed in an EDTA (145 g/L) solution. Trimmed fixed tissue sections were embedded in paraffin. Paraffin blocks were sectioned on a Leica RM 2165 microtome at 3 µm thickness and stained with hematoxylin and eosin (H&E) for histological examination. The presence of cancer or other diseases was diagnosed by an experienced animal veterinarian pathologist based on slide examination and consultation of necropsy reports. Blinded repeat samples were re-submitted for quality assurance with a 100% demonstrated precision record.

If two of the *same* type of cancer were found in a mouse, this was counted as a single cancer since it was not possible to distinguish whether the second observation was an independent primary cancer or a metastasis. If a mouse had a multiple *different* cancer types, these were each counted as one cancer. Both survival and cancer latency were defined as the time between treatment (7 or 8 weeks of age) and euthanasia.

4.3.3 Tissue Specific Lesions

Veterinary pathology reports provided information on the presence of lesions in each tissue section submitted. A lesion is defined as a localized pathological change in tissue. This could be related to malignant or non malignant disease. When a lesion was identified, the nature of the lesion was explained to allow for analysis of various cancer types as described in the section above. The radiation exposure associated with a PET scan results in a non-uniform dose distribution throughout the mouse following injection of the radiopharmaceutical ^{18}F-FDG (Table 4.1). The majority of organs will receive a total absorbed dose of ≈10 mGy whereas others will receive doses exceeding this value. The frequency of lesions were compared among treatment groups in tissues receiving doses >10mGy from the 0.74 MBq injection of ^{18}F-FDG.

Table 4.1 Absorbed dose estimates for a 20 ± 0.08 g mouse injected with 0.75 ± 0.0050 MBq ^{18}F-FDG

Structure	**Absorbed Dose (mGy)**
Whole Body †	11.88 ± 0.08
Whole Body *	10.57 ± 0.07
Bladder Wall *	399.31 ± 2.64
Brain *	9.81 ± 0.06
Heart *	22.8 ± 0.15
Kidneys *	19.63 ± 0.13
Reproductive Organs *‡	17.37 ± 0.15

Data are expressed mean ± SEM.
* Obtained using absorbed dose values normalized to administered activity (MBq) from Taschereau *et al.* [33]
† Obtained using an approximate dose calculation and S value (22.1×10^{-13} Gy/Bq s) from Funk *et al.* [31]
‡ Averaged value for reproductive organs from Taschereau *et al.* [33]

4.3.4 Statistical Analysis

Statistical analyses were performed using SigmaPlot version 11.0 (Systat Software Inc., Germany). Data is presented as median ± standard error (SE) with two-sided $P \leq 0.05$ considered statistically significant, unless otherwise specified. Differences in the frequencies of disease were tested for statistical significance using Fisher's exact test or χ^2 test. Differences in overall lifespan and cancer latency (calculated as days after radiation exposure) were analyzed with the non-parametric Mann-Whitney Rank Sum test. Survival curve probabilities were analyzed using Kaplan-Meier analysis and

significant differences in survival were tested with a Log Rank test. Survival analyses were corrected for competing causes using competitive censoring.

4.4 **Results**

4.4.1 Overall Survival

The survival curves associated with the various treatment regimes is shown in Figure 4.1. The 4 Gy radiation exposure significantly decreased the median lifespan in *Trp53+/-* mice relative to unirradiated *Trp53+/-* mice by 252 ± 8 days ($P<0.001$) (Table 4.2). The 10 mGy γ-ray exposure did not significantly change the lifespan of mice relative to unirradiated controls ($P=0.861$). Similarly, the 10 mGy PET scan did not significantly change lifespan relative to the unirradiated controls ($P=0.710$) nor was there a difference in survival between mice receiving the 10 mGy γ-ray exposure and the 10 mGy PET scan ($P=0.715$). A PET scan administered 24 hours prior to a 4 Gy dose did not significantly change the lifespan from mice receiving 4 Gy only ($P=0.513$).

Table 4.2 Treatment groups & number of mice per group

Treatment	**Number of Mice (n)**	**Median Survival (days+SEM)** †
0 Gy	199	433 ± 7
10 mGy γ-rays	187	441 ± 8
10 mGy PET	189	438 ± 8
4 Gy γ-rays	203	191 ± 4*
10 mGy PET + 4 Gy γ-rays	185	201 ± 4

* P = <0.001 relative to control mice
† Median survival post-treatment (at 7 or 8 weeks of age)

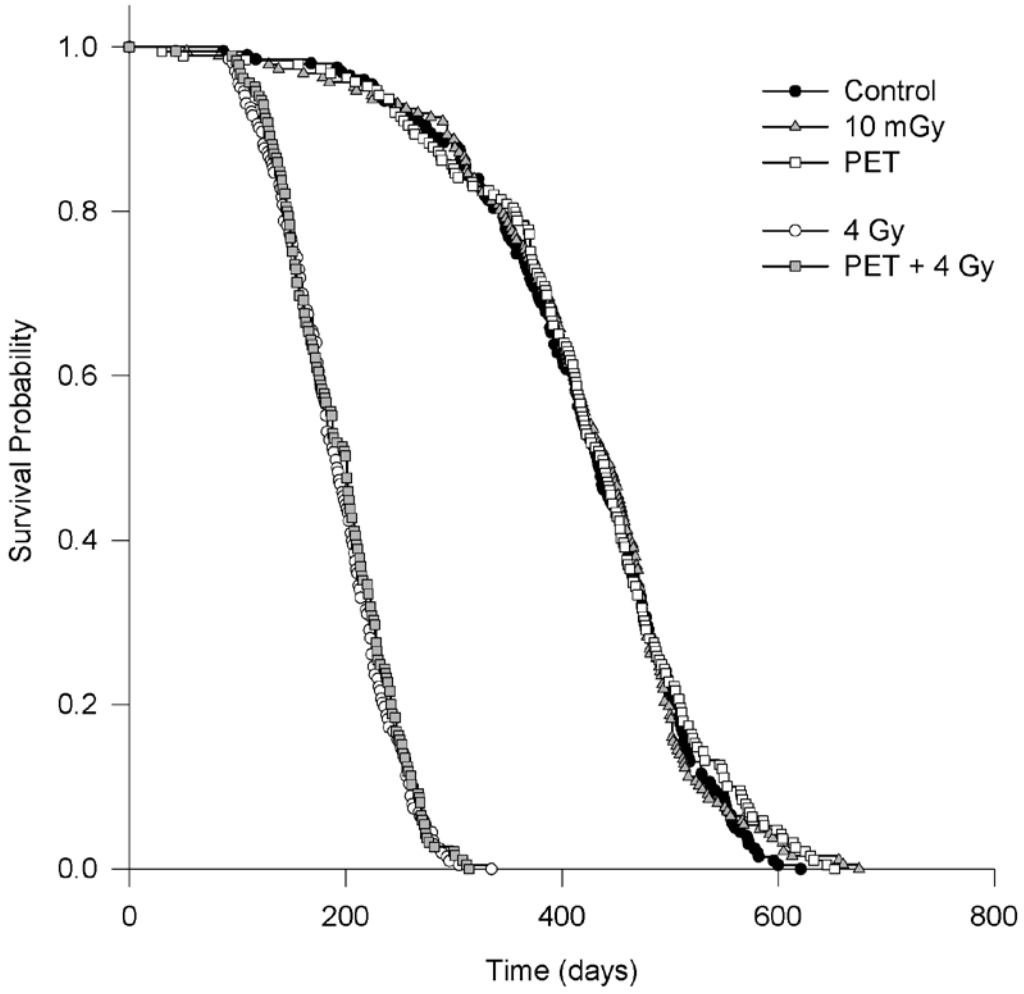

Figure 4.1 Survival probability of *Trp53+/-* mice. The Kaplan Meier method was used to estimate the survival curves and differences between the curves were evaluated with the log rank test. Time represents the number of days since radiation exposure (days at risk). All causes of mortality are included. The 4 Gy radiation exposures caused a significant decrease in lifespan ($P<0.001$).

4.4.2 Frequency and Latency of Malignant Tumours

The *Trp53+/-* mice in this study developed malignant tumours, benign tumours and non-cancer diseases such as chronic nephropathy and dermatitis. Malignancy was the most common cause for euthanasia with at least 84% of mice in each treatment group developing at least one malignant cancer during their lifetime. Many mice were diagnosed with more than one type of malignancy following histological examination.

The 4 Gy γ-ray treatments significantly increased the number of mice with malignant tumours (94%) relative to the 0 Gy (84%) (P=0.005) (Table 4.3). The PET scan administered 24 hours before the 4 Gy exposure (10 mGy PET + 4 Gy γ-rays) did not modify the frequency of malignancy associated with 4 Gy (97%) (P = 0.233). Similarly, a 10 mGy dose (γ-rays or PET) did not significantly modify the frequency of mice with malignant cancers from the 0 Gy group (P>0.830). In addition, there was no difference (P=0.917) between the number of malignant tumours in the two low dose groups (10 mGy γ-rays or 10 mGy PET).

The most frequent malignancies observed were lymphomas, sarcomas and carcinomas (Table 4.3). Unirradiated mice developed sarcomas most frequently (76%) followed by lymphomas (18%) and carcinomas (10%). In contrast, mice irradiated with 4 Gy developed lymphomas predominantly (61%) followed by sarcoma (43%) and carcinoma (12%). The frequency of these cancer types in the low dose irradiated groups (10 mGy

γ- rays or 10 mGy PET) did not vary significantly from the unirradiated controls (P>0.286) or between each other (P>0.258). The frequency of these cancer types in the 10 mGy PET + 4 Gy γ-ray group did not vary significantly from the 4 Gy group (P>0.724).

The latency period for malignant tumours was measured from the time of radiation exposure to endpoint. The latency of malignant tumours in *Trp53*+/- mice was significantly decreased following 4 Gy (194±4 days) relative to unirradiated controls (451±9 days) (P <0.001). The latency of malignant tumours in mice receiving a PET scan prior to the 4 Gy exposure was not significantly modified relative to the 4 Gy latency period (P=0.775). The latency of malignant tumours in mice receiving 10mGy γ-rays (460±6 days) or 10 mGy PET (453±7 days) was not significantly modified relative to the 0 Gy group (P>0.260). There was also no difference between the 10 mGy γ-rays and 10 mGy PET radiation doses in terms of malignant tumour latency (P=0.701).

Table 4.3 Number of *Trp53+/-* mice with malignant tumours and the frequencies of various subtypes

Treatment	Number of Mice with Malignant Tumours	Total Lymphomas		Total Sarcomas			Total Carcinomas
				Osteosarcoma		Other	
		T-Cell	B-Cell	All	Spinal		
0 Gy	168	11	25	104	71	48	20
10 mGy γ-rays	160	8	35	92	60	48	17
10 mGy PET	162	6	30	105	65	50	17
4 Gy γ-rays	*190	97	26	36	31	52	25
10 mGy PET + 4 Gy γ-rays	178	92	21	36	30	48	22

* P=0.005 relative to unirradiated controls

4.4.3 Frequency and Latency of Lymphoma

The 4 Gy γ-ray radiation dose significantly increased the frequency of T-Cell lymphoma relative to unirradiated controls ($P<0.001$) (Table 4.3). The frequency of B-Cell lymphoma did not vary with any of the treatments ($P>0.05$) (Table 3). The 4 Gy γ-ray radiation dose also reduced the latency period associated with lymphoma relative to unirradiated controls (Figure 4.2).

There was no difference in the frequency of lymphoma (T-cell, B-Cell, total) between the 10 mGy γ-ray group, the 10 mGy PET group and the 0 Gy group ($P>0.286$). The latency period of lymphoma for these treatment groups is shown in Figure 4.2 A. Competing causes of death were censored. There was no difference in the latency period of lymphoma between the 10 mGy γ-ray group, the 10 mGy PET group and the 0 Gy group ($P=0.502$).

There was no difference in the frequency of lymphoma (T-cell, B-Cell, total) between the 10 mGy PET + 4 Gy γ-ray group and the 4 Gy γ-ray group ($P>0.738$). The latency period of lymphoma for these treatment groups is shown in Figure 4.2 B. Competing causes of death were censored. There was no difference in the latency period of lymphoma between the 10 mGy PET + 4 Gy γ-ray group and the 4 Gy group ($P=0.965$).

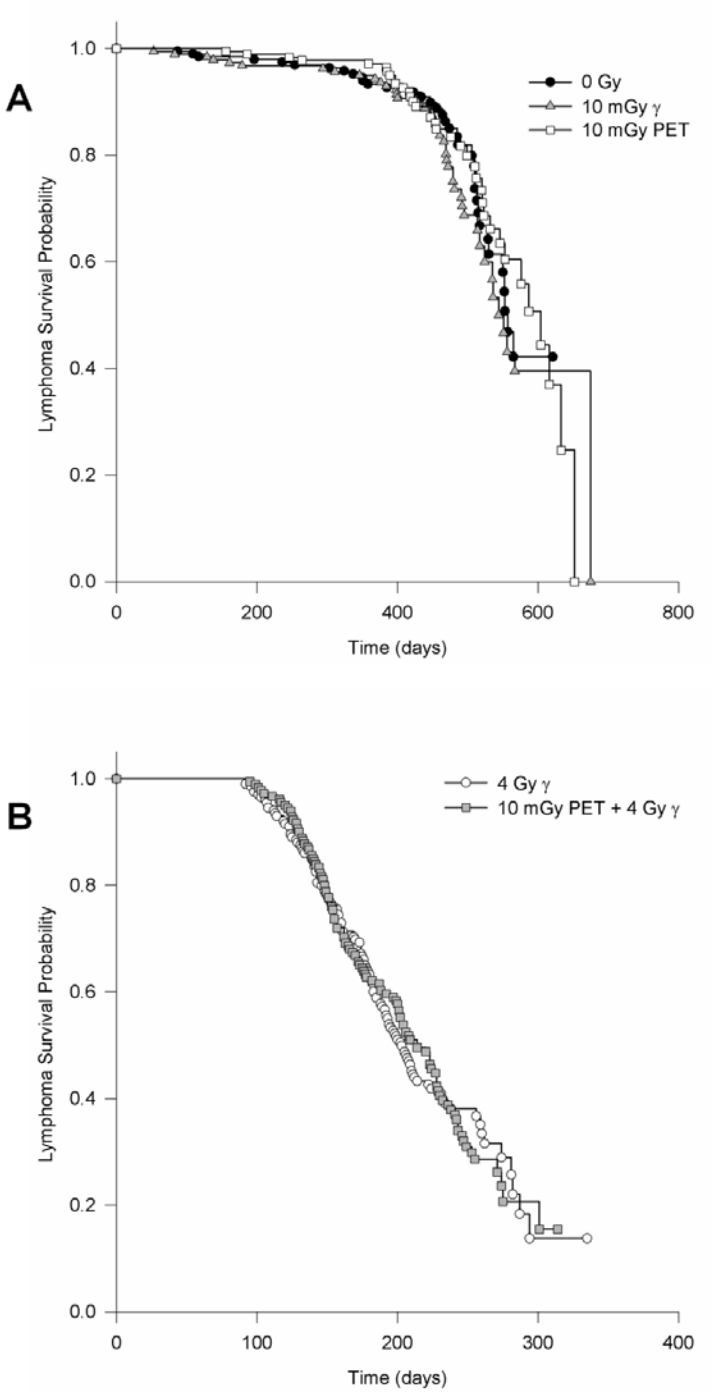

Figure 4.2 Survival probability of *Trp53+/-* mice with lymphoma. Time represents the

number of days since radiation exposure (days at risk) **(A)** Survival of mice treated with 10 mGy (γ-rays or PET) relative unirradiated controls (0 Gy) **(B)** Survival of mice treated with 10 mGy PET + 4 Gy relative 4 Gy only controls.

4.4.4 Frequency and Latency of Spinal Osteosarcoma

Unirradiated mice had a higher frequency of spinal osteosarcoma (and osteosarcoma in general) than 4 Gy irradiated mice ($P<0.001$) (Table 4.3). There was no difference in the frequency of spinal osteosarcoma between the 10 mGy γ-ray group, the 10 mGy PET group and the 0 Gy group ($P>0.412$). The latency period of spinal osteosarcoma for these treatment groups is shown in Figure 4.3A. Competing causes of death were censored. There was no difference in the latency period of spinal osteosarcoma between the 10 mGy γ-ray group, the 10 mGy PET group and the 0 Gy group ($P = 0.509$).

There was no difference in the frequency of spinal osteosarcoma between the 10 mGy PET + 4 Gy γ-ray group and the 4 Gy group ($P=0.889$). The latency period of spinal osteosarcoma for these treatment groups is shown in Figure 4.3B. Competing causes of death were censored. There was no difference in the latency period of spinal osteosarcoma between the 10 mGy PET + 4 Gy γ-rays group and the 4 Gy group ($P=0.965$).

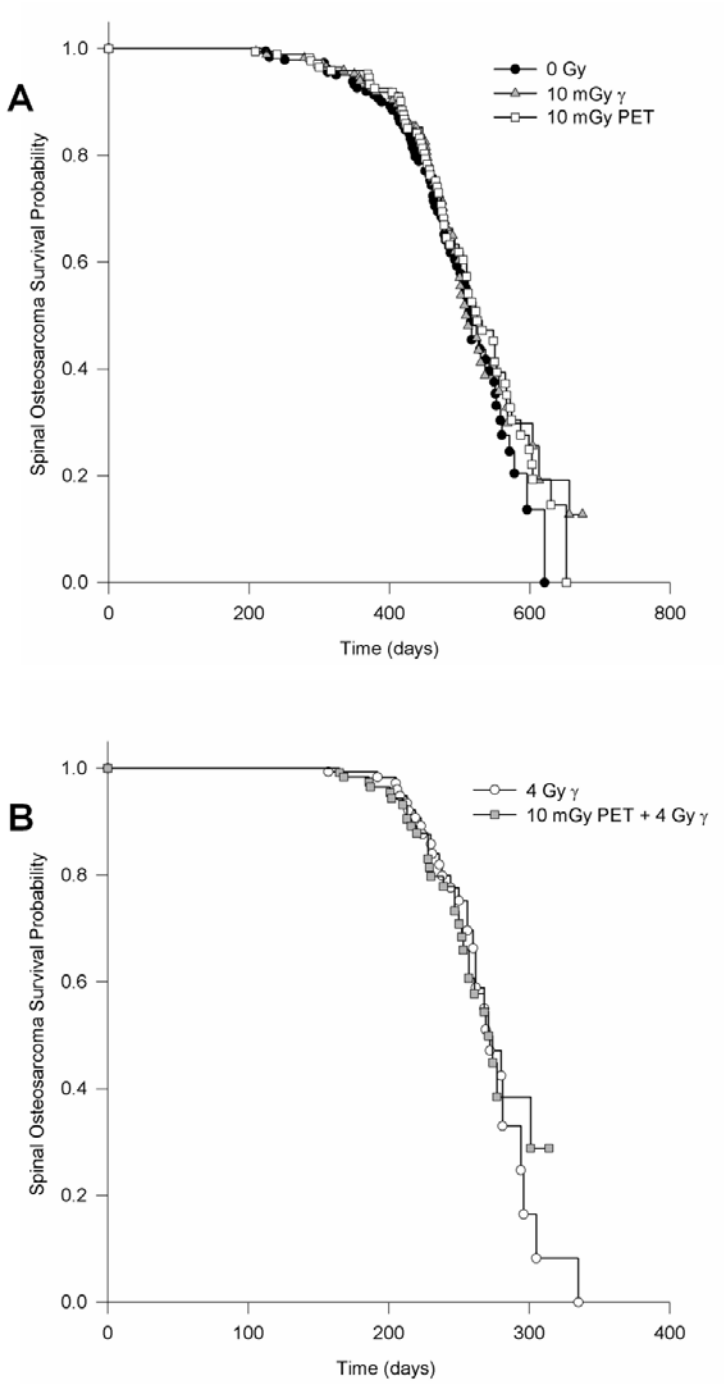

Figure 4.3 Survival probability of *Trp53+/-* mice with spinal osteosarcoma. Time represents the number of days since radiation exposure (days at risk) **(A)** Survival of mice

treated with 10 mGy (γ-rays or PET) relative unirradiated controls (0 Gy) **(B)** Survival of mice treated with 10 mGy PET + 4 Gy relative 4 Gy only controls

4.4.5 Tissue Specific Lesions

The spontaneous frequency of lesions in the bladder and heart of *Trp53+/-* mice were too low to allow for accurate comparisons between groups. When the number of mice with lesions in the reproductive organs were compared, there was not a significant difference between any of the treatment groups (P>0.261). There was however a significant decrease in the number of mice with kidney lesions that had received a single PET scan relative to unirradiated controls (P = 0.021). Lymphoma and chronic nephropathy (Figure 4.4) are the largest contributors to lesions in the kidneys of *Trp53+/- mice*. A 0.75 ± 0.00050 MBq injection of ^{18}F-FDG results in an approximate absorbed dose of 19.63 ± 0.13 mGy to the kidneys (Table 4.1). Otherwise, there were no significant differences between any of the other groups in terms of the number of mice with kidney lesions (P>0.215).

Table 4.4 Number of *Trp53+/-* mice with tissue specific lesions

Treatment	**Kidneys**	**Bladder**	**Heart**	**Reproductive Organs**
Control	32	3	0	28
10 mGy	23	6	0	20
PET	15*	3	0	27
4 Gy	25	0	0	38
PET + 4 Gy	32	0	0	36

* P=0.021 relative to unirradiated control mice

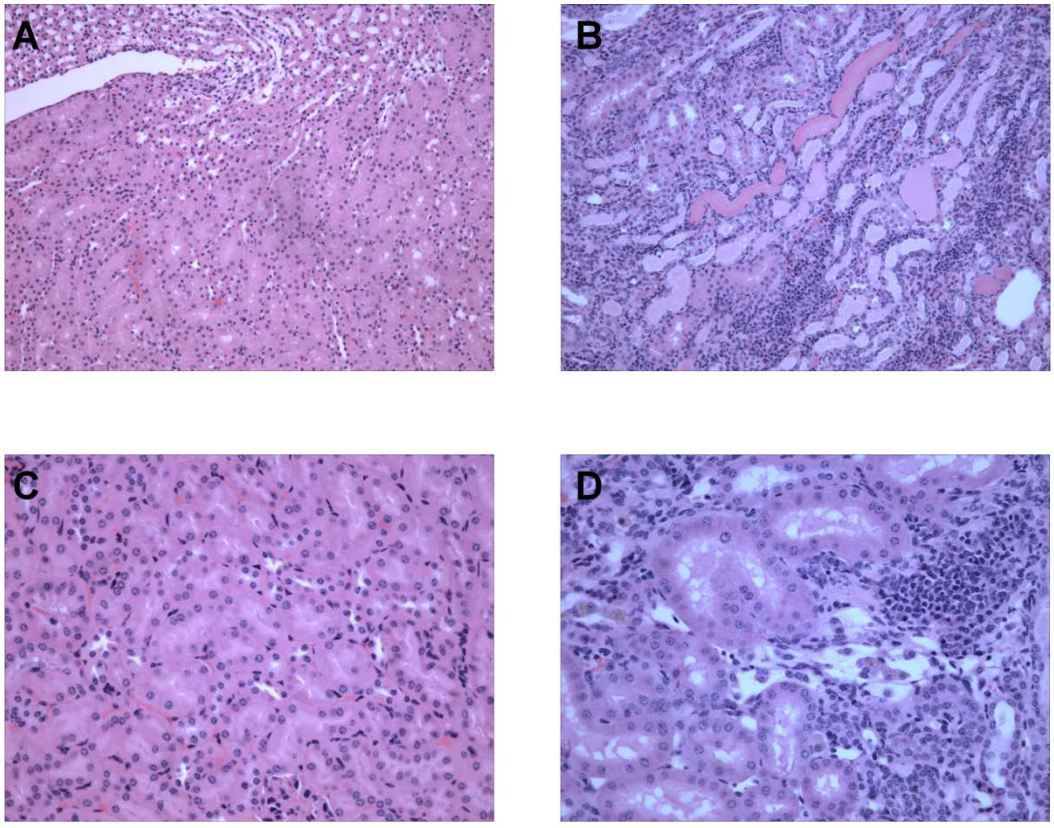

Figure 4.4 Histological features of chronic nephropathy in *Trp53*+/- mice. **(A)** and **(C)** are 20x and 40x normal kidney **(B)** and **(D)** are 20x and 40x severe chronic nephropathy

4.5 Discussion

It has been demonstrated previously that low doses of radiation can extend the lifespan or latency period of tumour formation in mice [14, 15, 36]. This is related to an up-regulation of antioxidants[35], increased DNA repair capacity[36], immune system up-regulation [14, 36, 39-42] and apoptosis of pre-malignant cells [39, 43] following low dose radiation exposure. This adaption has the capacity to protect the organism when subsequently irradiated with a high dose of radiation[12, 39]. The goal of this research was to investigate how modification of cancer risk associated with exposure to low dose ionizing radiation in *Trp53+/-* mice is influenced by radiation quality from Positron Emission Tomography (PET).

An injection activity of 0.75 ± 0.00050 MBq ^{18}F-FDG was used in this study to simulate human radiation exposure during a clinical PET scan (≈10 mGy). Human scans involve the administration of 350-750 MBq ^{18}F-FDG [20] and result in a whole body dose of approximately 10mGy whereas mouse imaging protocols require 18.5 MBq ^{18}F-FDG and result in a whole body dose of approximately 260 mGy [33]. This discrepancy stems from the difference in the size between mice and humans, compounded by the higher spatial resolution requirements in small animal imaging [43].

It was found that the 10 mGy PET scan did not significantly change risk (latency period or frequency of cancer) relative to unirradiated controls. Moreover, the 10

mGy PET scan did not significantly modify the risk associated with the 4 Gy dose. The hypothesis that a 10 mGy PET scan would increase latency as a single exposure and in the context of an adaptive response is therefore rejected and the null hypothesis is accepted. It is likely that the low dose-rate associated with the 10 mGy PET scan was too low to effectuate an up regulation of protective mechanisms. It has been identified previously that there is a lower dose threshold for protective effects and that the rate of dose delivery is an important factor [9]. In terms of investigating the tissue specific risk associated with PET scans, it was found that the number of mice with lesions in the kidney was decreased following a 10 mGy PET scan relative to unirradiated mice. An injection of 0.75 ± 0.0050 MBq ^{18}F-FDG results in an approximate absorbed dose of 20 mGy to the kidneys. It was originally hypothesized that the risk in tissues receiving >10 mGy would be increased. This finding may be related to our previous observations that the low dose-rate associated with PET scans reduces the risk associated with higher total doses[44].

This study did not replicate the previous result in *Trp53+/-* mice with respect to the extension of the latency period for lymphoma and spinal osteosarcoma following a 10 mGy γ-ray dose [15]. This may be related to a number of factors. In the previous study, the 10 mGy dose was delivered at a different dose-rate (0.5 mGy/minute) and with a different source (Co-60). The importance of these factors on tumorigenesis has been studied previously [10, 11, 34, 45]. This may

also be a result of different housing conditions as the unirradiated control mice in this experiment lived on average 100 days longer.

It was recently reported that acute radiation exposure in 7-8 week old *Trp53+/-* female mice results in a reduction of lifespan of 38.9 ± 1.9 days per Gy for overall survival and a reduction of 45.4 ± 2.6 days for malignant tumours[46]. These values were based on high radiation doses (1-4 Gy) at an acute dose-rate of 0.5 Gy/minute. Using the linear no threshold model and extrapolating these results to a 10 mGy dose (from the PET scan or the γ-ray exposure), a *reduction* of 0.39 days and 0.45 days would be expected in terms of overall survival and tumour latency, respectively. This study did not have adequate statistical power to measure differences in survival and latency of that magnitude. Regardless, our results present a *gain* of 5 (PET) and 8 (γ-rays) days in terms of survival and 2 (PET) and 9 (γ-rays) days in terms of malignant tumour latency. Similarly, the *loss of life* following PET+4 Gy would be expected to exceed that of 4 Gy alone by 0.39 days and 0.45 in terms of overall survival and tumour latency, respectively. We found that the mice treated with a PET scan before the 4 Gy dose developed tumours 6 days *later* and lived 10 days *longer*. While this study did not have adequate statistical power to directly address the linear no threshold model, the trends seen within the data suggest that if a larger sample had been used, the trend would be toward protection and not added risk.

We have considered whether the brief period of caloric restriction associated with the protocol may have affected the outcome of this study. Mice receiving an injection of radiopharmaceutical were fasted for a single period of 12-14 hours. While it is well established that moderate caloric restriction regimes extend lifespan and reduce tumorigenesis in mice, there is no evidence in *Trp53+/-* mice to suggest that a single incidence of fasting will impact lifespan [47]. The potential alteration in metabolism generated by the radiopharmaceutical has also been reviewed and the concentration used is suspected to be too low to have any effect based on the tracer principle (0.02 pmol ^{18}F-FDG per injection). In any case, these factors are intrinsic to the process of undergoing a PET scan and any results found reflect the total risk associated with the procedure.

It was observed that the primary tumour type shifted from sarcomas in unirradiated and low dose irradiated *Trp53+/-* mice to lymphoma in high dose irradiated *Trp53+/-* mice. This may be explained by the enhanced radiation sensitivity of lymphatic tissues (lymphoma) relative to mesenchymal tissues (sarcoma) in this mouse model and reliance on p53 function for the elimination of pre-cancerous lesions. It has been shown that the strongest expression of *p53* mRNA occurs in the thymus and spleen (sites of T and B cell lymphoma) in response to ionizing radiation exposure which leads to high levels of p53-dependent apoptosis [48]. With reduced p53 function, the thymus and spleen are most likely to be affected by a lack of apoptosis in response to ionizing radiation in *Trp53+/-* mice leading to enhanced tumour development.

It has been identified in previous studies that low doses of radiation act by increasing the latency period of tumour formation in *Trp53+/-* mice [15]. This may be due in part because the initiation of cancer may have already occurred in *Trp53+/-* mice at the time of radiation treatment (7-8 weeks of age). Other studies have shown that a low dose radiation regime administered prior to a tumour causing treatment (initiating event) reduces the frequency of tumours [41, 51]. For example, Cheda *et al.* showed that when 0.1 or 0.2 Gy x-rays was administered 2 hours before the injection of sarcoma cells into BALB/c mice, the number of pulmonary colonies were significantly reduced [39]. Similarly, Sakai *et al.* showed that chronic low dose irradiation for a period of 35 days reduced the tumours induced by 20-methylcholanthrene [49]. In this study, it was observed that a single PET scan significantly reduced the incidence of kidney disease in *Trp53+/-* mice relative to untreated *Trp53+/-* control mice. A major contributor to kidney disease in *Trp53+/-* mice is chronic nephropathy, an autoimmune related condition [50] associated with aging. A representative image is shown in Figure 3. The development of chronic nephropathy presumably occurred after the radiation treatment which makes a reduction in incidence plausible. Moreover, it may be hypothesized that the protective action of the PET injection on the kidneys is immune-mediated. Ina and Sakai [34] identified previously that low dose-rate irradiation (1.2 mGy/hour x 5 weeks) improved glomerulonephritis, an autoimmune disease specific to the kidney, in *Fas* defective MRL-*lpr/lpr* mice. This finding was accompanied by systemic activation of the immune system.

4.6 Conclusion

It was found that single 10 mGy γ-ray or 10 mGy PET doses did not significantly modify the frequency or latency of cancers in *Trp53+/-* mice from unirradiated *Trp53+/-* mice. When administered 24 hours prior to a 4 Gy dose, the 10 mGy PET dose did not significantly modify the frequency or latency of cancers in *Trp53+/-* mice from *Trp53+/-* mice irradiated with 4 Gy only. The risk of disease in specific tissues which receive higher doses following an injection of ^{18}F-FDG, such as the kidney, was reduced. While an exact mechanism behind these observations was not elucidated, it is likely that this is related to enhancement of immune function, repair capacity, antioxidants or apoptosis.

4.7 References

[1] R. E. J. Mitchel, “Low doses of radiation reduce risk in vivo.,” *Dose-response,*, vol. 5, no. 1, pp. 1-10, Jan. 2007.

[2] L. E. Feinendegen, “Evidence for beneficial low level radiation effects and radiation hormesis,” *British Journal of Radiology*, vol. 78, no. 925, pp. 3-7, Jan. 2005.

[3] D. L. Preston, Y. Shimizu, D. A. Pierce, A. Suyama, and K. Mabuchi, “Studies of mortality of atomic bomb survivors. Report 13: Solid cancer and noncancer disease mortality: 1950-1997,” *Radiation Research*, vol. 160, no. 4, pp. 381–407, 2003.

[4] M. Tubiana, A. Aurengo, D. Averbeck, and R. Masse, “Recent reports on the effect of low doses of ionizing radiation and its dose-effect relationship,” *Radiation and environmental biophysics*, vol. 44, no. 4, pp. 245-51, Mar. 2006.

[5] *Health Risks From Exposure to Low Levels of Ionizing Radiation Beir VII Phase 2*. Washington, DC: , 2006.

[6] M. P. Little, “Cancer and non-cancer effects in Japanese atomic bomb survivors.,” *Journal of radiological protection : official journal of the Society for Radiological Protection*, vol. 29, no. 2, pp. A43-59, Jun. 2009.

[7] R. L. Ullrich and B. Ponnaiya, “Radiation-induced instability and its relation to radiation carcinogenesis.,” *International journal of radiation biology*, vol. 74, no. 6, pp. 747-54, Dec. 1998.

[8] A. C. Upton, “Radiation hormesis: data and interpretations,” *Critical reviews in toxicology*, vol. 31, no. 4-5, pp. 681-95, Jul. 2001.

[9] R. E. J. Mitchel, P. Burchart, and H. Wyatt, “A lower dose threshold for the in vivo protective adaptive response to radiation. Tumorigenesis in chronically exposed normal and Trp53 heterozygous C57BL/6 mice.,” *Radiation research*, vol. 170, no. 6, pp. 765-75, Dec. 2008.

[10] A. Ootsuyama and H. Tanooka, “Threshold-like dose of local beta irradiation repeated throughout the life span of mice for induction of skin and bone tumors,” *Radiation research*, vol. 125, no. 1, pp. 98-101, Jan. 1991.

[11] O. Yamamoto T. Seyama H. Itoh N. Fujim, “Oral administration of tritiated w ater (HTO) in mouse . III : Low dose-rate irradiation and threshold dose-rate for radiation risk,” *International Journal of Radiation Biology*, vol. 73, no. 5, pp. 535-541, Jan. 1998.

[12] R. E. Mitchel, J. S. Jackson, R. a McCann, and D. R. Boreham, “The adaptive response modifies latency for radiation-induced myeloid leukemia in CBA/H mice.,” *Radiation research*, vol. 152, no. 3, pp. 273-9, Sep. 1999.

[13] H. Ishii-Ohba et al., “Existence of a threshold-like dose for gamma-ray induction of thymic lymphomas and no susceptibility to radiation-induced solid tumors in SCID mice.,” *Mutation research*, vol. 619, no. 1-2, pp. 124-33, Jun. 2007.

[14] Y. Ina, H. Tanooka, T. Yamada, and K. Sakai, “Suppression of thymic lymphoma induction by life-long low-dose-rate irradiation accompanied by immune activation in C57BL/6 mice.,” *Radiation research*, vol. 163, no. 2, pp. 153-8, Feb. 2005.

[15] R. E. J. Mitchel, J. S. Jackson, D. P. Morrison, and S. M. Carlisle, “Low doses of radiation increase the latency of spontaneous lymphomas and spinal osteosarcomas in cancer-prone, radiation-sensitive Trp53 heterozygous mice.,” *Radiation research*, vol. 159, no. 3, pp. 320-7, Mar. 2003.

[16] E. J. Calabrese, *Hormesis*. Totowa, NJ: Humana Press, 2010.

[17] R. E. J. Mitchel, J. S. Jackson, and S. M. Carlisle, “Upper dose thresholds for radiation-induced adaptive response against cancer in high-dose-exposed, cancer-prone, radiation-sensitive Trp53 heterozygous mice.,” *Radiation research*, vol. 162, no. 1, pp. 20-30, Jul. 2004.

[18] S. Wolff, “Aspects of the adaptive response to very low doses of radiation and other agents,” *Mutation Research/Fundamental and Molecular Mechanisms of Mutagenesis*, vol. 358, no. 2, pp. 135-142, Nov. 1996.

[19] F. A. Mettler et al., “Nuclear medicine exposure in the United States, 2005-2007: preliminary results.,” *Seminars in nuclear medicine*, vol. 38, no. 5, pp. 384-91, Sep. 2008.

[20] H. R. Schelbert et al., “Society of Nuclear Medicine procedure guideline for tumor imaging using F-18 FDG,” *Society of Nuclear Medicine Procedure Guidelines Manual*, 2002.

[21] H. M. Deloar et al., “Estimation of absorbed dose for 2-[F-18] fluoro-2-deoxy-D-glucose using whole-body positron emission tomography and magnetic resonance imaging,” *European Journal of Nuclear Medicine and Molecular Imaging*, vol. 25, no. 6, pp. 565–574, 1998.

[22] H. M. Deloar, T. Fujiwara, M. Shidahara, T. Nakamura, A. Yamadera, and M. Itoh, “Internal absorbed dose estimation by a TLD method for -FDG and comparison with the dose estimates from whole body PET,” *Physics in Medicine and Biology*, vol. 44, no. 2, pp. 595-606, Feb. 1999.

[23] M. T. Hays, E. E. Watson, S. R. Thomas, and M. Stabin, “MIRD dose estimate report no. 19: radiation absorbed dose estimates from (18)F-FDG.,” *Journal of Nuclear Medicine*, vol. 43, no. 2, pp. 210-4, Feb. 2002.

[24] G. Brix et al., “Radiation exposure of patients undergoing whole-body dual-modality 18F-FDG PET/CT examinations,” *Journal of Nuclear Medicine*, vol. 46, no. 4, p. 608, 2005.

[25] A. A. Mejia, T. Nakamura, I. Masatoshi, J. Hatazawa, M. Masaki, and S. Watanuki, “Estimation of absorbed doses in humans due to intravenous administration of fluorine-18-fluorodeoxyglucose in PET studies,” *Journal of Nuclear Medicine*, vol. 32, no. 4, p. 699, 1991.

[26] D. J. Brenner and E. J. Hall, “Computed tomography--an increasing source of radiation exposure.,” *The New England journal of medicine*, vol. 357, no. 22, pp. 2277-84, Nov. 2007.

[27] R. T. Griffey and A. Sodickson, “Cumulative radiation exposure and cancer risk estimates in emergency department patients undergoing repeat or multiple CT.,” *AJR. American journal of roentgenology*, vol. 192, no. 4, pp. 887-92, Apr. 2009.

[28] B. Huang, M. W. M. Law, and P. L. Khong, “Whole-Body PET/CT Scanning: Estimation of Radiation Dose and Cancer Risk,” *Radiology*, vol. 251, no. 1, p. 166, 2009.

[29] *ICRP publication 103: The 2007 Recommendations of the International Commission on Radiological Protection*, vol. 37, no. 2-4. 2007, pp. 1-332.

[30] T. Jacks et al., “Tumor spectrum analysis in p53-mutant mice.,” *Current biology*, vol. 4, no. 1, pp. 1-7, Jan. 1994.

[31] T. Funk, M. Sun, and B. H. Hasegawa, “Radiation dose estimate in small animal SPECT and PET,” *Medical Physics*, vol. 31, no. 9, p. 2680, 2004.

[32] R. Chirakal, "Base mediated Decomposition of a Mannose Triflate During the Synthesis of 2-Deoxy-2-18F-fluoro-D-glucose," *Applied Radiation and Isotopes*, vol. 46, no. 3, pp. 149-155, Mar. 1995.

[33] R. Taschereau and A. F. Chatziioannou, "Monte Carlo simulations of absorbed dose in a mouse phantom from 18-fluorine compounds," *Medical Physics*, vol. 34, no. 3, p. 1026, 2007.

[34] Y. Ina and K. Sakai, "Prolongation of life span associated with immunological modification by chronic low-dose-rate irradiation in MRL-lpr/lpr mice.," *Radiation research*, vol. 161, no. 2, pp. 168-73, Feb. 2004.

[35] K. Otsuka, T. Koana, H. Tauchi, and K. Sakai, "Activation of antioxidative enzymes induced by low-dose-rate whole-body gamma irradiation: adaptive response in terms of initial DNA damage.," *Radiation research*, vol. 166, no. 3, pp. 474-8, Sep. 2006.

[36] M. Pollycove and L. E. Feinendegen, "Radiation-induced versus endogenous DNA damage: possible effect of inducible protective responses in mitigating endogenous damage.," *Human & experimental toxicology*, vol. 22, no. 6, pp. 290-306; discussion 307, 315-7, 319-23, Jun. 2003.

[37] S. C. Shin, Y. M. Kang, and H. S. Kim, "Life span and thymic lymphoma incidence in high- and low-dose-rate irradiated AKR/J mice and commonly expressed genes.," *Radiation research*, vol. 174, no. 3, pp. 341-6, Sep. 2010.

[38] E. M. Nowosielska, J. Wrembel-Wargocka, A. Cheda, E. Lisiak, and M. K. Janiak, "Enhanced Cytotoxic Activity of Macrophages and Suppressed Tumor Metastases in Mice Irradiated with Low Doses of X- rays," *Journal of Radiation Research*, vol. 47, no. 3/4, pp. 229-236, 2006.

[39] A. Cheda, J. Wrembel-Wargocka, E. Lisiak, E. M. Nowosielska, M. Marciniak, and M. K. Janiak, "Single low doses of X rays inhibit the development of experimental tumor metastases and trigger the activities of NK cells in mice.," *Radiation research*, vol. 161, no. 3, pp. 335-40, Mar. 2004.

[40] Y. Ina and K. Sakai, "Activation of immunological network by chronic low-dose-rate irradiation in wild-type mouse strains: analysis of immune cell populations and surface molecules.," *International journal of radiation biology*, vol. 81, no. 10, pp. 721-9, Oct. 2005.

[41] D. I. Portess, G. Bauer, M. A. Hill, and P. O'Neill, "Low-dose irradiation of nontransformed cells stimulates the selective removal of precancerous cells via intercellular induction of apoptosis.," *Cancer research*, vol. 67, no. 3, pp. 1246-53, Feb. 2007.

[42] D. R. Boreham, J. A. Dolling, S. R. Maves, N. Siwarungsun, and R. E. Mitchel, "Dose-rate effects for apoptosis and micronucleus formation in gamma-irradiated human lymphocytes.," *Radiation research*, vol. 153, no. 5 Pt 1, pp. 579-86, May. 2000.

[43] A. F. Chatziioannou, "Instrumentation for molecular imaging in preclinical research: Micro-PET and Micro-SPECT.," *Proceedings of the American Thoracic Society*, vol. 2, no. 6, pp. 533-6, 510-11, Jan. 2005.

[44] K. Taylor, N. Phan, and D. Boreham, "PET scans with 18F-FDG cause radiation induced biological changes in mice," *Prepared Manuscript*.

[45] M. A. Hill, "The variation in biological effectiveness of X-rays and gamma rays with energy.," *Radiation protection dosimetry*, vol. 112, no. 4, pp. 471-81, Jan. 2004.

[46] S. M. Carlisle, P. a Burchart, and R. E. J. Mitchel, "Cancer and non-cancer risks in normal and cancer-prone Trp53 heterozygous mice exposed to high-dose radiation.," *Radiation research*, vol. 173, no. 1, pp. 40-8, Jan. 2010.

[47] D. Berrigan, S. N. Perkins, D. C. Haines, and S. D. Hursting, "Adult-onset calorie restriction and fasting delay spontaneous tumorigenesis in p53-deficient mice.," *Carcinogenesis*, vol. 23, no. 5, pp. 817-22, May. 2002.

[48] E. A. Komarova, K. Christov, A. I. Faerman, and A. V. Gudkov, "Different impact of p53 and p21 on the radiation response of mouse tissues.," *Oncogene*, vol. 19, no. 33, pp. 3791-8, Aug. 2000.

[49] K. Sakai, Y. Hoshi, T. Nomura, and T. Oda, "Suppression of carcinogenic processes in mice by chronic low dose-rate gamma-irradiation," *International Journal of Low Radiation*, vol. 1, no. 1, pp. 142-146, 2003.

[50] D. Percy, "Pathology of laboratory rodents and rabbits," 2007.

Chapter 5

Conclusion

This research has helped to clarify the role of p53 and radiation quality in low dose radiation responses and cancer risk. The main findings are:

- The initial DNA damage response following radiation exposure as measured by γH2A.X is no different between mice with different cancer risks (*Trp53*+/+ and *Trp53*+/-)

- A suppressed apoptotic response to doses of radiation between 0.1 and 2 Gy correlates with an increase in cancer risk in *Trp53*+/- mice. This suppression is only evident between 0 and 12 hours post-irradiation *in vitro*.

- *Trp53*+/+ and *Trp53*+/- mice exhibit similar MN-RET levels following radiation exposure although p53-deficient *Trp53*+/- mice show a slightly slower rate of MN-RET clearance between 43 and 137 hours post-irradiation. While the decreased rate of disappearance from the peripheral blood stream may be responsible for increased cancer risk in *Trp53*+/- mice, the similar maximum level of radiation induced damage at 43 hours between the two genotypes suggests that the clearance of severely damaged precursors in bone marrow is independent of p53.

- There is a threshold below which there is no measurable increase in DNA damage following a PET scan as measured by MN-RET formation. This threshold was found to be 3.70 MBq ^{18}F-FDG, which corresponds to a bone marrow dose of

approximately 35 mGy in mice. A much lower acute dose of γ-rays (10mGy whole body) will significantly elevate MN-RET levels. This highlights the increased tolerance to DNA damage associated with the protracted dose-rates used in PET scans. It was consequently found that the RBE of ^{18}F-FDG was less than 1 indicating that the mixed radiation quality and/or low dose-rate from PET scans is less damaging than equivalent doses of gamma radiation.

- A 20% reduction in residual γH2A.X fluorescence (indicative of DNA DSBs) was observed in mice injected with 14.80 MBq relative to controls at 24 hours (P=0.019) which corresponds to a bone marrow dose of 150 mGy. The isotope exposure has likely stimulated damaged cells to undergo apoptosis or has stimulated enhanced repair.

- While a high dose of radiation was shown to increase cancer risk in *Trp53+/-* mice (as measured by the frequency and latency of specific cancer types), a 10 mGy PET scan did not significantly modify risk from the background rate. When tissue specific risk was considered however, the PET scan reduced the number of mice with kidney disease (absorbed dose of approximately 20 mGy). A 10 mGy PET scan administered prior to the high dose of radiation did not significantly modify its effect.

An important question is how radiation responses and risks in a mouse compare to that of humans given that the goal was to understand radiation exposures relevant

to clinical imaging. An excellent review of this topic is provided in [1]. The mouse represents a high level of mammalian organization and shares organs systems, systemic physiology and genes with humans. The basal metabolic rate of mice however is 7 times higher than in humans which contributes to the comparatively short lifespan of mice (30-50 times less). The cancer types that develop in the two species are also quite different. In general, laboratory mice develop lymphomas and sarcomas (mesenchymal tissue cancers) whereas humans develop carcinomas (epithelial cancers). Human diet and tobacco use is thought to be a contributor but otherwise the biological mechanism is not clear. It is thought that differences in telomere length and regulation may play a role.

There were two major challenges associated with the experiments presented in this thesis. The first was finding endpoints that would provide a comprehensive assessment of the biological effects associated with *in vivo* isotope exposure. Sampling before the complete biological or physical decay of the isotope would lead to an underestimation of potential biological effects. As shown in Chapter 2, the optimal sampling time for the use of the γH2A.X fluorescence and apoptosis assays as direct measures of radiation exposure was 30 minutes and 8 hours post-irradiation, respectively, which made these endpoints unsuitable for measuring the direct effects of PET isotopes. Moreover, the sensitivity of these two endpoints in measuring doses of radiation below 100 mGy was not verified in Chapter 2. This was in part because other research in our laboratory has showed that γH2A.X fluorescence can only detect acute doses ≥100 mGy and that apoptosis, detected

with Annexin 7AAD staining, may only detect acute doses ≥50 mGy [2]. The micronucleated reticulocyte endpoint investigated in the Chapter 2 is not only sensitive to very low doses of radiation (10 mGy acute) but manifests itself 43 hours after radiation exposure which is why it was chosen to investigate the effects of PET scans in mice in Chapter. In Chapter 3, γH2A.X was used to measure residual fluorescence at 24 hours post-irradiation and 24 hours was generally chosen as the time for the adaptive response studies to allow for decay of the isotope. Moreover, there was an emphasis in Chapter 3 on measuring residual effects rather than direct effects. Chapter 4 circumvented the issue of timing by measuring late effects.

The second issue was mouse PET dosimetry. While the dosimetry of ^{18}F-FDG in humans is well characterized, there are limited studies focused on mouse dosimetry for nuclear medicine agents. Two studies in particular [3, 4] were used to provide an approximate dose for the injection activities of PET agent ^{18}F-FDG used in this work. An in-depth dosimetry assessment was beyond the scope of this project and resources available. Of particular interest would be evaluating the absorbed doses in female mice as the estimates currently available are reflective of male mouse anatomy only [3]. As mentioned in Chapter 3 and 4, the injection activities used in small animal imaging result in high absorbed doses to many organs so this type of investigation would be of interest for toxicity purposes. Throughout this study, both dynamic and static scans of 7-8 week old female mice were acquired following injection with various activities of ^{18}F-FDG. Moreover, a

subset of mice containing various tumour types were also imaged using ^{18}F-FDG. The imaging data available for future collaborative use is listed in Appendix B.

Although this research was focused specifically on the biological effects of ^{18}F-FDG, the findings may be helpful in understanding the health effects associated with other nuclear medicine procedures. Nuclear medicine procedures are generally characterized by low absorbed doses, partial body irradiation and low, decaying dose-rates which we have shown increase the tolerance for radiation damage associated with a total given dose.

In the context of murine lifespan studies, it has been shown that low dose radiation exposure can affect the risk of disease in two ways and it is hypothesized that this relies on the timing of the exposure relative to the initiation of cells. Mitchel *et al.* [5] showed that radiation exposure at 7-8 weeks of age in *Trp53*+/- mice significantly increased the latency period of lymphoma and spinal osteosarcoma without influencing the frequency of these cancers. It was hypothesized that cancers had already been spontaneously initiated by 7-8 weeks of age. In contrast, two groups [6, 7] have shown that pre-treatment of mice with low dose/low dose-rate radiation reduced the frequency of cancers initiated by the injection of cancer cells or treatment with a chemical agent. The finding presented in Chapter 4 of this thesis supports this theory. A reduction in kidney disease was observed in mice receiving a low dose PET scan which was due to a reduction in chronic nephropathy, a disease of aging mice. The initiation of this disease likely

occurred after the radiation exposure at 7-8 weeks of age. Moreover, our group recently showed that repeated CT scans administered after an initiating radiation exposure of 4 Gy significantly delayed the latency period of lymphoma but no modification of frequency was observed [8]. In the future, the goal should be to further investigate the temporal characteristics of hormetic responses using medical radiation exposures and possibly in combination with other known carcinogens.

Finally, the data presented in this thesis reflects only a fraction of the data acquired during the lifetime study. The study contains 1625 *Trp53*+/- heterozygous mice treated with various types of low dose radiation (γ-rays, CT, PET) and high dose radiation (4Gy γ-rays, CT + 4Gy γ-rays, PET + 4Gy γ-rays) in addition to a single group of 200 *Trp53*+/+ wild-type mice. Multiple tissues have been collected in formalin from each mouse in addition to data on disease progression and symptoms. We are currently investigating immnohistochemistry array analysis and gene expression analysis.

References

[1] A. Rangarajan and R. A. Weinberg, “Comparative biology of mouse versus human cells: modelling human cancer in mice,” *Nature Reviews Cancer*, vol. 3, no. December, pp. 952–959, 2003.

[2] N. Phan, K. Taylor, and D. R. Boreham, “Single computed tomography scans prolong survival by increasing cancer latency in Trp53 heterozygous mice,” *Manuscript*, 2011.

[3] R. Taschereau and A. F. Chatziioannou, “Monte Carlo simulations of absorbed dose in a mouse phantom from 18-fluorine compounds,” *Medical Physics*, vol. 34, no. 3, p. 1026, 2007.

[4] T. Funk, M. Sun, and B. H. Hasegawa, “Radiation dose estimate in small animal SPECT and PET,” *Medical Physics*, vol. 31, no. 9, p. 2680, 2004.

[5] R. E. J. Mitchel, J. S. Jackson, D. P. Morrison, and S. M. Carlisle, “Low doses of radiation increase the latency of spontaneous lymphomas and spinal osteosarcomas in cancer-prone, radiation-sensitive Trp53 heterozygous mice.,” *Radiation research*, vol. 159, no. 3, pp. 320-7, Mar. 2003.

[6] A. Cheda, J. Wrembel-Wargocka, E. Lisiak, E. M. Nowosielska, M. Marciniak, and M. K. Janiak, “Single low doses of X rays inhibit the development of experimental tumor metastases and trigger the activities of NK cells in mice.,” *Radiation research*, vol. 161, no. 3, pp. 335-40, Mar. 2004.

[7] Y. Ina and K. Sakai, “Prolongation of life span associated with immunological modification by chronic low-dose-rate irradiation in MRL-lpr/lpr mice.,” *Radiation research*, vol. 161, no. 2, pp. 168-73, Feb. 2004.

[8] N. Phan, K. Taylor, and D. R. Boreham, “Computed tomography scans modify acute biological effects and tumorigenic consequences of prior high-dose radiation exposures in Trp53 heterozygous mice,” *Manuscript*, 2011.

Appendix A: Other Material Prepared During PhD studies

Published Papers

Taylor K, Dingwall S, Mills CE, Phan N, Boreham DR. Human Health and the Biological Effects of Tritium in Drinking Water: Prudent Policy Through Science - Addressing the ODWAC New Recommendation. *Dose-response : a publication of International Hormesis Society*. 2011; 9(1):6-31.

Completed Manuscripts

Phan N, **Taylor K**, Boreham DR. Single computed tomography scans prolong survival by increasing cancer latency in Trp53 heterozygous mice

Phan N, **Taylor K**, Boreham DR. Computed tomography scans modify acute biological effects and tumorigenic consequences of prior high-dose radiation exposures in Trp53 heterozygous mice

Phan N, **Taylor K**, Boreham DR**.** Computed tomography scans induce protection against high-dose radiation exposures in the hematopoietic system of Trp53 wild-type mice

Appendix B: Imaging Inventory

A number of images were acquired during this study for the purpose of verifying the distribution of ^{18}F-FDG in the experimental mice and potentially developing better dosimetry models. They represent an untapped resource and may be used by other researchers. Figure B-1 provides a sample image from the tumour localization study.

Sept 4 2008
Objective: Representative Uptake values in WT mice
5 x 7 week old WT
Static Acquisition
30 m wait time between injection & acquisition
Injection Activities: 500, 200, 100, 50, 10 µCi (1 mouse per injection activity)

Sept 11 2008
Objective: Representative Uptake values in HET mice
4 x 7 week old HET
Injection Activities: 500, 200, 100, 50 (1 mouse per injection activity)
2 x 12 week old (1 HET, 1 WT)
Static Acquisition
30 m wait time between injection & acquisition

May 28 2008
Objective: Biological Half Life in HET + WT mice
2 hets, 2 wt
Dynamic Acquisition (mice under anaesthesia, 2-3 hour scan)
First hour: 5 m frames in the first hour, 15 m frames after the first hour (list mode acquisition)

April 14 2009
Objective: Fast versus Feed Trial
Replicate biology experiment conditions. Manual restraint, fast – inject – feed or fast – image
6 mice 8 week old WT
Injection Activity: 20 µCi
File ID: M002 versus M007 (PET Files ONLY)

Tumour Localization
July – October 2009
8 mice at endpoint scanned (PET/CT)
Mouse ID: PM69, PM132, PM133, PM134, PM135, PM137, PM175, PM192
PM 69 – [18F]Na used

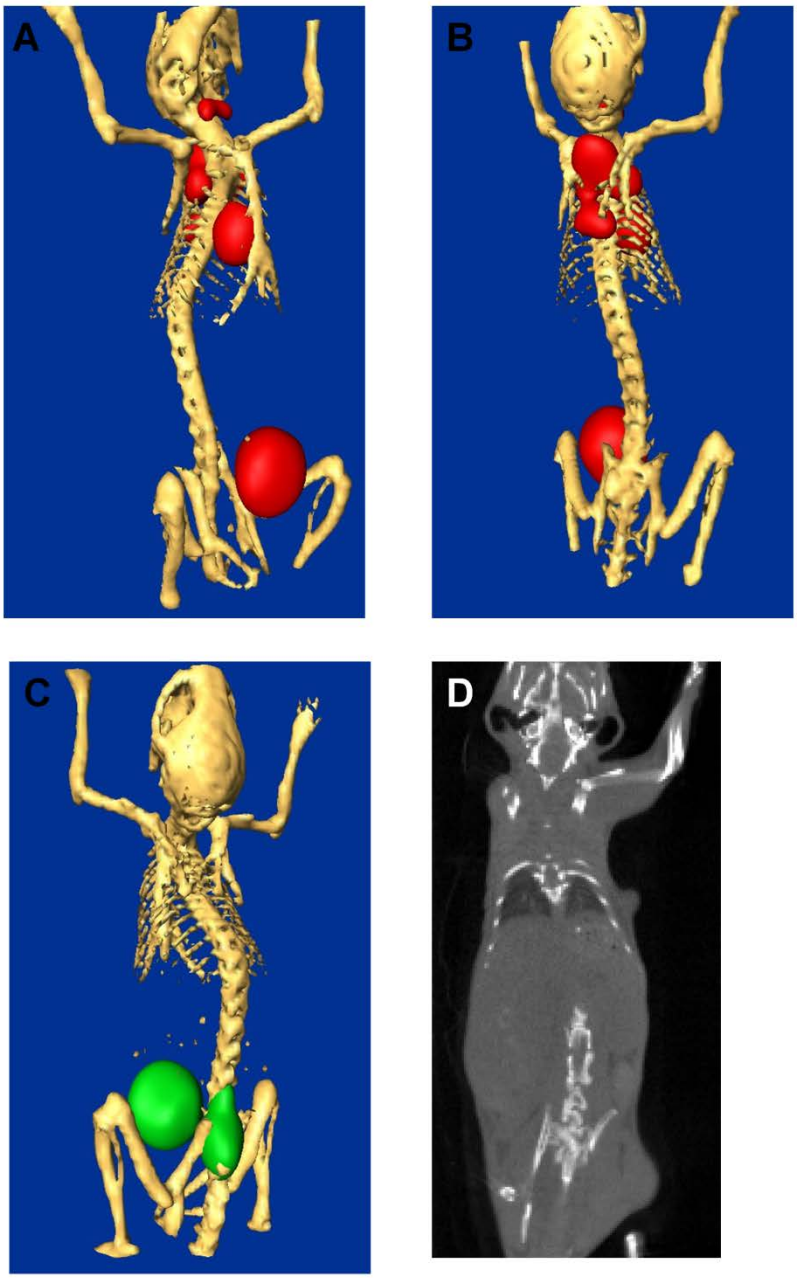

Figure B.1 *Trp53+/-* mouse with spinal osteosarcoma imaged at endpoint (A) and (B) PET/CT with [^{18}F]FDG (red) (C) PET/CT with [^{18}F]Na (green) (D) CT only